Karlsruher Institut für Technologie

Smart Polymer Materials With Orthogonal Responsiveness: From Polymers To Hydrogels

Zur Erlangung des akademischen Grades einer

DOKTORIN DER NATURWISSENSCHAFTEN

(Dr. rer. nat.)

von der KIT-Fakultät für Chemie und Biowissenschaften
des Karlsruher Instituts für Technologie (KIT)

genehmigte

DISSERTATION

von

M.Sc. Vaishali Pruthi

geboren in India

1. Referent: Prof. Dr. Patrick Théato
2. Referent: Prof. Dr. Pavel Levkin

Tag der mündlichen Prüfung: 22.04.2024

for my Parents

Declaration of Authorship (Erklärung)

Die vorliegende Arbeit wurde im Zeitraum von Dezember 2019 bis Februar 2024 am Institut für Technische Chemie und Polymerchemie (ITCP) am Karlsruher Institut für Technologie (KIT) unter der wissenschaftlichen Betreuung von Prof. Dr. Patrick Théato angefertigt.

Ich erkläre hiermit, dass ich die vorliegende Arbeit im Rahmen der Betreuung durch Prof. Dr. Patrick Théato selbstständig verfasst und keine anderen als die angegebenen Quellen und Hilfsmittel verwendet habe. Wörtlich oder inhaltlich übernommene Stellen sind als solche kenntlich gemacht und die Satzung des Karlsruher Instituts für Technologie (KIT) zur Sicherung guter wissenschaftlicher Praxis wurde beachtet. Des Weiteren erkläre ich, dass ich mich derzeit in keinem laufenden Promotionsverfahren befinde, und auch keine vorausgegangenen Promotionsversuche unternommen habe. Die elektronische Version der Arbeit stimmt mit der schriftlichen Version überein und die Primärdaten sind gemäß Abs. A (6) der Regeln zur Sicherung guter wissenschaftlicher Praxis des KIT beim Institut abgegeben und archiviert.

Karlsruhe, den 11.03.2024

_____

Vaishali Pruthi

Abstract

Recent advancements in materials science have sparked a heightened interest in smart and responsive materials, attributed to their unique ability to autonomously execute functions or respond in a controlled manner to external stimuli. Such materials are pivotal in creating advanced, efficient devices and systems, including sensors, actuators, and drug delivery systems. Within the diverse spectrum of stimuli-responsive materials, those exhibiting sensitivity to light command particular attention for their swift and precise control over material properties. However, the integration of varied stimuli-reactive attributes within a sole polymer structure presents a significant challenge which is essential for replicating the intricate behaviours observed in natural systems. The objective of the present thesis encompasses the development of smart materials with tunable properties and using state-of-the-art 3D printing techniques to fabricate complex polymer networks.

The first approach introduces a pioneering strategy for the creation of a distinct series of copolymers, integrating di(ethylene glycol)methyl ether methacrylate (DEGMA) with varying concentrations of spiropyran methacrylate (SpMA). These copolymers are characterized by the inclusion of spiropyran moieties capable of undergoing reversible photo-isomerization. Experimental findings reveal an increase in the glass transition temperature (T_g) of the copolymers upon exposure to ultraviolet (UV) light at a wavelength of 365 nm, attributable to the photo-induced isomerization of spiropyran to its merocyanine state. The observed photo-tunable T_g feature of these copolymers holds significant potential for their incorporation into advanced materials suited for photo-responsive applications.

The second study introduces a novel protocol for crafting *pH*-reactive interpenetrating polymer network (IPN) hydrogels by utilizing a sophisticated 3D printing technique that capitalizes on the photodegradable nature of the *ortho*-nitrobenzyl (*o*-NB) group. The synthetic strategy involves a delicate balance of embedding a polyelectrolyte complex (PEC), composed of hyaluronic acid (HA) and chitosan (CS), into a P(OEGMA-*co*-EGDEMA) scaffold, while temporally regulating the PEC formation with *o*-NB-modified HA during the 3D ink formulation. A diverse array of analytical techniques, including mechanical tests and *pH*-responsive swelling assessments, have been employed to investigate the mechanical and functional properties of these hydrogels. By manipulating the 3D ink's composition, hydrogels with adjustable mechanical strengths and elastic moduli, spanning 1 to 10 kPa, were

synthesized. These hydrogels exhibit superior flexibility, compressive strength, high strain resilience, *pH* sensitivity, and thermal robustness, demonstrating a harmonious fusion of natural polyelectrolyte complexes with 3D printing advancements.

Building upon the second project's groundwork, the third initiative advances the development of hybrid polymers that exhibit dual responsiveness to both light and *pH* changes. This research presents the fabrication of three distinct polymer networks, each embedding an Azo-modified polyelectrolyte and a β-cyclodextrin (CD)-functionalized polyelectrolyte within a P(OEGMA-*co*-EGDEMA) structural matrix. These newly synthesized IPNs and Supramolecular Polymer Networks (SPNs) were rigorously examined for their physical and chemical attributes, including their capacity for swelling, thermal stability, mechanical resilience, and reactive behaviours to variations in light and *pH* levels. Notably, the IPN hydrogels composed of HA-Azo/CD-CS demonstrated a superior storage modulus of 14 kPa, indicative of their advanced mechanical robustness, which arises from the synergistic effects of polymeric entanglements and supramolecular interactions. Conversely, the SPN hydrogels with CS-Azo/CD-CS and PDAC-Azo/CD-CS exhibited comparatively lower storage moduli of 10 kPa and 6 kPa, respectively, owing to their sole dependence on supramolecular interactions. The *pH*-responsive nature of these materials was further explored through three differentiated bilayer systems, manifesting variable bending behaviours. The seamless integration of these polymers with Digital Light Processing (DLP) technology was also assessed, leading to precise 3D-printed structures with complex floral patterns. These hydrogel networks hold extensive potential for bioinspired assemblies and soft robotic systems.

This thesis conclusively highlights a significant advancement in materials science, delivering dual light and *pH*-responsive polymer networks with exceptional control and adaptability. The innovative strategies outlined, from the photo-tunable copolymers of DEGMA and SpMA to the *pH*-responsive IPN hydrogels and the dual-responsive IPN and SPN hydrogels, exemplify the intricate control over material properties that modern science can achieve. Leveraging innovative 3D printing capabilities, these materials exhibit adjustable properties crucial for applications ranging from biomimetics to responsive actuation, reflecting a significant step toward replicating the complex functionality of natural systems.

Zusammenfassung

Jüngste Fortschritte in der Materialwissenschaft haben ein erhöhtes Interesse an intelligenten und reaktionsfähigen Materialien geweckt, was auf ihre einzigartige Fähigkeit zurückgeführt wird, Funktionen autonom auszuführen oder kontrolliert auf äußere Reize zu reagieren. Solche Materialien sind von entscheidender Bedeutung für die Entwicklung fortschrittlicher, effizienter Geräte und Systeme, einschließlich Sensoren, Aktoren und Arzneimittelverabreichungssystemen. Innerhalb des vielfältigen Spektrums an auf Reize reagierenden Materialien verdienen diejenigen mit Lichtempfindlichkeit besondere Aufmerksamkeit, da sie die Materialeigenschaften schnell und präzise steuern können. Allerdings stellt die Integration verschiedener reizreaktiver Eigenschaften innerhalb einer einzigen Polymerstruktur eine erhebliche Herausforderung dar, die für die Nachbildung der in natürlichen Systemen beobachteten komplexen Verhaltensweisen von entscheidender Bedeutung ist. Das Ziel dieser Forschung umfasst die Entwicklung intelligenter Materialien mit einstellbaren Eigenschaften und den Einsatz modernster 3D-Drucktechniken zur Herstellung komplexer Polymernetzwerke.

Der erste Ansatz stellt eine bahnbrechende Strategie für die Schaffung einer bestimmten Reihe von Copolymeren vor, bei der Di(ethylenglykol)methylethermethacrylat (DEGMA) mit unterschiedlichen Konzentrationen an Spiropyranmethacrylat (SpMA) integriert wird. Diese Copolymere zeichnen sich durch den Einschluss von Spiropyran-Einheiten aus, die eine reversible Photo-isomerisierung eingehen können. Experimentelle Ergebnisse zeigen einen Anstieg der Glasübergangstemperatur (T_g) der Copolymere bei Einwirkung von ultraviolettem Licht mit einer Wellenlänge von 365 nm, was auf die photo-induzierte Isomerisierung von Spiropyran in seinen Merocyaninzustand zurückzuführen ist. Die beobachtete photoabstimmbare T_g -Eigenschaft dieser Copolymere birgt ein erhebliches Potenzial für ihren Einbau in fortschrittliche Materialien, die für photo-responsive Anwendungen geeignet sind.

Die zweite Studie stellt ein neuartiges Protokoll zur Herstellung von *pH*-reaktiven Hydrogelen mit interpenetrierenden Polymernetzwerken (IPN) unter Verwendung einer hochentwickelten 3D-Drucktechnik vor, die sich die photoabbaubare Natur der *ortho*-nitrobenzylgruppe (*o*-NB) zunutze macht. Die Synthesestrategie beinhaltet ein empfindliches Gleichgewicht zwischen der Einbettung eines Polyelektrolytkomplexes (PEC), bestehend aus Hyaluronsäure (HA) und Chitosan (CS), in ein P(OEGMA-*co*-EGDEMA)-Gerüst und gleichzeitiger zeitlicher

Regulierung der PEC-Bildung mit *o*- NB-modifiziertes HA während der 3D-Tintenformulierung. Zur Untersuchung der mechanischen und funktionellen Eigenschaften dieser Hydrogele wurden vielfältige Analysetechniken eingesetzt, darunter mechanische Tests und *pH*-abhängige Quellungsbewertungen. Durch Manipulation der Zusammensetzung der 3D-Tinte wurden Hydrogele mit einstellbaren mechanischen Festigkeiten und Elastizitätsmodulen im Bereich von 1 bis 10 kPa synthetisiert. Diese Hydrogele zeichnen sich durch überragende Flexibilität, Druckfestigkeit, hohe Dehnungsbeständigkeit, *pH*-Empfindlichkeit und thermische Robustheit aus und demonstrieren eine harmonische Verschmelzung natürlicher Polyelektrolytkomplexe mit Fortschritten im 3D-Druck.

Aufbauend auf den Grundlagen des zweiten Projekts treibt die dritte Initiative die Entwicklung von Hybridpolymeren voran, die sowohl auf Licht- als auch auf *pH*-Änderungen doppelt reagieren. Diese Forschung präsentiert die Herstellung von drei unterschiedlichen Polymernetzwerken, die jeweils einen Azo-modifizierten Polyelektrolyten und einen β-Cyclodextrin (CD)-funktionalisierten Polyelektrolyten in eine P(OEGMA-*co*-EGDEMA)-Strukturmatrix einbetten. Diese neu synthetisierten IPNs und supramolekularen Polymernetzwerke (SPNs) wurden eingehend auf ihre physikalischen und chemischen Eigenschaften untersucht, einschließlich ihrer Quellfähigkeit, thermischen Stabilität, mechanischen Belastbarkeit und ihrem Reaktionsverhalten gegenüber Schwankungen des Licht- und *pH*-Werts. Bemerkenswert ist, dass die IPN-Hydrogele aus HA-Azo/CD-CS einen überlegenen Speichermodul von 14 kPa zeigten, was auf ihre fortschrittliche mechanische Robustheit hinweist, die aus den synergistischen Effekten polymerer Verflechtungen und supramolekularer Wechselwirkungen resultiert. Im Gegensatz dazu zeigten die SPN-Hydrogele mit CS-Azo/CD-CS und PDAC-Azo/CD-CS vergleichsweise niedrigere Speichermodule von 10 kPa bzw. 6 kPa, was auf ihre ausschließliche Abhängigkeit von supramolekularen Wechselwirkungen zurückzuführen ist. Die auf den *pH*-Wert reagierende Natur dieser Materialien wurde anhand von drei differenzierten Doppelschichtsystemen weiter untersucht, die ein unterschiedliches Biegeverhalten aufweisen. Auch die nahtlose Integration dieser Polymere in die Digital Light Processing (DLP)-Technologie wurde bewertet, was zu präzisen 3D-gedruckten Strukturen mit komplexen Blumenmustern führte. Diese Hydrogel-Netzwerke bergen ein umfangreiches Potenzial für bioinspirierte Baugruppen und weiche Robotersysteme.

Diese Arbeit unterstreicht abschließend einen bedeutenden Fortschritt in der Materialwissenschaft, der duale licht- und *pH*-responsive Polymernetzwerke mit

außergewöhnlicher Kontrolle und Anpassungsfähigkeit liefert. Die beschriebenen innovativen Strategien, von den photoabstimmbaren Copolymeren von DEGMA und SpMA über die *pH*-responsiven IPN-Hydrogele bis hin zu den dual-responsiven IPN- und SPN-Hydrogelen, veranschaulichen die komplexe Kontrolle über Materialeigenschaften, die die moderne Wissenschaft erreichen kann. Durch die Nutzung innovativer 3D-Druckfunktionen weisen diese Materialien anpassbare Eigenschaften auf, die für Anwendungen von der Biomimetik bis zur reaktiven Betätigung entscheidend sind, was einen bedeutenden Schritt in Richtung Nachbildung der komplexen Funktionalität natürlicher Systeme darstellt.

Table of Contents

1. Introduction

Nature has equipped various creatures with sophisticated structures, enabling them to respond dynamically to a range of external stimuli. These responses manifest in the form of alterations in stiffness, shape and color. This is evidenced by phenomena such as the sea cucumber's capacity for rapid stiffness modulation, the Venus flytrap's swift predatory action, and the adaptive coloration of cephalopods. [1] These natural strategies, governed by complex bio-macromolecules and polymers, provide a blueprint for the development of responsive polymer materials. Recent years have seen a surge in interest towards smart and responsive materials. "Smart" implies a material's ability to respond in a highly specific, controlled and often reversible manner, whereas "responsive" broadly refers to materials that change properties in reaction to environmental changes. The inherent capacity of smart materials to autonomously perform functions or respond to external influences is deemed essential for the innovation of drug delivery [2, 3], sensors [4, 5], and actuators [6, 7] in advanced technological sectors. [8, 9] The stimuli-responsive nature of smart polymers is principally governed by the functional groups present on or within the polymer chains. [10] A comprehensive range of such functionalities has been explored and well-documented in scientific literature. These polymers can respond to various environmental stimuli, including temperature [11], *pH* [12], light [13], ionic strength [14], electric [15] and magnetic fields [16]. An emerging trend in this area is the creation of polymers with multiple functional groups, each responsive to different stimuli.

This dissertation presents a comprehensive investigation into an innovative synthesis and detailed characterization of new polymer materials, focusing on their tunable properties and orthogonal responsiveness. Through a comprehensive exploration of their dynamic properties, the mechanisms that enable these materials to exhibit distinct responses under varying stimuli are elucidated. Additionally, utilizing photo stimuli as a control measure is particularly advantageous, offering unmatched remote precision, the ability to effect rapid state changes, and the capacity to direct stimuli to specific zones within material frameworks. [17] Simultaneously, polymers that are sensitive to *pH* changes take advantage of the slight, yet impactful, fluctuations in *pH* levels that are inherent to various ecological niches.

By embedding molecular entities like azobenzene [18, 19] and spiropyran [20, 21], known for their light-induced reversible isomerization, within polymer frameworks, one can fabricate dynamic materials that exhibit photo-induced structural alterations. Concurrently, the assimilation of

photo-labile *ortho*-nitrobenzyl groups [22], which are characterized by their propensity to cleave under UV light introduces a layer of control that is highly desirable for advanced materials design. These modifications enable the creation of sophisticated photo-responsive systems that can be finely tuned for applications requiring controlled light-induced reactions. Furthermore, natural polyelectrolytes stand out among *pH*-sensitive polymeric materials due to their widespread occurrence in nature, their environmentally friendly degradation profile, and the relative simplicity of modifying their chemical properties to suit specific applications. [23]

Moreover, the synergistic integration of varied polymeric systems, accompanied by the strategic utilization of a spectrum of crosslinking strategies could result in the creation of polymer networks that exhibit multiplexed responsiveness. The emergent polymeric structures demonstrate considerable improvements in terms of stability and mechanical durability, primarily due to the molecular reinforcement incurred through the interlaced networks formed by the confluence of various polymer species. [24]

Besides, advanced 3D printing technology has dramatically advanced the development of smart polymers and hydrogels, paving the way for a new era of functional materials. 3D printing offers enhanced adaptability, improved resource efficiency, and economic advantages, while also facilitating the integration of more sophisticated and intricate substructures. [25] The selection of materials that are compatible for use as 3D inks is an essential but challenging aspect in the development and implementation of 3D printing technologies. [26] Notably, hydrogels, with their significant water content and three-dimensional network formations, are highly appropriate as ink formulations for the construction of three-dimensional porous matrices. [27] Although significant successes have been achieved in designing single-component hydrogels, the lack of a larger variety of printable and responsive hydrogel systems has been identified as one major drawback that limits the rapid advancement of this field. [28]

In this thesis, naturally occurring and biocompatible polyelectrolytes as well as photo-sensitive moieties are employed to create intricate and responsive hydrogel structures through Digital Light Processing (DLP). The quest to efficiently 3D print hydrogels faces intriguing challenges, especially in understanding and manipulating their viscoelastic properties. This research gap is critical, as these properties are pivotal in material applications. Moreover, this research aims to underscore the vast potential of smart polymers in advancing technology, providing a significant contribution to the field of photo and *pH* responsive polymer science.

2. Theoretical Background

The current chapter briefly introduces the stimuli-responsive (smart) polymer materials, focusing specifically on orthogonal responsiveness, including photo-responsive and *pH*-responsive polymers and hydrogels. Additionally, it explores the architecture of polymer networks and the polymerization methods employed in the research presented in this thesis.

2.1 Smart Polymer Materials

Within the vast realm of polymer science, the advancement of stimuli-responsive polymer materials (smart or intelligent polymers) is one of the most intriguing and innovative areas. These materials have been integrated into various aspects of our everyday life due to their unique ability to change in response to specific environmental stimuli such as- temperature [11, 29, 30], light [31], *pH* [32], electric [33] or magnetic field [16, 34], biomolecules [35, 36] etc. On exposure to external stimuli, such materials tend to change their physical or chemical properties. [37] The design and creation of these materials frequently draw inspiration from nature. [1] They are extensively used in the biomedical sector for applications such as- biosensing [5, 38], controlled drug delivery [3, 39], environmental cleansing [40], and actuating devices [9, 41, 42].

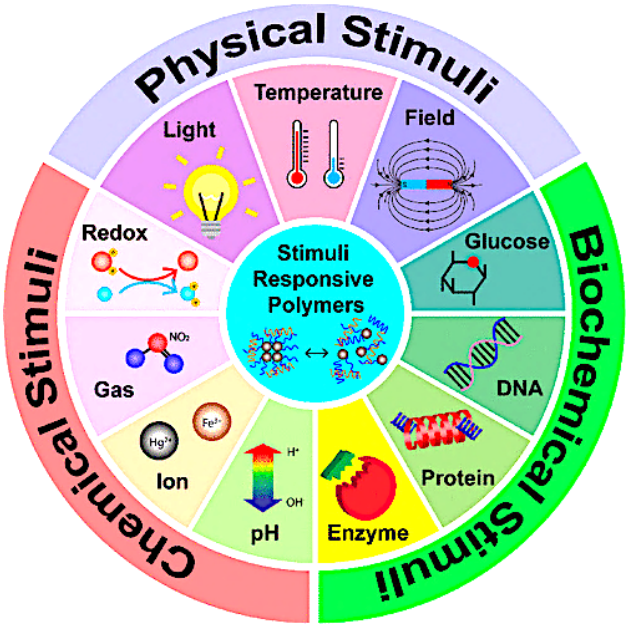

Figure 2.1 Diverse classes of stimuli-responsive polymer materials. Reproduced with permission from reference. [43] Copyright @2021 American Chemical Society.

Over the past decades, a spectrum of polymers, encompassing polymer films, nanoscale architectures, bulk formations, and hydrogels, have been innovatively developed to

demonstrate stimuli-responsiveness. [10] Within solutions, responsive materials are capable of rapid and intricate molecular responses. Conversely, materials in their bulk form permit substantial mechanical property alterations. Gels, an intermediary phase, amalgamate the distinctive features of both solvated and bulk states to offer versatile and tunable responses. Responsiveness originates from the shift of a molecule from one stable state to another, termed bistable molecules or isomers, with each state possessing unique geometrical or chemical features. In certain instances, the activation of the molecular switch is achieved not through a conformational alteration but through a change in its chemical structure detectable at the macro level. Triggered by various environmental stimuli such as temperature, light, electric and/or magnetic fields, chemical agents, mechanical stress, and biological agents, this transition allows for the engineering of actuators and materials at the molecular level, adaptable to the spatial requirements of their intended applications. [8, 44]

Polymers have the remarkable ability to react to a diverse array of stimuli, which are typically grouped into three principal categories: chemical, physical, and biological (**Figure 2.1**). Chemical stimuli encompass factors such as *pH*, ionic states and various chemical compounds, which alter the molecular interactions within polymer chains and between chains and solvents. In contrast, physical stimuli like- temperature, light, electric or magnetic fields, and mechanical stress affect the energy dynamics and molecular interactions at essential threshold points. [45] Additionally, biological stimuli include interactions with biological molecules like enzymes, antigens, or glucose, which can lead to significant alterations in the polymer's structure and function in response to the biological environment. [43]

The tailored responsiveness of smart polymers is a consequence of their unique molecular frameworks, the alignment of the polymer chains, and the characteristics of the integrated active molecules, enabling the polymers to exhibit distinct chemical, physical, and mechanical responses to designated stimuli. [8] Crosslinking these polymers fabricates complex polymer networks with enhanced three-dimensional architecture, amplifying their intelligent functionalities and the breadth of their potential applications. The following section will concisely introduce polymer networks and their various forms.

2.2 Polymer Networks

According to the International Union of Pure and Applied Chemistry (IUPAC), a polymeric network is described as a macromolecule in which each constituent unit is perpetually bonded not only to every other unit but also to the macroscopic phase boundary, ensuring connectivity

throughout the entire structure. [46] The formation of network structures can emerge from the formation of covalent bonds, ionic interactions, or the presence of physical forces such as Van der Waals forces and hydrogen bonds. [47]

Polymer networks are structurally characterized by the presence of network junctions, also known as crosslinks. These are bonds connecting one polymer strand to another. Each junction typically radiates three or more groups from a central point, linked by branch functionality strands. These strands may consist of linear polymer chains, flexible short molecules, or rigid struts/linkers. Based on the nature of junctions and strands, polymer networks are typically categorized into two types: "physical" (supramolecular) networks, which are formed by non-covalent interactions, and "chemical" (covalent) networks, where the connections are covalent bonds. [48]

2.2.1 Interpenetrating Polymer Networks

Within the diverse array of polymer-based matrices, the interpenetrating polymer networks (IPNs) and semi-IPNs distinguish themselves with their extraordinary versatility in terms of composition and their physicochemical characteristics. IPNs first emerged in 1914 with Aylsworth's pioneering work in creating synthetic IPNs for phonograph record production. [49] However, it wasn't until the 1950s and early 1960s that the scientific community began to take a keen interest in these intricate structures. Millar conducted groundbreaking research on their properties and formally introduced the term “Interpenetrating Polymer Network”. [50] According to IUPAC, an Interpenetrating Polymer Network (IPN) can be defined as “A polymer comprising two or more networks which are at least partially interlaced on a molecular scale but not covalently bonded to each other and cannot be separated unless chemical bonds are broken.” [46]

IPNs stand out from polymer blends, graft copolymers, and block copolymers due to their unique molecular interlacing of two or more non-covalently bonded polymers, unlike the simple mixtures in polymer blends (**Figure 2.2**). Unlike graft copolymers with chemically grafted branches and block copolymers with covalently bonded segments, IPNs maintain the individual network structures of each polymer. This molecular interplay in IPNs often results in superior properties like enhanced mechanical strength and thermal stability, which are not achievable in standard polymer blends, graft, or block copolymers. [51] Based on the chemical preparation of IPN hydrogels, they can be broadly divided into two categories. Firstly, simultaneous IPNs are created when both network precursors are combined and simultaneously

synthesized through distinct, non-conflicting processes such as chain and stepwise polymerization. In contrast, sequential IPNs are produced by immersing an already-formed single-network hydrogel in a solution that contains a monomer, initiator and optionally a crosslinker. The presence of a crosslinker leads to the formation of a fully interpenetrating network, whereas its absence results in a network containing linear polymers interwoven within the initial network, known as a semi-IPN. [52, 53]

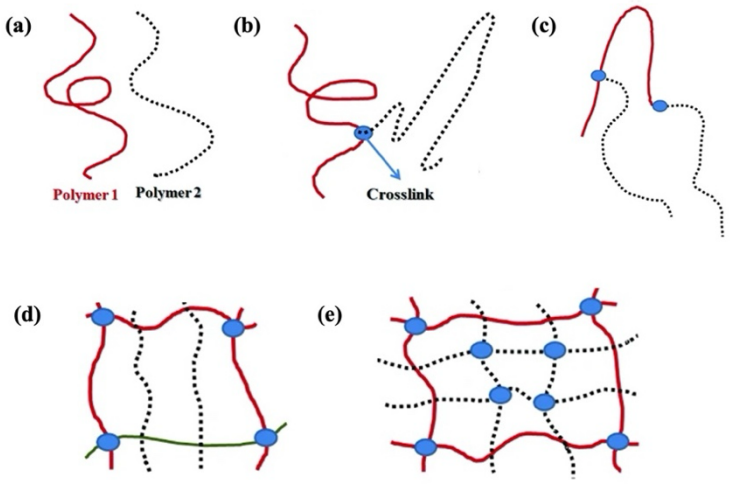

Figure 2.2 Schematic representations of (a) mechanical blends, (b) graft copolymers, (c) block copolymers, (d) semi-IPN, and (e) full IPN. Reproduced with permission from reference. [51] Copyright @2012 Springer Nature Switzerland AG.

2.2.2 Supramolecular Polymer Networks

Supramolecular Polymer Networks (SPNs) are composed of macromolecules that are linked by reversible, non-covalent supramolecular interactions, encompassing hydrogen bonds, coordination bonds involving metals, interactions based on hydrophobicity, and electrostatic attractions. [54] The outstanding properties of SPNs have made them increasingly popular in the field of smart materials innovation, particularly in the production of tough hydrogels and elastomers. [55-57] Within these networks, numerous non-covalent bonds act as sacrificial elements, dissociating prior to the rupture of the material's covalent backbone. [58] The reversible reformation of these dynamic bonds elevates the energy threshold required to fracture the material, thereby providing an effective means of enhancing toughness. [59]

The reversible nature of supramolecular interactions in SPNs enables these materials to demonstrate extraordinary properties, including self-healing, responsiveness to stimuli, adaptability, and the ability to be reprocessed. [60, 61] Moreover, the type of noncovalent

interactions and the architecture of the employed building blocks are key determinants of the materials' sensitivity to environmental changes. Thus, the careful selection and combination of these noncovalent interactions and building blocks enable the precise fabrication of responsive supramolecular polymeric materials. [60] Despite ongoing investigations, the field of SPNs remains largely in a preliminary phase, underscoring the necessity for the development of SPNs with innovative architectures and/or improved characteristics.

2.2.3 Hydrogels

Hydrogels are three-dimensional, hydrophilic, polymeric networks capable of imbibing large quantities of water or biological fluids. They consist of crosslinked polymers, which can be either naturally derived or synthetic, forming a matrix that swells in aqueous environments while maintaining distinct structural integrity (**Figure 2.3**). [62] They are characterized by their extensively porous architecture and a pliable surface, closely mimicking the properties of natural living tissues. Hydrogels that are able to respond to various stimuli, including temperature, pressure, *pH* levels, and electric and magnetic fields, are aptly categorized as intelligent or 'smart' materials. [63]

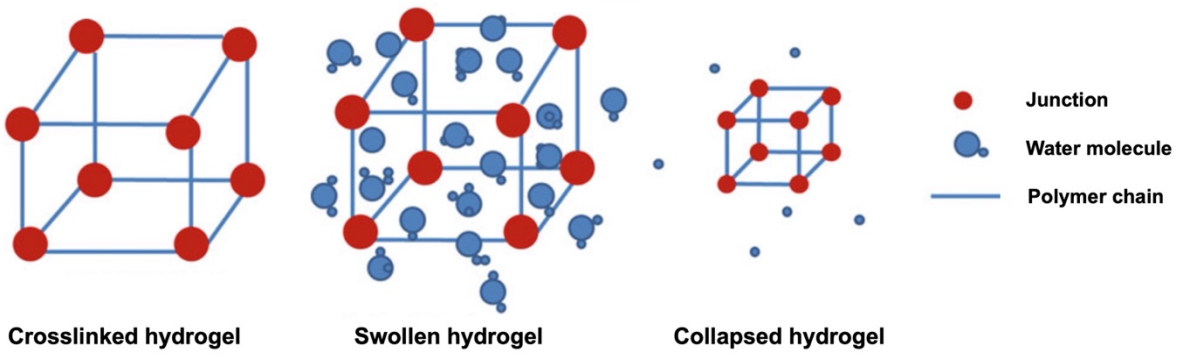

Figure 2.3 Diagrammatic illustration of hydrogel architecture and swelling behavior Reproduced with permission from reference. [51] Copyright @2012 Springer Nature Switzerland AG.

Hydrogels have emerged as highly adaptable materials utilized across a broad spectrum of fields such as- drug delivery [39, 64, 65] and tissue engineering [66, 67], as well as in the creation of smart actuators [6, 67], flexible electronic devices [68], sensors [5], functional coatings [69], and water harvesting systems [70]. The diverse applications of these materials arise from their distinctive properties, including their tunable mechanical features, their responsive nature, biocompatibility, their unique viscoelasticity, inherent moisture content, and their proficiency in facilitating mass transport. [71] Hydrogels can be divided into two main categories:

"chemical" or "permanent" hydrogels, which are bound by covalent crosslinks, and "physical" or "reversible" hydrogels, which rely on physical interactions like ionic bonds, van der Waals forces, hydrogen bonding, and physical entanglements for stability. [72] A particularly interesting type of physical hydrogel is the polyelectrolyte complex hydrogel, which is a product of ionic interactions between polyelectrolytes (PEs) carrying opposite charges, which are discussed in detail later in **Section 2.5.2.**

The transition to the forthcoming chapter marks a shift in focus from the static properties of polymer networks to the dynamic behaviors exhibited by polymers under various stimuli. Subsequent sections provide a comprehensive examination of the integration of various responsive behaviors within polymeric matrices.

2.3 Types of Responsiveness

The incorporation of various stimuli-responsive groups into a polymer can enhance or refine the polymer’s response to external stimuli. The interaction of multiple stimuli-responsive groups can manifest in parallel, serial, or causal manners. As studies have shown over time, examples exist for each type.

Orthogonal/ Parallel Responsiveness:

Specifically, "parallel" implies that one chemical group's response doesn't interfere with another's, defining it as an orthogonal system. [10] Integrating multiple interactions or responsiveness often results in enhanced properties. [73] One such example of an orthogonal responsive system is a copolymer created from poly(*N*-isopropylacrylamide) (PNIPAM) and fulgimide that shows a remarkable dual-responsive behavior. [74] PNIPAM, widely recognized for its temperature-sensitive nature, consistently exhibits a lower critical solution temperature (LCST) in water. In contrast, fulgimides are characterized by their light-induced photochromic features. Notably, the LCST of PNIPAM remains constant even after light exposure, suggesting that the photochromic transition in fulgimides is distinct from PNIPAM's thermal response. This indicates a system that is responsive to multiple, independent stimuli.

Serial Responsiveness:

A serial responsive system refers to a system where the response or behavior of one component is directly influenced or amplified by the response of another component in a sequential manner. [10, 75] One notable example is seen in acrylamide copolymers composed of PNIPAM

and TEMPO moieties (4-*N*-amino-2,2,6,6-tetramethylpiperidin-1-oxyl-4-yl). These polymers demonstrate a considerable increase in the LCST of PNIPAM in a statistical copolymer by merely oxidizing and reducing the TEMPO groups, known for their redox-active properties. [76]

Casual Responsiveness:

When a casual responsive system encounters an external stimulus, the respective responsive group within the polymer is activated, leading to changes such as- a structural evolution at the molecular level or a broader environmental transition within the polymer matrix, shifting from hydrophilic to hydrophobic states. This causes the activation of a second responsive group, which reacts in its own distinct manner, contrasting to the first group's behavior. [10] Iwai et al. developed one such system involving a copolymer, composed of *N,N*-dimethylaminopropylacrylamide, *N*-*t*-butylacrylamide, and a benzofurazan-based compound, with the latter being integrated into the main structure via an ester linkage. [77] The benzofurazan part of this copolymer changes its fluorescence in response to environmental changes. This copolymer uniquely changes its fluorescence under different conditions. When heated, it becomes more hydrophobic, causing the benzofurazan part to fluoresce at a different wavelength, showcasing the casual interplay of responsiveness. [77]

Inspired by these instances, we can envision that incorporating various stimulus-responsive groups into a single polymer could result in a stronger or more nuanced reaction to external stimuli. Therefore, carefully selecting the right responsive elements could enable the creation of a versatile polymer that shows diverse behaviors in response to one or more external triggers. Moreover, out of the multitude of stimuli responsiveness, light and *pH* has gained particular interest, especially in the field of materials and biomedical research. Light, with its ability to be precisely controlled in terms of intensity, wavelength, duration, and location, offers a unique tool for manipulating materials and biological systems in real-time. [78] This has led to groundbreaking developments in photodynamic therapy for cancer treatment, where light-sensitive drugs are activated at the tumor site, minimizing damage to healthy tissues. [79-81] On the other hand, *pH* responsiveness taps into the subtle but critical variations in acidity or alkalinity that occur in different parts of the body or in various environmental conditions. This sensitivity has been ingeniously exploited in drug delivery systems, where capsules or nanoparticles are designed to release their payload only when they encounter the specific *pH* of a target tissue, like the acidic environment of a tumor or an inflamed tissue, thereby

enhancing the efficacy and reducing side effects of therapeutic agents. [32, 82] These two fields, often intersecting, are paving the way for fabricating tailorable "smart" functional materials and biomedical devices. Accordingly, the following sections will provide a detailed discussion on the photo-responsive and *pH*-responsive polymer materials.

2.4 Photo-Responsive Polymer Materials

Photo-responsiveness gains its attractiveness from the essential benefits that light as a stimulus brings. Light, being non-invasive, can be precisely controlled in space and time, along with the possibility of external activation. [83] Furthermore, the photochemical processes it initiates generally do not require the addition of reagents and tend to have limited by-products. The ability to finely tune irradiation parameters like light intensity, wavelength, and exposure time also adds to its suitability for different systems. [78] Owing to these properties, photo-responsive polymer (PRP) materials have been used for a variety of applications, including soft-actuators [84, 85], photo-electric films [86], optical devices [87, 88], biomedicine [89], sensors [90], smart coatings and information storage [91].

Upon exposure to light, PRPs demonstrate the ability to precisely alter their physical or chemical properties. Typically, they incorporate chromophoric groups like- spiropyran (SP) [20, 21], azobenzene (Azo) [18, 19] or stilbene [92, 93], which experience structural changes at the molecular level under light. [93] Embedding these groups into polymers leads to conformational changes in or at the polymer chains, thereby altering the polymer's physical and chemical properties through mechanisms such as photo-isomerization and light-driven expansion or contraction. [94, 95]

In 1866, Fritzsche first introduced photochromism, describing it as a phenomenon triggered by light. [96] Photochromism is characterized by the reversible conversion of a chemical species between two isomeric states, triggered by light absorption, leading to a shift in absorption spectra. The mechanisms encompass a range of reactions such as pericyclic changes, *cis-trans* isomerizations, breaking of molecular bonds, internal transfers of hydrogen or functional groups, and electron movements involving oxidation and reduction processes. [17] Besides altering their color, these transformations also bring about changes in the physical and chemical characteristics of the species, including modifications in the dipole moment, refractive index, and geometric structure. These dynamic changes are pivotal as they can concurrently modify the optical, chemical, electrical, and aggregate properties of the encompassing system. Photochromic molecules, therefore, hold a central role in photo-responsive systems, adept at

capturing optical signals and translating them into advantageous changes in properties through their isomerization. [17, 95]

Photo-responsive polymers are invariably composed of photo-responsive units and a bulk polymer matrix. Here, our primary focus is on the photo-responsive units, which can be categorised into two types: reversible and irreversible. Reversible units, exemplified by Azo and SP, are capable of undergoing cyclic isomerization between their isomers when exposed to certain light wavelengths. In contrast, the irreversible units, like *o*-nitrobenzyl and coumarinyl, are characterized by a one-time photo-induced bond disruption (**Figure 2.4**). [89]

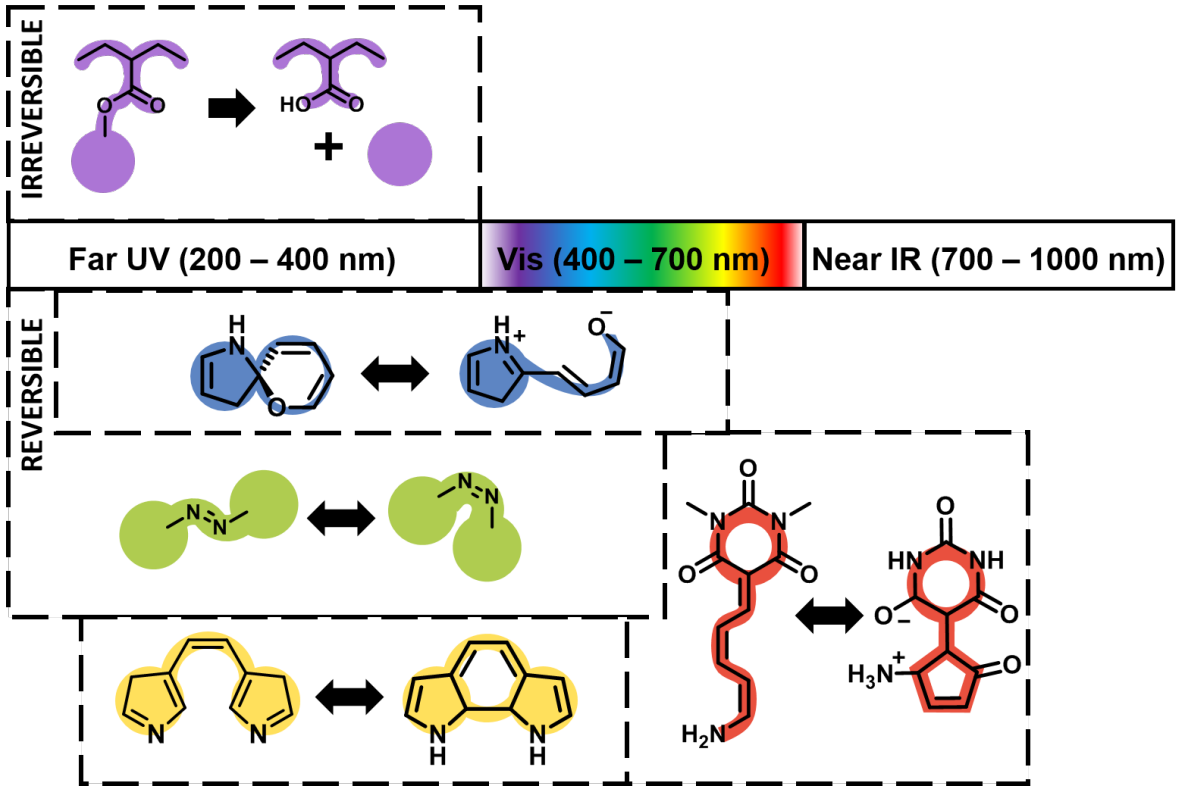

Figure 2.4 Graphical representation showing reversible and irreversible photo-induced responses. Reproduced with permission from reference [97]. Copyright@2017 MDPI, Basel, Switzerland.

Reversible Systems:

Typically, reversible units exhibit two primary isomerization mechanisms: one is the *cis-trans* isomerization, which occurs without any bond cleavage, such as in Azo, and the other is a dissociation mechanism involving bond cleavage, as seen in SP. [98] The Azo group switches between its planar *trans* configuration to its angular *cis* configuration through light-triggered rearrangement. [99] On the other hand, exposure to UV light triggers an electrocyclic ring-opening reaction in spiropyran or spirooxazine, leading to the conversion of the spiro form into

an open, planar merocyanine structure. This newly formed structure possesses an extended conjugated system, which exhibits strong absorption in the visible spectrum. Besides, the interaction of diarylethenes and fulgides with UV light triggers the closure of their intrinsic six-membered rings, forming colored isomers that are resistant to thermal reversal. This phenomenon of photochromic transition between different isomeric states at different wavelengths is often referred to as 'switching'. [17] Such reversible photochromic systems offer the versatility of alternating between two photo-stationary states, making them ideal for use as switches in applications ranging from artificial muscles to actuators.

Irreversible Systems:

Whereas, the irreversible units essential in the fabrication of PRPs include *o*-nitrobenzyl (*o*-NB), coumarinyl, pyrenylmethyl and 2-diazo-1,2-naphthoquinone. The photocleavage of chemical bond in these chromophores, exposes the carboxyl groups on the surface of the PRP materials, hence switching the wettability of the surface from hydrophobic to hydrophillic. [89] The photolytic cleavage of *o*-nitrobenzyl moieties can be triggered by either one-photon UV (365 nm) or two-photon near-infrared (700 nm) absorption and leads to the detachment of the chromophore from the polymer. [78] However, protonic solvent is needed for the UV-induced photolysis reaction in pyrenylmethyl moieties. In case of coumarinyl moieties, exposure to UV causes variations in chemical structure as well as properties like-fluorescence, absorbance spectra and reactivity. [100] Conversely, in 2-diazo-1,2-naphthoquinone (DNQ), photolysis initiates a Wolff rearrangement. The exposure to light causes the decomposition of diazo group, resulting in the formation of a reactive ketene. Such a reaction plays a crucial role in the field of photoresist technology within semiconductor manufacturing, as it facilitates the creation of patterns on substrate surfaces. [89]

SP, Azo and *o*-NB, serving as photo-sensitive groups, place polymers containing them at the forefront of photo-responsive polymer research. Therefore, a more detailed examination of these compounds is discussed in the subsequent sections.

2.4.1 Spiropyran-based Photo-responsive Systems

SP-based photochromic molecules stand out as one of the leading types of photo-switchable materials, boasting advantages like synthetic flexibility and a high isomerization yield triggered by various stimuli such as light, temperature, mechanical force, and *pH* changes. [101] Fischer and Hirshberg were the pioneers in discovering the photochromic behavior and associated color

shifts of spiropyran (SP) when exposed to visible and near UV light in 1952. [102] SP is highly adaptable, offering a wide range of functionalities that include temperature-induced color changes (thermochromism), solvent-dependent color changes (solvatochromism), pressure-induced color changes (mechanochromism), electron transfer properties (redox-properties), reaction to acid-induced color changes (acidochromism), and *pH*-responsive isomerization. [101, 103] Multifunctional SP compounds have been instrumental in creating functional materials that respond to various stimuli. These materials include versatile porous films [104] that react to multiple conditions and self-assembled polymeric nanoparticles [105] that can regulate the release of encapsulated molecules. Moreover, their functional attributes can be finely adjusted through chemical modifications or by altering the surrounding environmental conditions. [106]

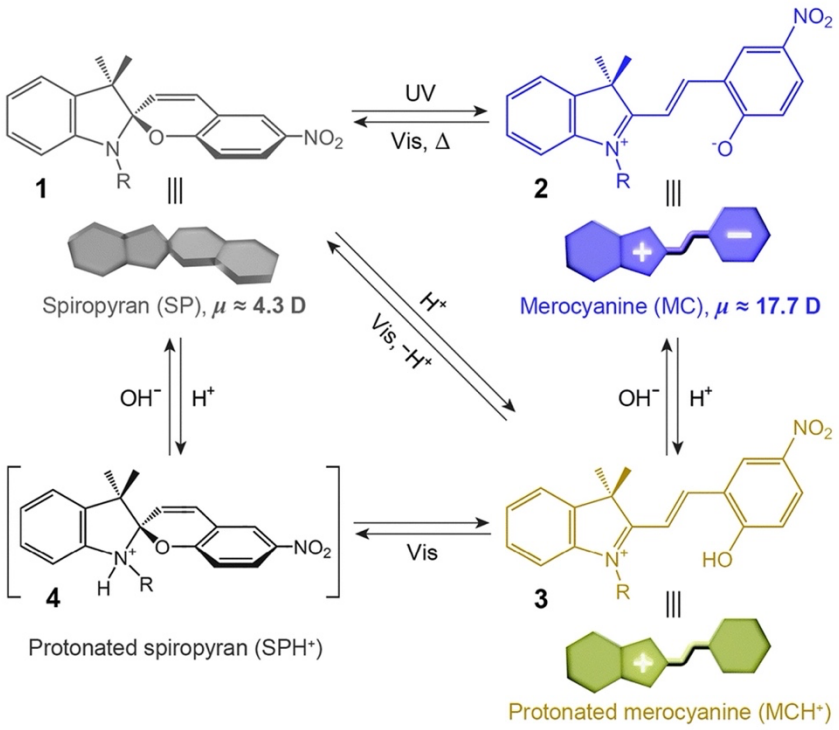

Figure 2.5 Depiction of reversible photochromic and acidochromic transitions in SP amongst four distinct states. Reproduced with permission from reference [20]. Copyright @2014 Royal Society of Chemistry.

2.4.1.1 Photochromism in SP

Upon exposure to UV light, SP undergoes photo-isomerisation from a neutral closed form to an open merocyanine (MR) form, is zwitterionic. This switch is reversible, with the MR form reverting back to spiropyran under visible light or heat. The SP structure features a benzopyran ring connected to an indoline group, which is orthogonally linked to the spiro carbon (as shown

in **Figure 2.5**). In contrast, the MR form allows for an extended configuration of the π electrons across both rings. The change to MR not only reshapes the molecule but also significantly increases its polarity due to the new electric charges formed under irradiation. [107]

These dynamic molecules represent a significant category of smart or stimuli-responsive materials, capable of reacting to light exposure by breaking the C–O spiro bond and reversibly transitioning between SP with a dipole moment of 4–6 D and merocyanine (MR), with a dipole moment of 14–18 D isomers. [108] There are pronounced differences in the properties of two isomers, including structural properties, color, dipole moment, absorption spectra, fluorescence and stability. The SP isomer exhibits optical transparency in the visible spectrum, while the MC isomer has a strong absorption peak at λ_{max} = 550–600 nm, resulting in a deep blue or violet appearance. SP and MR also show significant differences in their emission properties: the SP isomer lacks strong emission, but upon ring-opening, an intense emission band emerges at $\lambda_{max} \approx$ 650 nm. On exposure to UV, the photochromic SP molecules in solution exhibit a color change, which diminishes rapidly once the UV irradiation ceases. Conversely, in the solid state, the limited scope for structural rearrangements within these photochromic compounds results in a reduced rate of photo-isomerization. [101] Additionally, the zwitterionic MR molecules have a tendency to cluster together, forming various types of molecular aggregates. [107] These significant shifts in its properties enable the precise manipulation of molecular behaviors through external triggers, paving the way for innovative photo-switchable devices.

When subjected to UV light (λ = 365 nm), the closed-ring isomer of SP undergoes a transition to the open-ring isomer (MR) through a first-order process, which has been studied extensively, as shown in **Figure 2.6** [20, 109]. The conversion starts with the breakage of C_{spiro}– O bond, resulting in the formation of *cis*-MR. This is followed by a rotation around the central C– C bond in *cis*-MR, which ultimately yields *trans*-MR. The ring-opening reaction of the molecule can be depicted in two ways: heterocyclic C– O bond cleavage or a 6π-electrocyclic ring opening. These processes lead to the formation of zwitterionic (7) and quinoidal (8) resonance structures, respectively. [110] The resultant MR structure represents a hybrid of these structures. The planar configuration of MR, coupled with the extended π-conjugation connecting its indoline and chromene components, results in a distinct delocalized transition, evident in the λ = 550–600 nm range, particularly in most non-polar solvents. The exact position of the absorption band is influenced by the relative dominance of the two resonance forms. In non-polar solvents, which tend to stabilize the quinoidal form, the energy difference between the

ground and excited states of MR narrows, leading to a bathochromic shift of its absorption band, a phenomenon known as 'negative solvatochromism' of MR. [20]

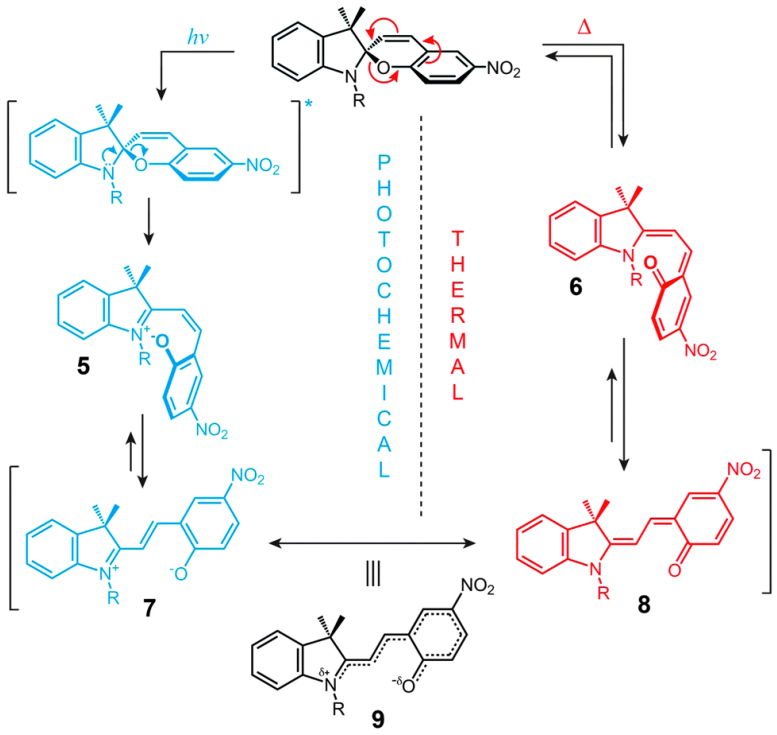

Figure 2.6 Schematic representation of spiropyran isomerization dynamics: photo-induced and thermal pathways. Reproduced with permission from reference [20]**.** Copyright @2014 Royal Society of Chemistry.

Additionally, the isomerization kinetics of photochromic SP to zwitterionic MR are determined by the nature of the substituent groups on the benzopyran ring and the environmental medium. Introducing electron-withdrawing groups at the para position of the benzopyran ring in SP aids in the delocalization and stabilization of the negative charge on the benzopyran oxygen, which allows for the detection of the open-ring MR isomer through UV/Vis spectroscopy. Whereas, the presence of weak electron-withdrawing substituents or hydrogen results in the MR isomer being undetectable, except by employing ultrafast spectroscopy. [101] The environment surrounding the molecules, such as the presence of polymer chains, can facilitate the stabilization of the zwitterionic MR form through either dipolar or ionic interactions. This stabilization is so effective that the transformation from SP to MR can spontaneously occur under normal ambient conditions, or even without light exposure. However, the process of reverting from MR back to SP typically demands a greater consumption of energy. [101]

The photo-stationary state (PSS) of SP mainly consists a mixture of the energetically lower spiro (closed) form and the more stable transoid MR (open) structure. The commencement of

the photochemical reaction is commonly attributed to the dissociation of the C_{spiro}–O bond when the molecule is in an excited electronic state. The activation of SP to its excited SP* state results in diminishing the double bond properties via a typical π-π* transition, which subsequently raises its energy level as a direct consequence of the change in hybridization. [103]

2.4.1.2 Synthesis of SP

SP mechanophores are typically synthesized through a reaction between salicylaldehyde and indole. [111] The method reported by Raymo and Giordani is commonly used for the synthesis of polymerizable SP derivatives (**Scheme 2.1**). [94, 112] Moreover, methacrylated SP derivative (SpMA) monomer is commonly utilized as a monomer for the incorporation of SP as a polymer, expanding its application significantly in materials science, particularly in smart materials.

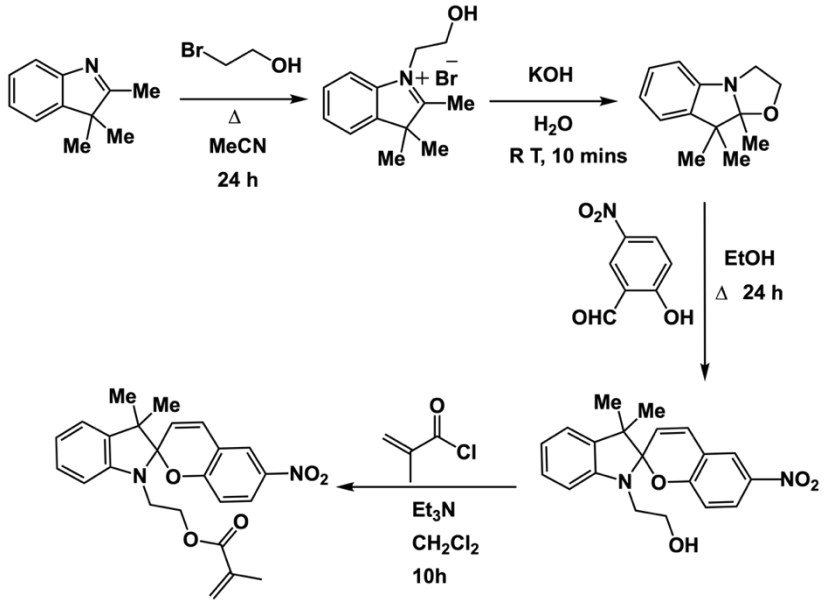

Scheme 2.1 Synthesis of SP derivatives. Reproduced with permission from reference [94]. Copyright @2023 Wiley-VCH GmbH.

2.4.1.3 SP-based Polymers

Typically, the integration of SP units into polymer matrices is achieved through the polymerization of modified SP monomers or by copolymerizing these monomers with other compatible units. During this process, the SP group can be added either as a side chain or as a component of the primary polymer chain. [113] Alternative approaches include embedding SP derivatives into diverse polymer matrices via non-covalent doping or entrapment, or by grafting onto pre-formed polymer chains. [114] The grafting-on method has been employed to

introduce functionality to a range of polymers, such as polytetrafluoroethylene, polyaniline, polyacrylates, polysulfones, polyphosphazenes, and Pluronic®.

For the synthesis of homopolymers, the most common approach includes Ring-opening metathesis polymerization (ROMP). [115, 116] In contrast, the synthesis of random copolymers is commonly achieved by initiating free radical polymerization (FRP) with azobisisobutyronitrile (AIBN), employing terminal alkenes [117, 118], frequently methacrylates, or through polycondensation reactions. [119, 120] In contrast, block copolymers are effectively produced using controlled polymerization methods like atom transfer radical polymerization (ATRP) [121] and reversible addition-fragmentation transfer (RAFT) polymerization [122]. These precise techniques are also applicable for surface modification with spiropyran polymers, by pre-functionalizing the solid surfaces with polymerization initiators. [123, 124]

2.4.2 Azobenzene-based Photo-responsive System

Nearly two centuries ago, Mitscherlich pioneered the synthesis of Azo, quickly followed by the creation of the first azo dye, aniline yellow, in 1861, marking a significant shift towards synthetic dyes over natural pigments. [125, 126] Since then, the field of Azo has witnessed continual growth, diversifying in synthesis techniques and applications. Initially, Azo compounds were solely explored for dye manufacturing, with a focus on developing light-stable, cost-effective dyes. [99] A significant milestone was reached in 1937 when Hartley reported the photo-isomerization of Azo from its *E* form to the *Z* form, along with the isolation and analysis of the *Z* isomer. [127] The Azo derivatives have advanced beyond their original use as simple dyes, emerging as sophisticated molecules instrumental in manipulating the attributes of diverse materials, including but not limited to biomacromolecules [128] and polymers. [129]

2.4.2.1 Photochromism in Azobenzene

The molecular structure of Azo is distinguished by two phenyl rings linked via an azo bond (–N=N–). This molecule can adopt either a *trans* or *cis* isomeric state, with the *trans* isomer (*Z*-form) being thermodynamically favored and characterized by a rigid, planar configuration (**Figure 2.7**). In contrast, the *cis* isomer (*E*-form), which is less stable, features the phenyl rings at an angle close to 90°. [18] With an energy advantage of 10–12 kcal/mol over the *cis* isomer, the *trans* form of Azo is substantially more stable. The reason for this can be attributed to the absence of delocalization and the distorted structure of the *cis*-form, as opposed to the more orderly arrangement found in the *trans*-isomer. [130] As a consequence, the *trans* isomer is found

to be the dominant isomer, approximately 99.99%, in dark equilibrium conditions. Irradiating it with the UV light of ~ 340 nm can significantly generate the *cis* isomer. While the *trans* isomer maintains a dipole moment of zero, the *cis* isomer which has its phenyl rings angled at ~ 55° from the plane of the Azo group, exhibits a dipole moment of 3 D. [128]

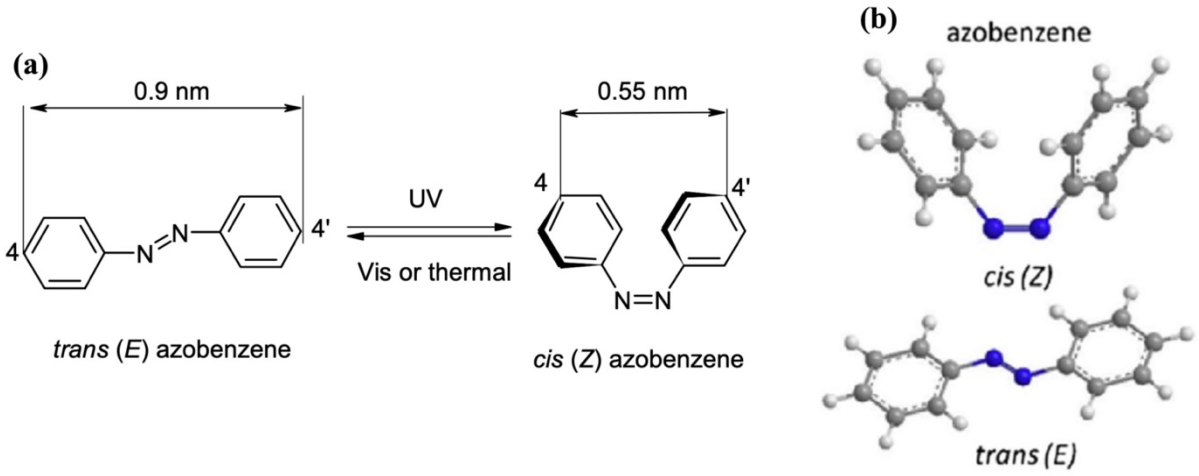

Figure 2.7 (a) Reversible photo-isomerism in azobenzene, (b) structural models of *cis* and *trans* isomers of azobenzene. Reproduced with permission from reference [131]. Copyright @2018 Springer Nature.

The ultraviolet-visible absorption spectrum of *trans*-Azo is characterized by two principal absorption bands. The first, in the visible range at roughly 440 nm represents an n–π* transition (S_1) that is symmetry-forbidden, reflected by a lower intensity. The second, a highly intense band located at around 320 nm corresponds to a symmetry-permitted π–π* transition (S_2). [99] Whereas, in *cis*-Azo, the π–π* electronic transition's absorption band experiences a hypsochromic shift and shows a notable reduction in intensity compared to the *trans*-isomer. In contrast, the n–π* electronic transition band (ranging from 380 to 520 nm) is permitted in the *cis* form, leading to a substantial increase in its intensity. [130]

Furthermore, Rau categorized Azo into three distinct classifications based on the energy levels of their n–π* and π–π* transitions: these are the Azo type, the amino-Azo type, and the pseudo-stilbene type (**Figure 2.8 (a)**). The introduction of the electron-donating substituents like hydroxy or amino groups at the para position of Azo leads to bathochromic shift in the absorption peak of the π–π* band without altering the n–π* band, resulting in a reduced separation between them, indicative of the amino-Azo type. Conversely, appending strong electron-accepting substituents, like cyano or nitro groups, to the 4′ position of 4-aminobenzene creates pseudo-stilbene-type Azo. [99]

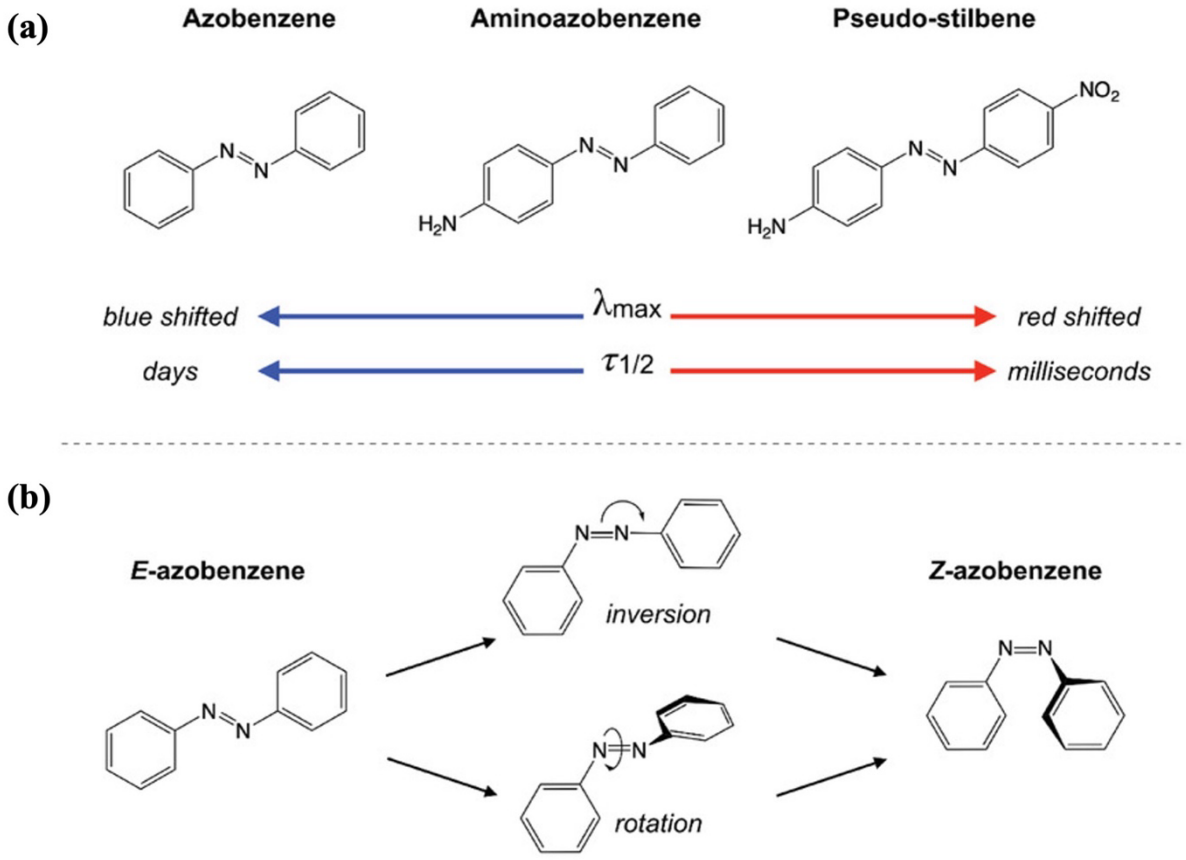

Figure 2.8 (a) Categorization of azobenzene into three types as per Rau's classification, including differences in the absorption peak (λ_{max}) of the *E*-form and the room temperature half-life ($\tau_{1/2}$) of the *Z*-form, (b) Depiction of the rotation and inversion pathways in the *E* to *Z* isomerization process of azobenzene. Reproduced with permission from reference [132]. Copyright @2019 Wiley-VCH Verlag GmbH.

The distinct spectroscopic properties of *cis* and *trans* isomers and the distribution of their excited state electronic levels facilitate isomerization upon light exposure. This process generally leads to a photo-stationary state (PSS) that contains varying amounts of both *cis* and *trans* isomers. The composition of this mixture varies based on the modifications to the Azo core and the irradiation wavelength. [130]

In E- Azo, the ground singlet state is referred as S_0, while the subsequent first and second excited states are designated as S_1 (n–π*) and S_2 (π–π*). The transition of Azo from E to Z configuration can be triggered by exciting the molecule from S_0 to S_1 or from S_0 to S_2. In Azo, excitation to the S_1 state initiates C-N=N-C rotation, reaching the lowest point on the S_1 potential energy surface, assuming no interference from substituents. A conical intersection that is geometrically and energetically close to this state, usually higher by just 1–2 kcal/mol,

facilitates the transfer to the ground state, resulting in photo-isomerization. Excitation to the S_2 state often leads to a similar rotational path due to a degenerate energy region, although different paths can return the molecule to its initial state. These variations in photo-isomerization pathways contribute to differences in quantum yield, dependent on the excited state achieved and the allowable geometries. [133]

Numerous studies have investigated the isomerization pathways of Azo, revealing that the process is influenced by the substituents on the aromatic rings and other factors, leading to a multifaceted mechanism. [130, 134, 135] Typically, two fundamental mechanisms are proposed for the isomerization process in Azo derivatives: the expansion of the Ph-N=N angle within the molecular plane (known as the inversion mechanism), and the molecular rotation around the N=N bond (referred to as the rotation mechanism), as depicted in **Figure 2.8 (b)**. Although there remains a discrepancy in the mechanistic specifics across various Azo derivatives, the pivotal attribute of Azo photochromism lies in the light-triggered isomerization reaction, which is notably efficient and resistant to degradation, occurring with high quantum efficiency and negligible decomposition. [132] Interestingly, recent studies have identified novel azo derivatives, specifically those incorporating tetra-*ortho*-methoxy and tetra-*ortho*-chloro groups, which exhibit the ability to transition from trans to cis configurations under the influence of visible light. This trans-to-cis isomerization, driven by visible light opens up new avenues for research and applications in the field of photo-induced biomedical technology.[136]

2.4.2.2 Synthesis of Azobenzene

Griess, a Victorian brewer, pioneered a widely utilized synthesis approach for Azo, which involves the diazotization of aromatic amines and their subsequent coupling with electron-rich aromatic nucleophiles like aromatic amines or phenols. [137] Subsequent developments have led to alternative methods (**Scheme 2.2**). For instance, the Mills reaction [138] is the reaction of aromatic nitroso derivatives with anilines in glacial acetic acid. The synthesis of symmetrical Azo often employs the reductive coupling of aromatic nitro derivatives, utilizing reducing agents such as $LiAlH_4$, Zn/NaOH, $NaBH_4$, KOH, and Bi. [139] Alternatively, anilines can be oxidized using oxidants such as sodium perborate/acetic acid, H_2O_2/Na_2WO_4, AgO, Ag_2O, or Ag_2CO_3. [140] The Wallach reaction transforms Azo into 4-hydroxy or sometimes 2-hydroxy Azo derivatives in the presence of a strong acid. [141] While numerous methods have been reported for generating a variety of Azo derivatives, diazotization remains the most favored

and primary synthesis technique for Azo derivatives, owing to its straightforward process and aqueous medium application. [99]

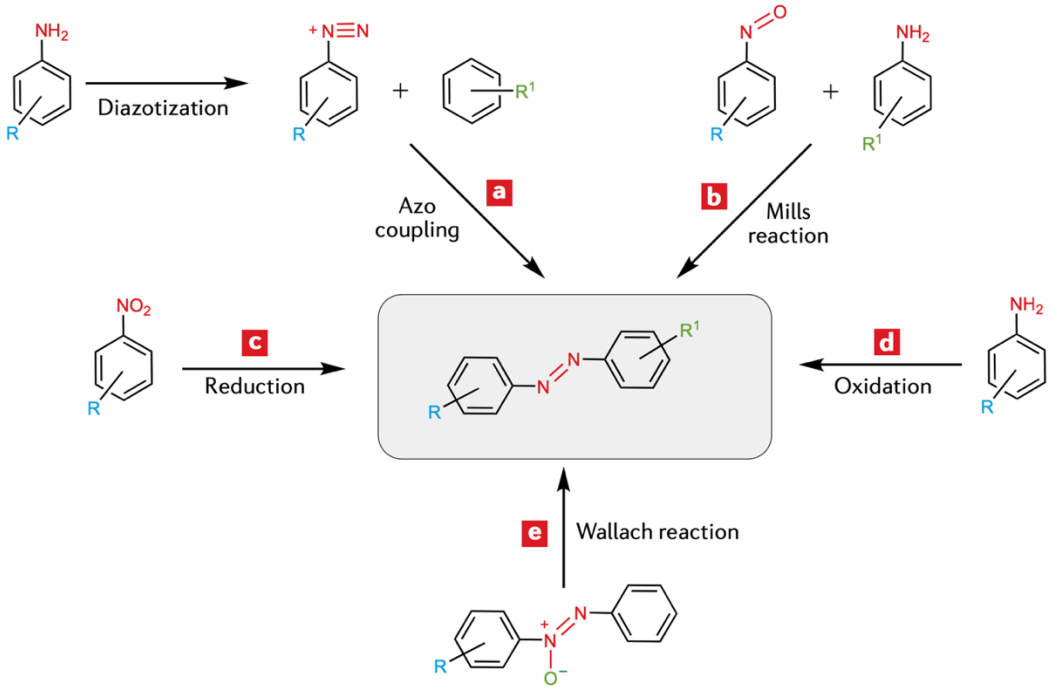

Scheme 2.2 Synthetic routes for preparation of azobenzenes. Reproduced with permission from reference [99]. Copyright @2021 MDPI, Springer Nature Limited.

2.4.2.3 Azo-based Polymers:

Azo-containing polymers, known as Azo-polymers, blend the photo-switchable characteristics of Azo with excellent mechanical properties and ease of processing, establishing themselves as photo-responsive materials. [142] Over the years, these Azo-polymers have been the focus of extensive fundamental research in the past. The complex and advanced structures of Azo-polymers, as opposed to the simpler Azo molecules, open up a wide array of possibilities for crafting innovative materials. These have been utilized in numerous fields, ranging from information storage [143], photonics [144], actuators [19, 145, 146], drug delivery [147], lithography [148] and the storage of solar energy [149, 150].

For the fabrication of photo-responsive materials, a diverse array of Azo-polymers have been synthesized in the literature, encompassing structures like homopolymers, random copolymers, block copolymers, and Azo-terminated polymers. [142] Azo functional groups are usually integrated into the polymer's main chain or more commonly attached to the backbone as side-chain pendant groups, either directly or through a spacer group. Azo-polymers are commonly synthesized using two methods: (a) through the polymerization and copolymerization of

monomers already containing Azo functional groups, and (b) by chemically modifying a precursor polymer to incorporate the Azo functional groups post-polymerization. [19] The homopolymers and copolymers with comparatively simple structures are synthesized using standard addition and condensation polymerizations. Moreover, for the synthesis of block or graft polymers and Azo-polymers with narrow dispersity, controlled radical polymerization is utilized. [99] Additionally, the Azo content within Azo-polymers is a key determinant for their photo-responsive qualities and practical applications. The innovative approach of triggering an isolated chromophore on a polymer backbone to extend its influence has pioneered novel and vibrant research directions in polymer science. [151]

Azo -based Hydrogels:

The incorporation of Azo into the fabrication of photo-responsive hydrogels has garnered significant interest in recent years. In the past several decades, the development of hydrogels has transitioned from static bulk materials to smart materials that are sensitive to changes in their surroundings. [83, 152]

Photo-responsive hydrogels are notable for their substantial water retention, exceptional pliability, and compatibility with biological tissues. Furthermore, they possess the unique ability to perform a variety of mechanical responses when subjected to light stimuli with precise spatial and temporal control. [153] Upon light irradiation, changes in their physical and chemical properties such as- viscosity, shape, elasticity and degree of swelling can be observed. This functionality positions them as highly promising materials for use in biomedical engineering and underwater bionics technologies. [154]

2.4.2.4 Azo and Cyclodextrin Inclusion Complex

Azo demonstrates an affinity for binding with the hydrophobic cavity in cyclodextrin (CD), leading to a noncovalent guest-host interaction. This interaction is reversible and gets easily disrupted when Azo converts to its *cis* isomer under UV light. [155] This phenomenon has been harnessed to create supramolecular hydrogels with the ability to switch from gel to sol phases under light. Additionally, this dynamic linkage offers a method for controlled ligand presentation, crucial for influencing biological events such as cell adhesion.

CDs are a group of cyclic oligosaccharides produced through the enzymatic breakdown of starch and are made up of α-(1,4)-D-glucopyranose subunits. Alpha (α), beta (β), and gamma (γ) CDs contain six, seven, and eight glucose molecules, respectively. These present as

truncated cones in three dimensions, featuring a hydrophilic external surface owing to their hydroxyl groups, while the inner cavity is inherently hydrophobic. [156] Out of the three types of CDs, β-CD stands out due to the optimal size of its cavity, with an internal diameter of 6.0 to 6.5 Å, making it exceptionally suitable for forming host-guest inclusion complexes with numerous molecules that have a hydrophobic part (**Figure 2.9**). [157] These are frequently employed as cyclic host molecules in pharmaceutical sciences, valued for their proficiency in elevating both the solubility and bioavailability of inherently hydrophobic drugs. [158] In the aqueous environment, CDs form an inclusion complex with the hydrophobic molecules. The formation of the inclusion complex is facilitated by the hydrophobic and van der Waals interaction between the CD's inner surface and the hydrophobic guest molecules. Moreover, there needs to be a match in the molecular size of the hydrophobic guests and the CD cavity. [159]

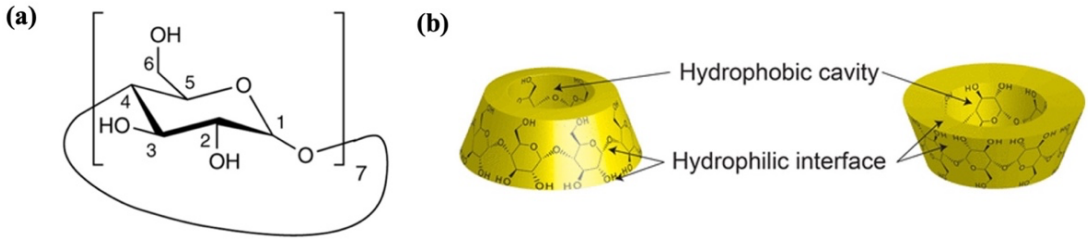

Figure 2.9 (a) Chemical structure of β-CD, (b) Schematic representation of CD structure. Reproduced with permission from reference [156] Copyright @2018 and reference [159] Copyright @2014 American Chemical Society.

Takashima and colleagues were the first to manipulate the properties of hydrogels by altering the cross-linking density within the host-guest complex. [160] They fabricated a light-responsive supramolecular hydrogel using CD and Azo, which displayed reversible macroscopic changes in both dimensions and form when exposed to UV light at 365 nm or visible light at 430 nm. The binding affinity of CD towards *trans*-Azo is greater compared to its affinity for *cis*-Azo as indicated by their respective association constants (for *trans*-Azo, K_a = 12,000 M^{-1}; for *cis*-Azo, K_a = 4.1 M^{-1}). Azobenzene contributes to the induction of photo-triggered morphological changes and remote actuation capabilities. Such features facilitate the use of host-guest polymer architectures in creating photo-responsive supramolecular hydrogels, optimized for expansion and contraction mechanisms.

2.4.3 *ortho*-nitrobenzyl Photo-labile Systems

Among the category of irreversible photo-responsive molecules, the derivatives of *ortho*-nitrobenzyl (*o*-NB) alcohol have demonstrated remarkable utility and adaptability across various polymer systems, making them a key group in polymer science. [161] Initially, employed as photo-protective groups (PPGs), their origin trace back to 1966 in the work of Barltrop and coworkers. [162] The UV light irradiation triggers a photo-isomerization process in which an o-nitrobenzyl alcohol derivative is transformed into an *o*-nitrosobenzaldehyde. This reaction also concurrently liberates a free carboxylic acid. [163]

The research conducted by Fréchet and colleagues revealed that this methodology could be broadened to synthesize organic bases. They achieved this by utilizing *o*-nitrobenzyl carbamates of amines and diamines, which ultimately facilitated the liberation of the respective alkylamines. [164] The application of this chemistry has been extended to utilize *o*-NB variants for the deprotection of both alcohols [165] and peptides [166].

2.4.3.1 Photo-isomerization in *o*-NB Derivatives

When exposed to UV light (300–365 nm), the *o*-NB chromophore in its excited state removes a hydrogen atom from the methylene or methine carbon at the γ-position, leading to the creation of aci-nitro tautomers. This initiates a molecular rearrangement resulting in benzoisoxaline derivatives. These derivatives eventually cleave, forming a carboxylic acid and *o*-nitrosobenzaldehyde as the main photoproducts (**Scheme 2.3**). Additionally, secondary photochemical reactions cause *o*-nitrosobenzaldehyde to dimerize, forming Azo groups. [161] The photocleavage can take place within less than 5 mins of light exposure when light intensities of 20-40 mW cm^{-2} is applied. On the other hand, it can also take a few hours when a low-intensity of 1.3 mW cm^{-2} is applied. [163] Using wavelengths near 300 nm tends to increase the effectiveness of photocleavage, as the *o*-NB absorption peak is at or around this wavelength. [167] It has been reported in literature that the introduction of substituents to the aromatic ring or the benzyl position of *o*-NB can alter the wavelength needed for photocleavage and also inhibit the generation of photo-dimerized byproducts. [168] Lately, there has also been advancements on developing *o*-NB based PPG with a red-shifted absorption spectrum, which enables the use of two-photon excitation methods for photolysis. [169]

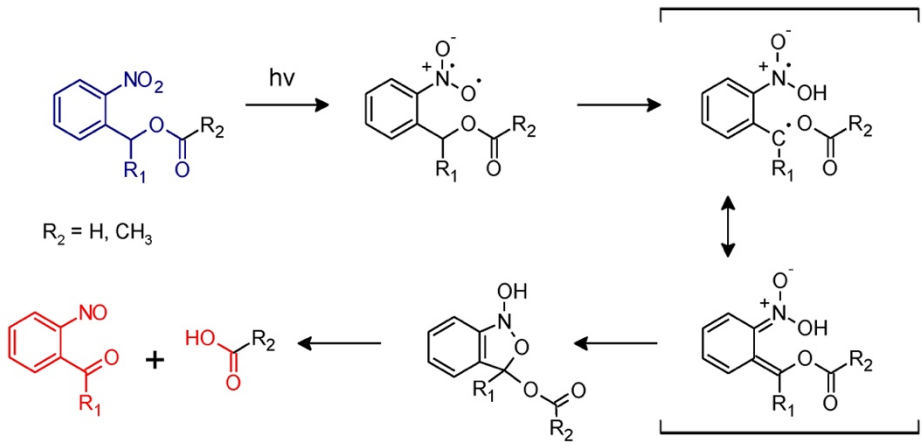

Scheme 2.3 Mechanism of photo-isomerization of *o*-NB alcohol derivatives into *o*-nitrosobenzaldehyde, releasing carboxylic acid. Reproduced with permission from reference. [161] Copyright @2020 MDPI, Basel, Switzerland.

2.4.3.2 *o*-NB- incorporated Polymers

In 1977, Petropoulos introduced the novel concept of employing *o*-NB alcohol derivatives as photo-labile groups in polymer chemistry, a first in the field. [170] These were incorporated in the polymer networks for developing UV-sensitive photoresists and gradually became popular as photocleavable crosslinkers. This adaptation extended to applications in light-triggered drug delivery systems and as photocleavable junctions in copolymer blocks. [161]

Interestingly, the incorporation of photo-labile groups into acrylate or methacrylate polymer networks could enhance their capabilities, offering significant benefits in the development of 'smart' materials and advancing 4D printing technologies. [161] In recent years, there has been a notable increase in the application of *o*-NB alcohol derivatives within methacrylate and acrylate frameworks, especially in the development of photoresists. [171] Various methodologies have been employed in the literature to leverage *o*-NB chemistry in the advancement of photoresist technologies.

Besides, in the early 1980s, Reichmanis et al. first reported the incorporation of *o*-nitrobenzyl cholate ester into a poly(methyl methacrylate-*co*-methacrylic acid) polymer matrix, aiming to control the network's solubility. [172] When exposed to UV light, the *o*-nitrobenzyl cholate ester fragmented into soluble components, facilitating the selective removal of the exposed areas using an aqueous alkali developer. Moreover, extensive research into *o*-NB chemistry has revealed its effectiveness in modifying the surface features of polymers, encompassing both their physical-chemical attributes and morphological aspects. Through UV irradiation, one can selectively adjust properties such as adhesion, cohesion, optical refraction, and surface

wettability, as well as the morphology at micro and nano levels. [173] Zhao et al. further reported the incorporation of *o*-NB as a side chain in amphiphilic block copolymers, which are engineered to form micelles that respond to light (**Figure 2.10**). [163] Utilizing *o*-NB for side chain functionalization within block copolymers can lead to the development of advanced materials. These materials are characterized by their modifiable hydrophobic and hydrophilic behaviors, as well as their LCST attributes, ultimately targeting the fabrication of micelles with controllable assembly and disassembly properties. [163]

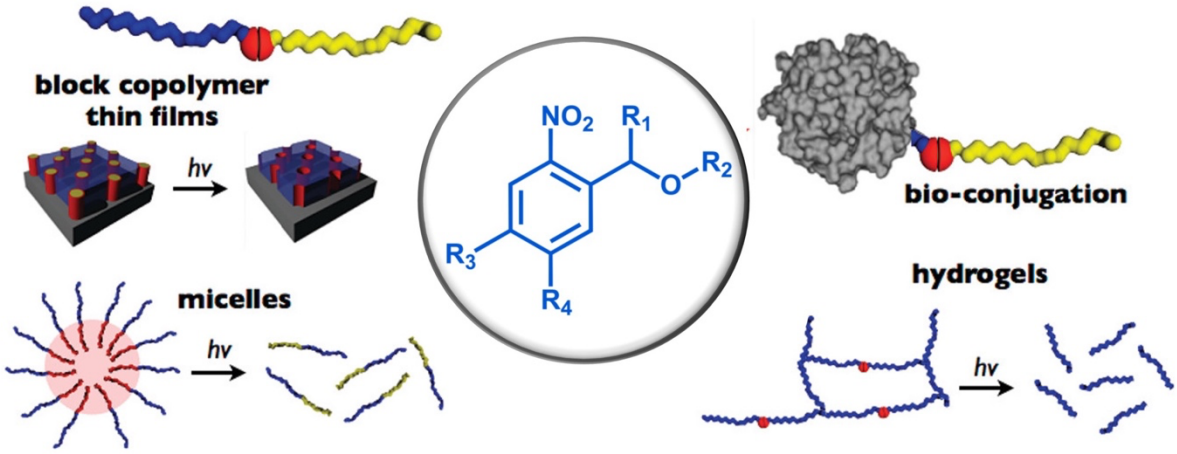

Figure 2.10 Possible applications of *o*-NB derivatives in polymer chemistry. Reproduced with permission from reference. [163] Copyright @2012 American Chemical Society.

o-NB integrated Hydrogels

Cross-linkers based on *o*-NB have been utilized to link hydrophilic PEG (poly(ethylene glycol)) chains, forming hydrogels that are frequently employed as scaffolds for tissue engineering and drug delivery. The introduction of *o*-NB group in the hydrogel was first reported by Anseth and co-workers, illustrating that these hydrogels, when created with *o*-NB -containing crosslinkers, had the capacity for targeted degradation through light exposure. [174] Additionally, the formation of biocompatible hydrogels was achieved by Kros and co-workers using the acrylate-thiol Michael addition reaction, where dithiolated PEG was added to dextran that had been functionalized with acrylate-modified *o*-NB moieties.

Furthermore, the scope of photo-labile chemistries was broadened by Luo et al. to include agarose and hyaluronan derivatives, fabricating three-dimensional structured materials with roles in tissue scaffold development and using the unveiling of photo-labile groups to bind biomolecules on hydrogel surfaces, influencing cell proliferation and motility. [175] Similarly, another study reported the production of cytocompatible three-dimensional hydrogels using

thiol-ene click chemistry and strain-promoted azide-alkyne cycloaddition, along with *o*-NB-based localized degradation. [176]

All in all, the use of photodegradable hydrogels with *o*-NB derivatives is paving the way for the development of specially tailored hydrogels, which can be refined through targeted photodegradation. Presently, these hydrogels are being explored as three-dimensional scaffolds for cell encapsulation and direction, with potential future uses in achieving adjustable feature sizes and innovative geometrical designs. [163]

2.5 *pH*-responsive Polymer Materials

Belonging to the class of stimuli-responsive polymers, *pH*-responsive polymers are distinguished by their ability to react to changes in the *pH* of solutions, resulting in notable modifications in properties like surface characteristics, chain structure, solubility, and overall configuration. These polymers are composed of ionizable acidic or basic units that adjust their ionization according to the *pH* of the solution. [82] Recently, the study of *pH*-responsive polymers has become increasingly popular, with new research emerging regularly. Their unique attributes render them highly effective for numerous applications, such as in drug and gene delivery systems, sensing devices, surface treatments, membrane technologies, and chromatographic methods. [32, 177, 178]

pH-responsive polymers are a category of polyelectrolytes characterized by the inclusion of weak acidic or basic groups in their structure. These groups are capable of proton exchange in response to environmental *pH* variations. Polymers that contain functional groups like carboxyl, pyridine, sulfonic, phosphate, and tertiary amines fall under this category, as the ionization of these components with *pH* changes leads to structural transformations. Typically, polymers composed of basic monomeric units act as cationic polymers when in an acidic environment, while those made up of acidic monomeric units function as anionic polymers in a basic environment. [82]

Moreover, hydrogels that are responsive to *pH* variation display distinct swelling and shrinking behaviors in response to changes in environmental *pH* levels. These dynamic responses are attributed to the presence of ionizable functional side groups in the polymeric structure of the hydrogel, which, upon *pH* variation, undergo ionization, thereby altering the charge density across the hydrogel network. This process facilitates the generation of electrostatic repulsion between closely situated polymer chains bearing like charges (either both positive or negative),

thereby promoting the uptake of water molecules throughout the hydrogel network, which in turn causes the hydrogel to swell and morphologically transform as depicted in **Figure 2.11.**

Anionic hydrogels exhibit swelling behavior that is contingent upon the ionization of their anionic functional groups (such as weak acidic carboxylic, sulphonic, phosphonic or boronic acid groups), a process that occurs when the ambient *pH* surpasses the acid dissociation constant (pK_a) of hydrogel, causing these groups to shed protons and render the hydrogel negatively charged. Consequently, the hydrogel expands due to osmotic pressure driven by electrostatic repulsion. Conversely, cationic hydrogels, incorporate cationic functional groups (such as amine groups, morpholino, pyrrolidine, imidazole, piperazine, and pyridine groups). [82], swell upon protonation when exposed to environments with a *pH* lower than their pK_a.

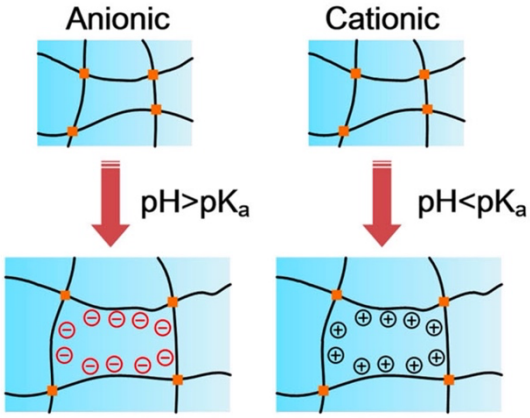

Figure 2.11. Illustration of *pH*-Induced swelling dynamics in anionic versus cationic hydrogels. Reproduced with permission from reference. [7] Copyright @2019 Springer Nature.

Therefore, depending on their pK_a values, these substances exhibit polyelectrolyte properties when exposed to either acidic or basic *pH* levels. The shift between ionic and non-ionic states enables the adjustment of their affinity for water in an aqueous environment. Consequently, this fine-tuning results in precipitation of the polymer or makes them soluble, causes their hydrogels to swell or deswell, or induces a transition between hydrophobic and hydrophilic properties on the surfaces of these polymers. Furthermore, natural polyelectrolytes, known for their abundance in nature, biodegradability, biocompatibility, and modifiability, are frequently the primary focus of research over synthetic polymers.

2.5.1 Natural Polyelectrolytes

Natural polyelectrolytes (PEs) command significant interest within the spectrum of *pH*-sensitive polymers, owing to their ubiquitous presence in nature, inherent biodegradability,

biocompatibility, and their facile functionalization. Prominent examples of such polyelectrolytes include alginate, hyaluronic acid (HA), chitosan (CS), cellulose, and gelatin.

Notably, HA and CS have been the subject of intensive research in the context of crosslinked hydrogels (**Scheme 2.4)**. Hyaluronan, a constituent of the extracellular matrix, is a glycosaminoglycan characterized by its high molecular weight. It is uniquely structured, comprising repetitive disaccharide units, specifically *N*-acetylglucosamine and glucuronic acid. HA's biological relevance and cytocompatibility are key features, complemented by its shear-thinning properties. Additionally, its unique viscoelastic nature and capacity for precise fine-tuning of desired attributes through chemical modifications further underscore its significant potential in the field. CS, a natural, mildly polycationic compound, consists of non-linearly structured units of *N*-acetyl-glucosamine and glucosamine. Owing to its desirable physicochemical characteristics, optimal viscosity, and cell adhesion capabilities, it is deemed fit for various biomedical applications.

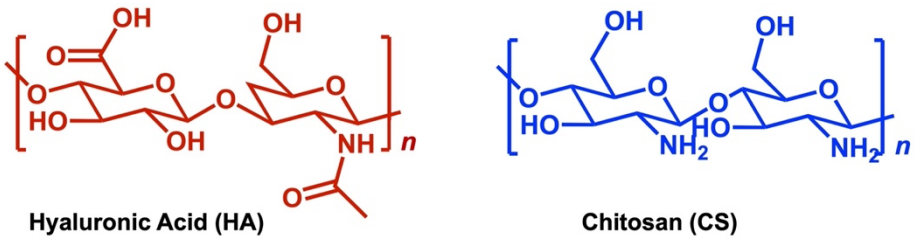

Scheme 2.4 Chemical structures of anionic polyelectrolyte (HA) and cationic polyelectrolyte (CS).

Natural polysaccharides possess unique and desirable physicochemical and biological properties, so hydrogels prepared from these biomaterials have found wide application. The formation of polyelectrolyte complex hydrogels, an intriguing category of physical hydrogels, results from the ionic cross-linking between charged polyelectrolyte species.

2.5.2 Polyelectrolyte Complex

A polyelectrolyte complex (PEC) is formed through a process of physical crosslinking initiated by the electrostatic attraction between polyelectrolytes of opposing charges, which also prompts the entropy-favored expulsion of small counterions (**Figure 2.12**).[179] PEC exhibits a greater sensitivity to swelling, particularly in response to *pH* variations, in contrast to covalently cross-linked hydrogels. This characteristic has opened the door to a broad spectrum of applications.[180] PECs made from natural polymers, including polysaccharides, offer the

extra benefits of being non-toxic and biologically absorbable. The characteristics of polyelectrolyte complexes are influenced by several factors: the anionic-to-cationic polymer charge ratio, the extent of neutralization, the ionic strength, and the valency of the ions present in the electrolyte solution. Strong polyelectrolyte complexes arise when the polymers include anions and cations from strong acids and bases or when polyions are completely ionized. [181]

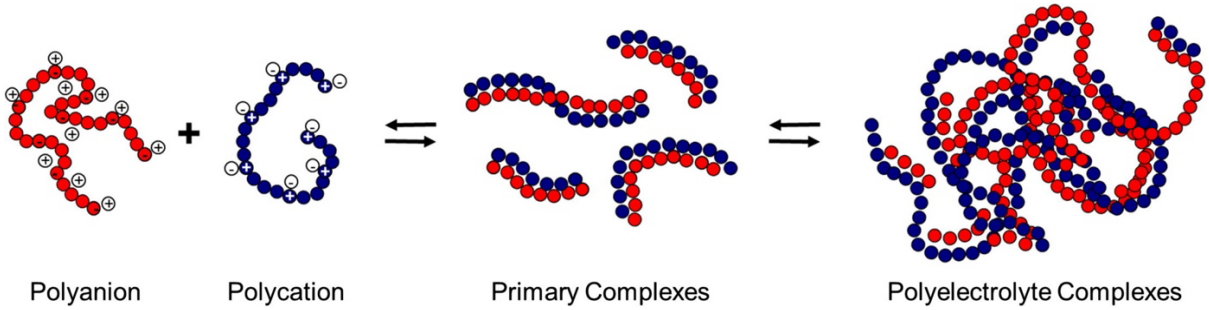

Figure 2.12 Formation of polyelectrolyte complex. Reproduced with permission from reference [182]. Copyright @2016 Elsevier B.V.

The formation of PEC provides an array of advantages, merging the positive aspects of distinct PE constituents, with a simple and benign production process and avoiding the adverse effects associated with organic solvents. The process is also noted for being cost-effective and energy-conserving, as it does not require special apparatus and takes place at standard room conditions. [182] The complexation is characterized by a two-step relaxation mechanism: an initial swift diffusion of polymer entanglements within 5 microseconds, influenced by molecular weight disparities and collision frequencies, leading to primary particle formation, and a subsequent slower phase where the polyelectrolyte chains undergo thermodynamic adjustments to reach an equilibrium conformation. [183]

PEC hydrogels emerge as a versatile class of soft materials, advancing applications in the biomedical field as platforms for tissue engineering [184], bioadhesive formulations [185], and drug delivery [186], besides their roles as ionic conductors [187] and applications in the food industry [188]. These hydrogels distinguish themselves by their quick self-assembly from aqueous solutions of oppositely charged block PEs, which organize into a hierarchical microstructure. Unlike typical ionically crosslinked hydrogels based on homo-PEs, PEC hydrogels feature a three-dimensional network of PEC domains interwoven with neutral blocks, endowing them with an exclusive set of characteristics. [189] These include tailored shear properties, the ability to respond to stimuli like salt and *pH*, injectability, self-healing features, and the capacity to incorporate charged macromolecules such as proteins and nucleic acids within their structure. [190, 191] In comparison to their isolated counterparts, PECs offer improved

stability in diverse *pH* swelling media and better structural and mechanical resilience. [72] However, their stability in limited in various pH and salt solutions due to the sensitivity of their electrostatic interactions to changes in ionic strength and hydrogen ion concentration. In the presence of aqueous media, PEC undergoes continuous swelling and eventuallly leading to their dissolution, undermining the material's structural cohesion. By engineering a tunable swelling response, one can avert material depletion, ensure the maintenance of structural and mechanical stability, and safeguard the intrinsic functional qualities of PEC hydrogels. Yet, these enhancements still fall short of ideal. The pressing issue now is to figure out methods to reinforce the stability of PECs during swelling across various media, while preserving their *pH*-dependent swelling properties.

One strategy to enhance polyelectrolyte complexes involves introducing additional crosslinks, either covalent or ionic. Presently, glutaraldehyde is the predominant crosslinking agent for chitosan/alginate complexes. Gierszewska et al. have recently documented a pioneering chitosan/alginate polyelectrolyte complex membrane designed for biomedical and industrial uses, which exhibits elevated structural, mechanical, and chemical robustness. [72]
Another interesting approach could be the incorporation of PEC within the interpenetrating polymer networks to achieve good mechanical stability and stimuli-responsiveness in hydrogels.

2.5.3 PEC-integrated Interpenetrating Polymer Network

Polysaccharide-based IPNs represent a remarkable category of biopolymeric materials, leveraging the inherent biocompatibility, biodegradability, and functional versatility of polysaccharides. These systems typically involve the integration of one or more polysaccharides, such as chitosan, alginate, or hyaluronic acid, with synthetic or natural polymers, creating a network structure with enhanced mechanical and chemical properties compared to their individual components. [192] The uniqueness of polysaccharide-based IPNs lies in their ability to mimic natural extracellular matrices, making them highly suitable for biomedical applications such as drug delivery, tissue engineering, and wound healing. [193]

A recent investigation conducted by Defu Li and colleagues introduced the development of PEC-IPN hydrogels, aiming to address the limitations of PEC through integration within a covalent framework (**Figure 2.13)**. Their study emphasized the combined enhancements in the hydrogel's mechanical strength as a result of embedding PEC into the IPN structure. [191] A

notable limitation of pure PEC hydrogels is that they are prone to excessive swelling when immersed in water, leading to eventual dissolution. This compromises the material's structural integrity, affecting its mechanical stability and functionality which are crucial for practical applications. [194] On the other hand, PEC integrated within IPN hydrogels imparts a controlled swelling behavior, significantly enhancing the material's resilience to aqueous environments. Therefore, the structural and mechanical properties remain intact in the PEC-IPN structure, making them more reliable and versatile for various applications.

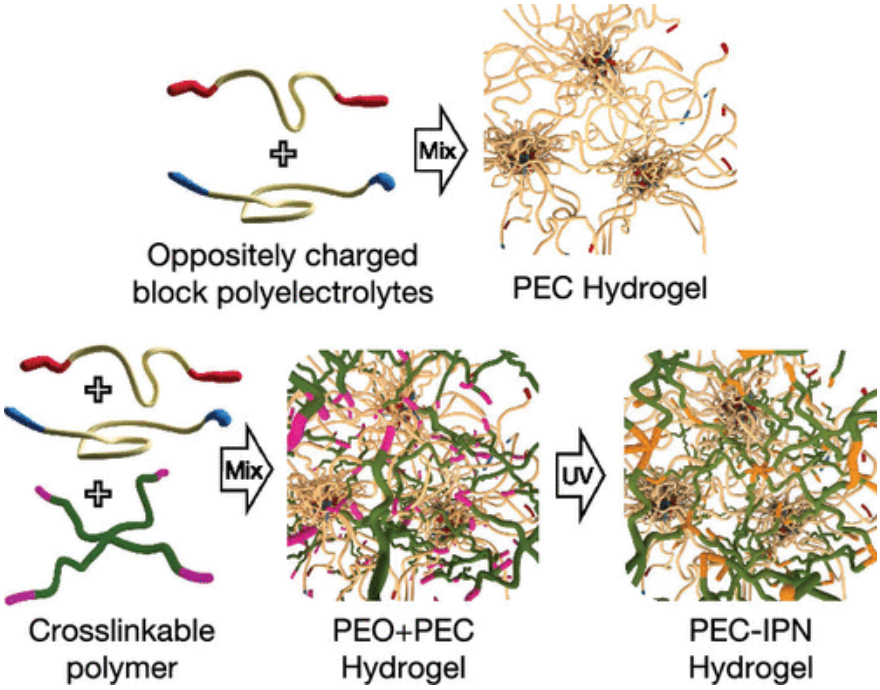

Figure 2.13 Conceptual outline depicting the assembly of PEC-IPN hydrogels. Reproduced with permission from reference [191]. Copyright @2022 American Chemical Society.

Integrating these advancements offers substantial benefits across various applications where photo-crosslinked hydrogels are used, especially where in situ crosslinking of precursor polymers is a critical step. [195] In light-based biofabrication techniques, such as extrusion-based 3D printing, which typically struggle with maintaining viscosity and structural integrity of the hydrogel precursor solution prior to photo-crosslinking, the addition of PEC networks can be transformative. [196] This inclusion improves initial shear strength, minimizes the leakage of precursors due to secondary flows, and strengthens inter-layer adhesion, which is essential for achieving high-fidelity printing. [191]

2.6 Polymerization Techniques: A Synthetic Overview

This chapter offers an overview of the polymerization methodologies applied within this dissertation, focusing on radical polymerization, photopolymerization techniques, and specifically on three-dimensional printing via Digital Light Processing.

2.6.1. Radical Polymerization

For the past decades, radical polymerization (RP) has been instrumental in the synthesis of synthetic polymers, making up half of the world's plastic production. Despite a modest decrease due to the rising prominence of metal-organic initiators for plastic and synthetic rubber creation, RP still significantly contributes to the industry. Presently, it is responsible for nearly 45% of the annual production of plastic materials, translating to roughly 100 million tons, and 40% of synthetic rubber, totaling about 4.6 million tons. [197] Its widespread adoption can be attributed to the simplicity of the polymerization process and the minimal requirements for solvent and reagent purity. Moreover, unlike ionic or coordination polymerization, RP exhibits a high tolerance for protic solvents and minor contaminants, including oxygen and monomer stabilizers. As a result, RP can efficiently proceed in polar solvents like alcohols, and notably, in water, even when using monomers that have not undergone excessive drying or purification processes. [198]

From a mechanistic perspective, polymerizations are classified into diverse categories, with RP being a distinguished type within the chain-growth polymerization class.

RP proceeds through a chain reaction mechanism with the key steps including initiation, propagation, chain transfer and termination as shown in **Scheme 2.5**. It starts with the formation of free radicals, usually through the decomposition of initiators like-Azobisisobutyronitrile (AIBN) or peroxides, especially under heat or UV light. These radicals react with monomer molecules, creating new radicals and starting the chain growth process. During propagation, the chain elongates as monomer units successively add to the reactive chain end, a step characterized by rapid growth and varying chain lengths. Termination occurs either through combination, where two radical chain ends join, or disproportionation, involving the transfer of a hydrogen atom from one chain to another, resulting in stable end products. This mechanism is widely used due to its simplicity and versatility, allowing the polymerization of various monomers, but it typically results in polymers with a broad molecular weight distribution due to the random nature of the initiation and termination phases. [199]

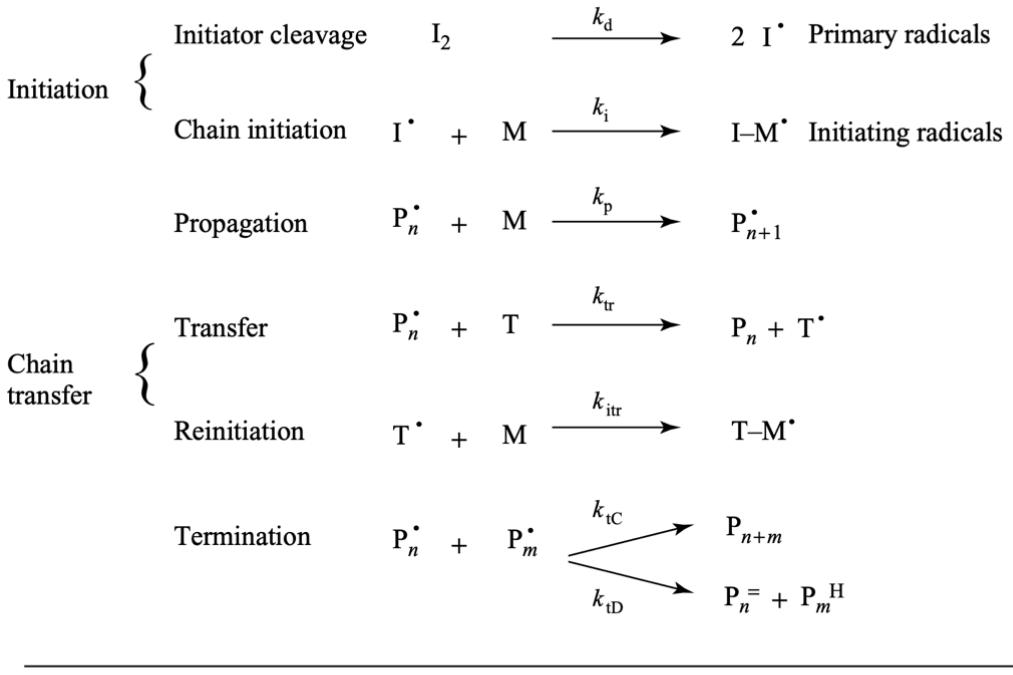

Scheme 2.5 General mechanism of radical polymerization. Reproduced with permission from reference. [198] Copyright @2012 John Wiley & Sons, Ltd.

2.6.2 Photopolymerization

Photo-induced polymerization is an increasingly popular technology due to its solvent-free process, energy efficiency, and cost-effectiveness. [200] It is widely used in the production of photoactive polymer systems for coatings, paints, printing inks, adhesives, composites, and dental restoratives. [201, 202] A distinctive characteristic of this method is that polymerization occurs only in exposed areas, allowing for high-resolution imaging in printing plates, optical discs, and microcircuit production. Additionally, recent developments include applications in three-dimensional stereolithography and holographic recording. [203] Acrylate-based resins are the most popular choice in light-curable systems, primarily due to the high reactivity exhibited by acrylate monomers.

PIs efficiently absorb electromagnetic radiation within the UV/Vis spectrum, specifically between 250 to 450 nm, and effectively transduce this photonic energy into chemical energy. This energy transition results in the formation of reactive intermediates, notably free radicals and cations, which serve as moieties driving the polymerization of functional monomers into

linear polymeric chains. In contrast, the presence of multifunctional monomers facilitates the formation of complex three-dimensional crosslinked polymeric networks. [204]

Photoinitiating System:

Photopolymers fall into two main groups based on their initiation reactions: free radical and ionic. The key difference lies in the type of reactive species produced by the photoinitiator (PI), whether radicals or reactive ions, upon light exposure, which begins the photopolymerization process. [205] Both groups share a common three-step process, comprising initiation (where PI absorbs UV light to generate reactive species), propagation (where these species bond with oligomers and monomers to form extended chains), and termination (which occurs due to recombination, disproportionation, or occlusion). Free radical systems can cross-link monomers like acrylates, styrenes, and thiols using bifunctional monomers (such as- ethylene glycol dimethacrylate, divinyl benzene, diethylene glycol diacrylate) that serve as cross-linkers. The polymerization and cross-linking proceed rapidly forming long chains upon light exposure and cease on removal of light. In contrast, ionic species drive the polymerization of different monomers such as ketones and aldehydes, which free radicals cannot polymerize. Cationic polymerization, predominant in ionic systems, requires longer exposure and continues even post light removal. [205]

Most commercial photopolymerization systems operate on the principles of free radical chemistry. These systems are typically made up of ethylene-based unsaturated compounds such as acrylates or methacrylates, complemented by a small quantity of a PI, which usually constitutes about 0.5% to 6% of the mixture. There are two primary categories of PIs: unimolecular type I and bimolecular type II, each functioning through distinct mechanisms to generate free radicals. [206] Type I PIs, including benzil ketals, acetophenones, aminoalkyl phenones, acyl phosphine, O-acyl-α-oximo ketones, R-hydroxyalkyl ketones, and acyl phosphine oxides, produce two free radicals following the homolytic bond cleavage induced by photon absorption. Conversely, type II PIs, typically derivatives of benzophenone and thioxanthone, operate by abstracting hydrogen or electrons from co-initiator molecules in their triplet state after UV radiation exposure, leading to free radical formation. [205]

Conversely, in ionic photoinitiating systems, polymerization is driven by anions in anionic systems and cations in cationic systems. Anionic polymerization involves the transfer of a nucleophilic group or an electron to a monomer, initiated by anionic PIs. However, managing anionic photoinitiating systems is more complex compared to radical-based systems, making

them a less preferred choice. On the other hand, cationic photoinitiating systems are more prevalent. In cationic PI systems, the principal categories include onium salts, diazonium salts, and organometallic complexes. [205, 207]

When PI absorbs light, its activation hinges on the spectral overlap between the emission spectrum of the light source and the PI's absorption band. [204] When such overlap occurs, the PI transitions to an electronically excited state **(**PI^***)** through the excitation of an electron to a higher energy orbital. The excited state PI^* typically has a brief lifetime, usually under 10^{-6} seconds. During this transient period, PI^* can undergo various pathways: it may revert to its ground state PI, releasing light and heat, or it can engage in a chemical reaction to form a reactive intermediate, such as $I^\bullet$ or I^+. This reactive intermediate, for instance, $I^\bullet$, can subsequently interact with another radical R, initiating the polymerization of a monomer M, leading to the formation of a polymer. [204]

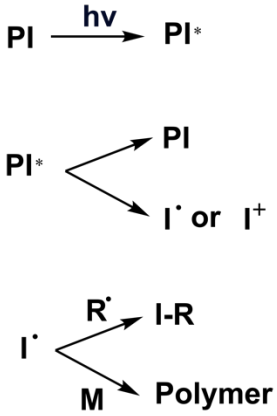

Rate of polymerization can be given by:

$$R_p = \frac{k_p}{\sqrt{k_t}}\sqrt{R_i}[M]$$

where k_p and k_t are the kinetic constants of propagation and termination, ***[M]*** is the monomer concentration and R_i is the rate of initiation, which can be given by:

$$R_i = I\phi[PI]$$

where I is the intensity of irradiation, ϕ is photoinitiation quantum yield (or efficiency of PI) which varies from 0 to 1 and ***[PI]*** is the concentration of PI.

Furthermore, 3D printing technology, taking advantage of photopolymerization, offers remarkable benefits including high precision and detail, rapid production speed, and versatile material properties. This method is exceptionally cost-effective for small production runs and prototypes, allowing for intricate designs and complex geometries that are difficult to achieve with traditional manufacturing. Therefore, it is discussed in detail in the next section.

2.6.3 3D Printing

Introduced in the 1980s, 3D printing technologies, also known as additive manufacturing, rapid prototyping, or layered manufacturing, revolutionized the fabrication of custom and complex structures, eliminating the need for conventional molds. [208, 209] Innovations in polymer chemistry have particularly enhanced photopolymerization-based 3D printing methods, drawing significant interest from the fields of polymer chemistry, materials science, and engineering. [203]

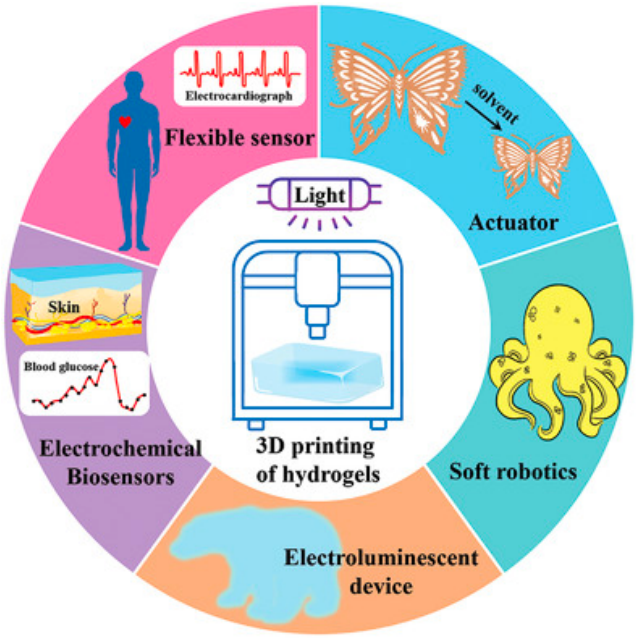

Figure 2.14 Functional applications for 3D-printed hydrogels. Reproduced with permission from reference [210]. Copyright @ 2021 Wiley-VCH GmbH.

In the recent decade, the development of functional material-based devices has been significantly influenced by the innovation of 3D printing smart hydrogels (**Figure 2.14**). Various techniques like extrusion-based printing [211], stereolithography (SLA) [212, 213], digital light processing (DLP) [214, 215], bioprinting [216], and inkjet printing [217] have been introduced for hydrogel fabrication. These techniques stand out for their ability to intricately craft multifunctional materials with specific control over their optical, chemical, and mechanical features. [203] 3D printing technology has been widely applied in crafting hydrogels for various applications, including tissue engineering [218], drug delivery systems [219], scaffolding [220], and the creation of microfluidic devices [221]. The use of natural, biocompatible, and biodegradable polymers in 3D printing allows for the construction of complex and dynamic hydrogel structures.

3D photopolymerization, also known as photocuring or photo-cross-linking, utilizes monomers or oligomers in their liquid form. These substances undergo curing or photopolymerization when exposed to a light source of a specific wavelength, resulting in the formation of thermosets. [203] Among all techniques, DLP is particularly noteworthy for its precision, speed, and flexibility. It will be discussed in detail in the following subsection.

2.6.3.1 Digital Light Processing

The recent development of DLP technology has significantly enhanced printing efficiency, achieving faster production times without compromising on precision. [222] This technique differs from SLA by illuminating each layer simultaneously, rather than point-by-point. In DLP systems, light is projected from underneath a resin bath, with the build platform immersing from above. This allows for efficient 3D printing using minimal resin volumes. [223] Additionally, the layers being cured are shielded from air at the bottom of the vat, reducing the risk of oxygen inhibition. DLP printing has diverse applications, ranging from creating luminescent 3D structures and stretchable polymers to engineering nerve conduits [224] and electrically conductive materials [225]. It's also used in forming organic-inorganic hybrids [226] and various complex shapes [227].

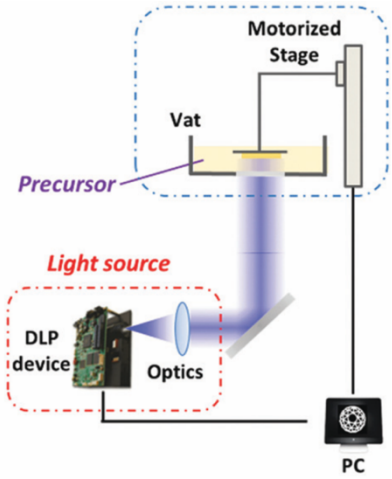

Figure 2.15 A representative setup of DLP-based printer. Reproduced with permission from reference. [223] Copyright @2020 Royal Society of Chemistry.

3. Motivation

The primary motivation of this thesis is to develop innovative smart polymer materials with precise tunability and orthogonal responsiveness to light and pH, opening avenues for technological advancements in adaptive material science. Therefore, this thesis presents a trio of pioneering projects, each offering a distinct contribution to this sophisticated arena. **Chapter 4.1** focuses on the synthesis of photo-responsive SP and DEGMA-based copolymers with a range of compositions, revealing their capability to exhibit photo-switchable glass transition temperatures (T_g). The development of a light-responsive mechanism for the control of T_g represents a significant extension in the applicability of these polymer-based materials, paving the way for new scientific and industrial uses.

Moreover, the fabrication of advanced materials by incorporation of stimuli-responsiveness coupled with cutting-edge 3D printing techniques serves as a further incentive. These techniques are distinguished by their proficiency in intricately fabricating multifunctional materials, meticulously tailoring their optical, chemical, and mechanical properties. However, the research in this field is still embryonic and presents challenges, particularly in comprehending and controlling the viscoelastic characteristics for printing such smart materials. Working towards this objective, **Chapter 4.2** aims at employing Digital Light Processing (DLP) as a methodical approach for the synthesis of *pH*-sensitive Interpenetrating Polymer Networks integrated with Polyelectrolyte complex (PEC-IPN), which exhibit a tailored response to *pH* variations, along with an adjustable mechanical robustness. Additionally, irreversible photo-responsive *ortho*-nitrobenzyl is employed in this network for targeting this approach.

As an extension of this approach, **Chapter 4.3** targets the goal of achieving dual responsiveness by incorporating a photo-responsive Azo group within PEC-IPN synthesized previously. Additionally, the objective includes 3D printing this IPN network, enhancing mechanical robustness and engineering properties that can be fine-tuned, via an added interplay between the Azo-modified polyelectrolyte and Cyclodextrin.

The projects outlined above are intended to lead to the synthesis of novel smart polymeric materials with modifiable features via state-of-the-art methods and to enhance the body of knowledge with the addition of 3D printable intelligent networks.

4. Results and Discussion

This chapter meticulously documents the research findings delineated throughout this thesis. It systematically addresses distinct topics within individual subchapters, aiming to equip the reader with a thorough understanding of each specialized area within the field of smart polymer materials.

In the first section, a series of copolymers containing photochromic spiropyran and DEGMA are synthesized and thoroughly characterized for their responsive, structural and thermal properties. A comprehensive analysis has been conducted to elucidate the effects of UV irradiation on the glass transition temperature (T_g) of the polymers. Subsequently, the second section leverages the photo-labile characteristics of the *o*-NB group, introducing an inventive strategy for fabricating *pH*-responsive IPN hydrogels with *o*-NB functionalized PEC, utilizing a 3D printing technique. Lastly, the third section further extends the approach established in the second project by incorporating azobenzene functionalities into PEC-containing polymer networks, thus forming dual-responsive SPN and IPN hydrogels. An exhaustive exploration of their responsive behavior and their compatibility with 3D printing technologies is also presented.

4.1 Photo-responsive Spiropyran and DEGMA-based Copolymers

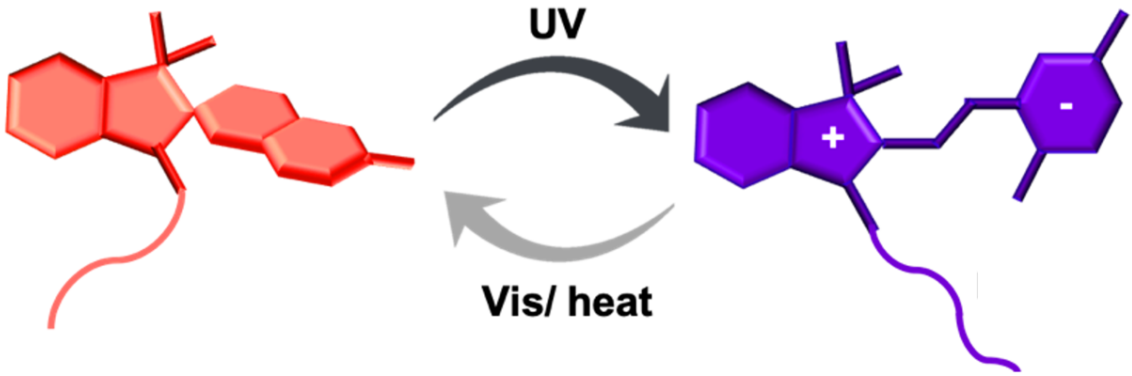

Parts of this chapter and the corresponding experimental section are published as “V. Pruthi, Y. Akae, and P. Théato. "Photoresponsive Spiropyran and DEGMA-based Copolymers with Photo-switchable Glass Transition Temperatures." Macromol. Rapid Commun., 2023, 2300270. https://doi.org/10.1002/marc.202300270 and adapted with permission from Wiley, 2023.

4.1.1 Prologue

The recent advent of SP-side groups in the creation of photochromic copolymers has opened new research avenues, with applications spanning chemical sensors, optical data storage and smart coatings. [228, 229] The work of Zhou et al. has been pivotal in demonstrating that polymers with Azo groups can exhibit a glass transition temperature (T_g) that is responsive to light, offering innovative strategies for designing self-healing polymers with high-resolution healing processes activated by light. [230] Building on this, Hu et al. reported on SP-based liquid crystalline materials that can be cross-linked, featuring controllable photochromism and an adjustable T_g. [231] The comprehensive impact of UV light on the T_g across various SP-based polymers remains under-explored. Furthermore, the ability to photo-modulate the T_g in such polymers heralds new possibilities for their integration into diverse applications, including photo-switchable adhesives and nanoimprint lithography, as a result of alterations in their polarity and rheological behavior. [232, 233]

This study involves the synthesis of a novel series of copolymers composed of di(ethylene glycol)methyl ether methacrylate (DEGMA) and spiropyran methacrylate (SpMA), each with a distinct proportion of spiropyran. A systematic investigation and comparison of their photo-responsive, structural, and thermal properties were conducted using a diverse array of analytical techniques. Essentially, a thorough examination has been carried out to understand the impact of UV irradiation on (T_g) of the polymers.

4.1.2 Monomers

For the synthesis of SP-based polymers, SpMA and DEGMA were used as monomers. Firstly, SpOH, a derivative of SP, was synthesized starting from the readily available 2,3,3-trimethyl-3H-indole, using a previously established protocol. [112] This was followed by the addition of a methacrylate group to the SP molecule, leading to the formation of SpMA, as depicted in **Scheme 2.1.** Further details of the synthetic pathway and characterization of intermediates and

final product are provided in the experimental **Section 6.3.1.** Additionally, DEGMA imparts superior flexibility to the polymers produced, thereby qualifying as an excellent co-monomer.

4.1.3 Synthesis of P(DEGMA-*co*-SpMA) Copolymers

Different copolymers of spiropyran methacrylate (SpMA) and DEGMA were synthesized using free-radical polymerization, varying the ratio of monomers **(Scheme 4.1, Table 4.1).** Polymerization of SpMA, DEGMA and 1 mol% initiator (AIBN) was conducted in 1,4-dioxane at 70 °C overnight and the polymers were purified by precipitation in petrol ether to remove the unreacted small molecule compounds. After filtration and drying under vacuum at 40 °C for 48 hours, the purified polymers P(DEGMA-*co*-SPMA) with various ratios were obtained with a reddish-orange color.

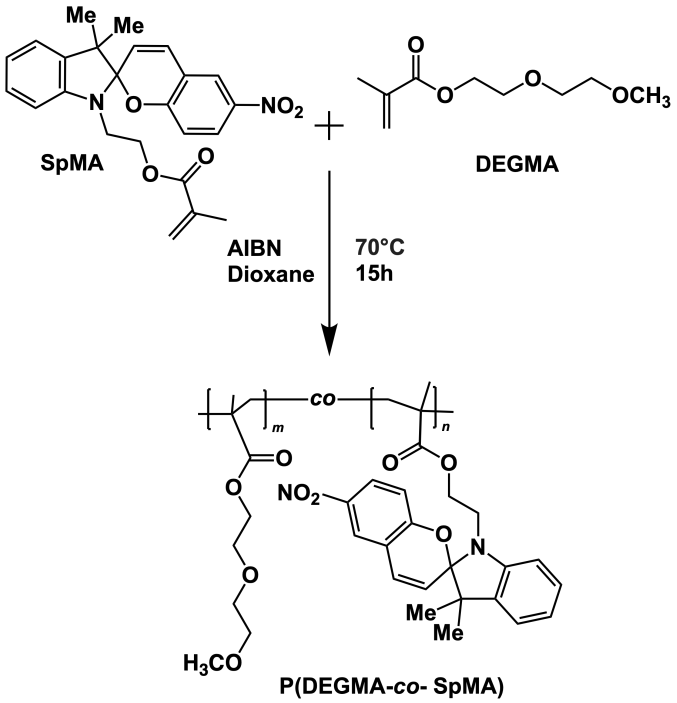

Scheme 4.1 Synthesis of P(DEGMA-*co*-SPMA).

^{1}H NMR spectra of the synthesized polymer P(DEGMA-*co*-SPMA) measured in $CDCl_3$ confirmed the successful copolymerizations (**Figure 4.1 and 4.2**). The presence of aromatic peaks between 5.75 ppm to 7.88 ppm verified the presence of SP in the copolymers, along with significant peaks originating from the incorporation of the DEGMA monomer. The composition of copolymers was calculated from the ratio of peak integral attributed to protons of the benzopyran phenyl group and the protons of the methylene group next to the ester group of DEGMA, as listed in **Table 4.1**.

Table 4.1 Synthesis of different copolymers P(DEGMA-*co*-SpMA).

Co-polymer	DEGMA [mmoles]	SpMA [mmoles]	Feed SpMA %	Incorporated SpMA% [a]	M_n [b]	M_w [b]	$Đ$ [b]	T_g [c] [°C] (before UV)	T_g [c] [°C] (after UV)	T_d(5 %) [d] [°C]
1	0.25	0.6	70	69.9	17600	31000	1.7	111.8	127.5	257
2	0.75	0.5	40	37.5	25300	71500	2.8	45.7	63	254
3	1.17	0.5	30	25.6	41300	102400	2.4	34.8	51.3	272
4	2.0	0.5	20	20.0	49000	226000	4.6	24.6	39.3	273
5	3.0	0.33	10	7.2	52300	100300	1.9	-4.4	1	272
6	3.0	0.16	5	4.8	65700	267900	4.1	-20.8	-9.4	277
7	5.5	0.055	1	1.4	80000	194200	2.4	-28.2	-7.2	266
Homo-polymer	5.5	0	0	0	82000	223100	2.7	-37.8		218

[a)] % SpMA in the synthesized copolymers determined by NMR; [b)] Number average molecular mass M_n , weight average molecular mass M_w and dispersity Đ determined by GPC analysis; [c)] glass transition temperature T_g determined by DSC analysis; [d)] decomposition temperature T_d (5%) determined by TGA analysis.

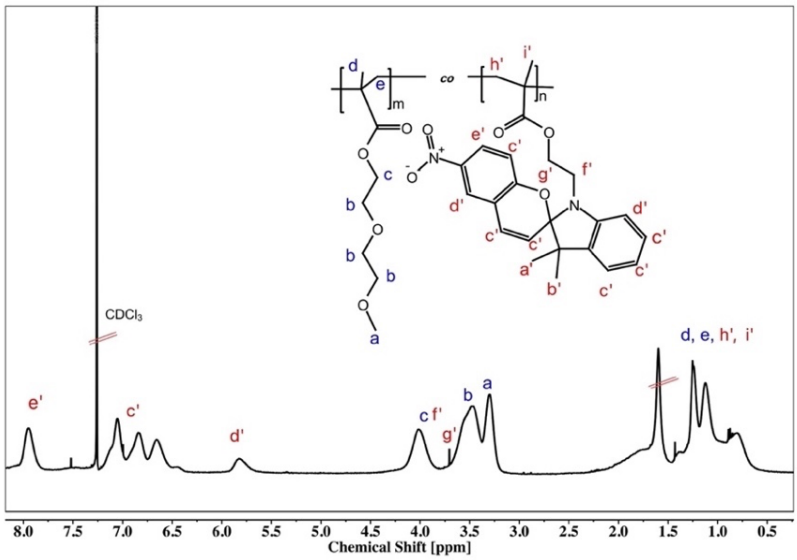

Figure 4.1 [1]HNMR spectra of P(DEGMA-*co*-SpMA) copolymer with 70% SpMA (400 MHz, 298 K).

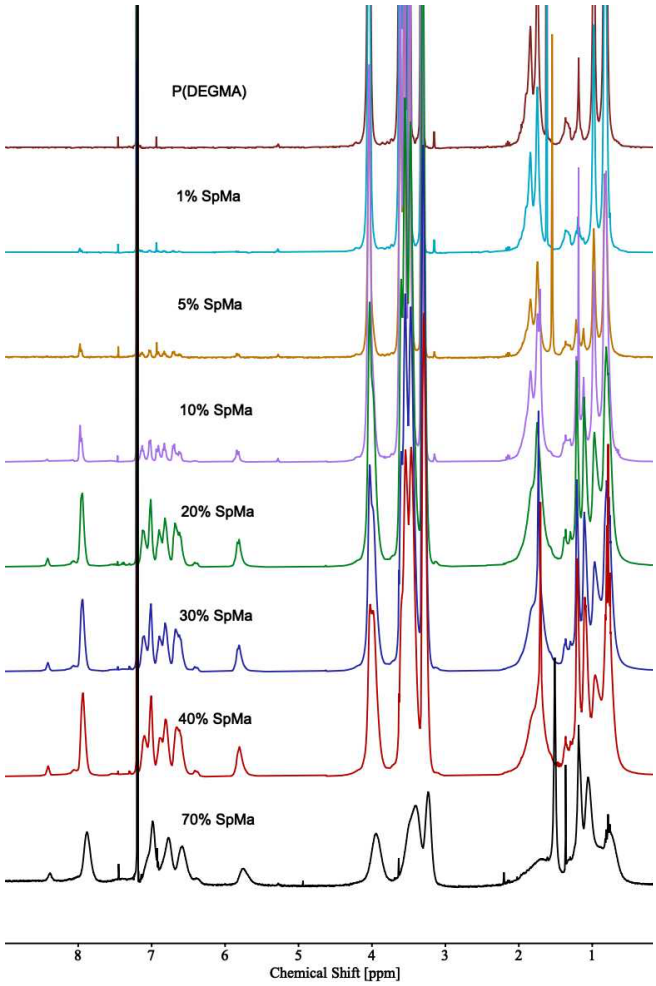

Figure 4.2 ^{1}HNMR spectra of P(DEGMA-*co*-SpMA) copolymers containing different percentages of spiropyran methacrylate (SpMA) ((400 MHz, 298 K).

Furthermore, to determine the number average molecular mass (M_n) and the molecular mass distribution (M_w/M_n, Đ), GPC measurements were carried out for all synthesized P(DEGMA-*co*-SPMA) copolymers with varying composition of SpMA and DEGMA, as shown in **Figure 4.3**. As shown in **Table 4.1**, the number average molecular mass (M_n) of the polymer increased with an increase in the percentage of DEGMA and a decrease in the percentage of SP. The elution time in the GPC traces was longer, i.e., M_n was smaller, and the molecular mass distribution was narrower for the copolymers with less amount of DEGMA in their composition. The properties of the polymer, including the color and viscosity also changed with the increasing DEGMA content. P(DEGMA-*co*-SPMA) with 1 to 20% SpMA were extremely viscous polymers, while copolymers with 30% or more SpMA content were completely solid.

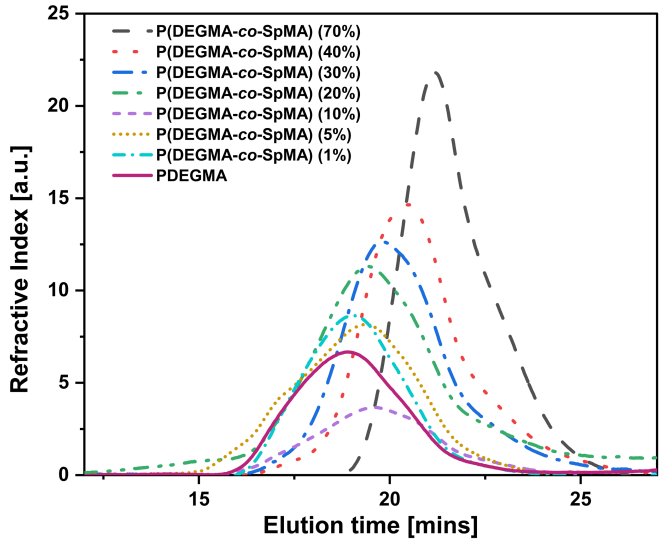

Figure 4.3 Comparison of GPC chromatography (eluent: THF) of the synthesized P(DEGMA-*co*-SpMA) copolymers.

4.1.4 Photochromism of SP in P(DEGMA-*co*-SpMA)

UV/Vis absorption spectroscopy was conducted to investigate the photo-isomerization of P(DEGMA-*co*-SpMA). When dissolved in $CHCl_3$, the SP polymer solution appeared to be pale yellow in color. Upon irradiation of UV light (λ = 365 nm) on the copolymer solution with a concentration of 0.03 mg mL^{-1} in $CHCl_3$, SP present in the copolymer underwent photo-isomerization into its open-ring form MR as shown in **Figure 4.4 (a).** Also, the solution turned bright purple in color. Two localized transitions can be noted in the absorbance spectrum of the closed SP form, one corresponding to the π-π^* transition in the indoline molecule (275 nm) and the other (360 nm) attributed to the chromene group. [20, 234, 235] Whereas, the photo-induced open ring MR isomer showed one transition (560 nm) in the visible region, responsible for the coloration of the solution. The UV spectra of MR isomer of P(DEGMA-*co*-SpMA) copolymers with variable SP composition, after UV irradiation for 2 mins are shown in **Figure 4.4 (b)**. Noticeably, the absorbance at 560 nm increased with an increase in percentage incorporation of SP.

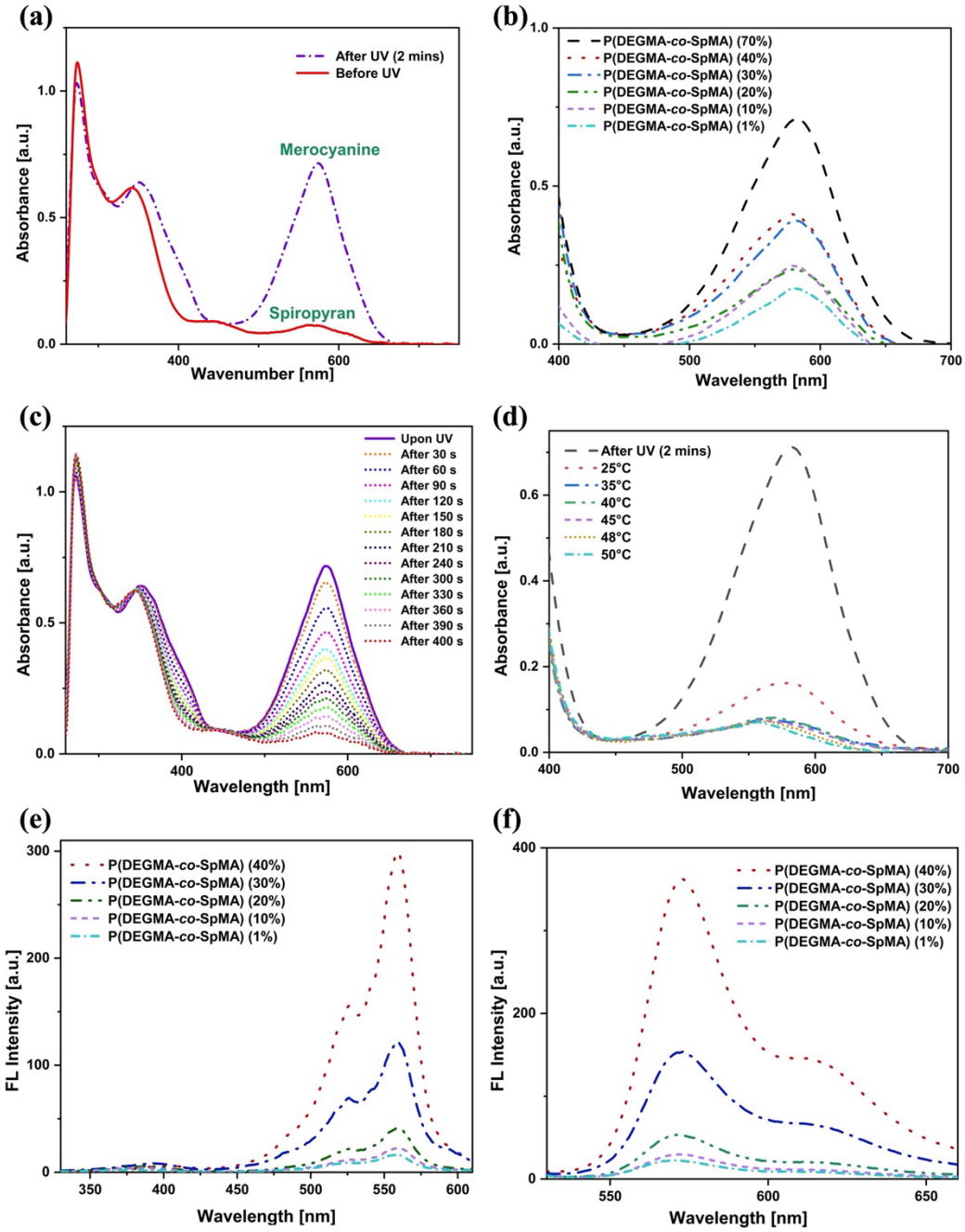

Figure 4.4 (a, b) UV–vis absorption spectra of P(DEGMA-*co*-SpMA) copolymers upon UV irradiation for 2 min, (c) when kept under visible light after UV irradiation showing photo-reversibility back to MR form with time evolution at room temperature, (d) UV–vis spectra showing reversibility with temperature evolution, (e) fluorescence excitation spectra, and (f) emission spectra of P(DEGMA-*co*-SpMA) with different % SP.

Moreover, in order to investigate the reversibility with time evolution, the UV-irradiated polymer solution was kept under visible light at room temperature and the absorbance was measured at different time intervals. Clearly, the reversible conversion of MR back to SP at

room temperature was detected as shown in **Figure 4.4 (c).** The absorbance of P(DEGMA-*co*-SpMA) at 275 nm and 365 nm increased and at 560 nm decreased with increasing time of exposure to visible light, as per the fact that the ring-closing photo-isomerisation gradually transforms MR form to SP form. Therefore, on account of the instability of the MR form at room temperature, P(DEGMA-*co*-SpMA) exhibits good reversibility. Additionally, the reversibility with temperature evolution was also studied using UV/Vis absorption spectroscopy (**Figure 4.4 (d)**). With an increase in temperature, the transformation occurred very rapidly. When the UV-irradiated polymer solution was kept at 50 °C for 1 min, the absorbance of the SP group at 560 nm completely recovered back to its original state.

Owing to their great potential applications in imaging and detection, the fluorescence properties of SP have been extensively studied in the past years. [20] Thus, the fluorescence spectra were recorded for polymers with varying SP content in chloroform. As shown in **Figure 4.4 (e)**, the excitation spectra of the polymers showed two absorption bands at around 390 nm (minor) and 550 nm (major). A gradual decrease in the intensity of these bands with respect to the decrease in the SP content in the polymers was observed. **Figure 4.4 (f)** represents the emission spectra of polymers at an excitation wavelength of 550 nm. A similar trend was observed in the emission spectra as well. The emission maximum was observed at around 570 nm for all polymers.

Furthermore, photochromism was observed in P(DEGMA-*co*- SpMA) in solution as well as solid state within a minute of UV irradiation at 365 nm (**Figure 4.5 (a, b)**). The reversibility of photo-isomerization and accompanying photochromism of the polymers was investigated in both solid and solution. While, the MR form in solution transformed back to its SP form at room temperature within a couple of mins, the MR form in solid reversed back to its SP form over a time period of 2-3 hours. The probable reason for this would be the closed packing of molecules in solid state that hinders structural transformation and photo-switching. [236] Besides, smart photo-responsive polymer-coated polypropylene fabrics were prepared by simply coating the surface of the fabric with P(DEGMA-*co*-SpMA) by spin-coating a solution of the copolymer in $CHCl_3$. After drying, the photo-isomerization on the fabric was also investigated. Upon exposure to UV light at 365 nm, the fabric's surface underwent photo-isomerization, as evidenced by the change in color. Moreover, a localized irradiation within the irradiated spot and a visible bright fluorescence was observed on the P(DEGMA-*co*-SpMA) coated PP fabric, when irradiated with UV laser (365 nm) as shown in **Figure 4.5 (d)**.

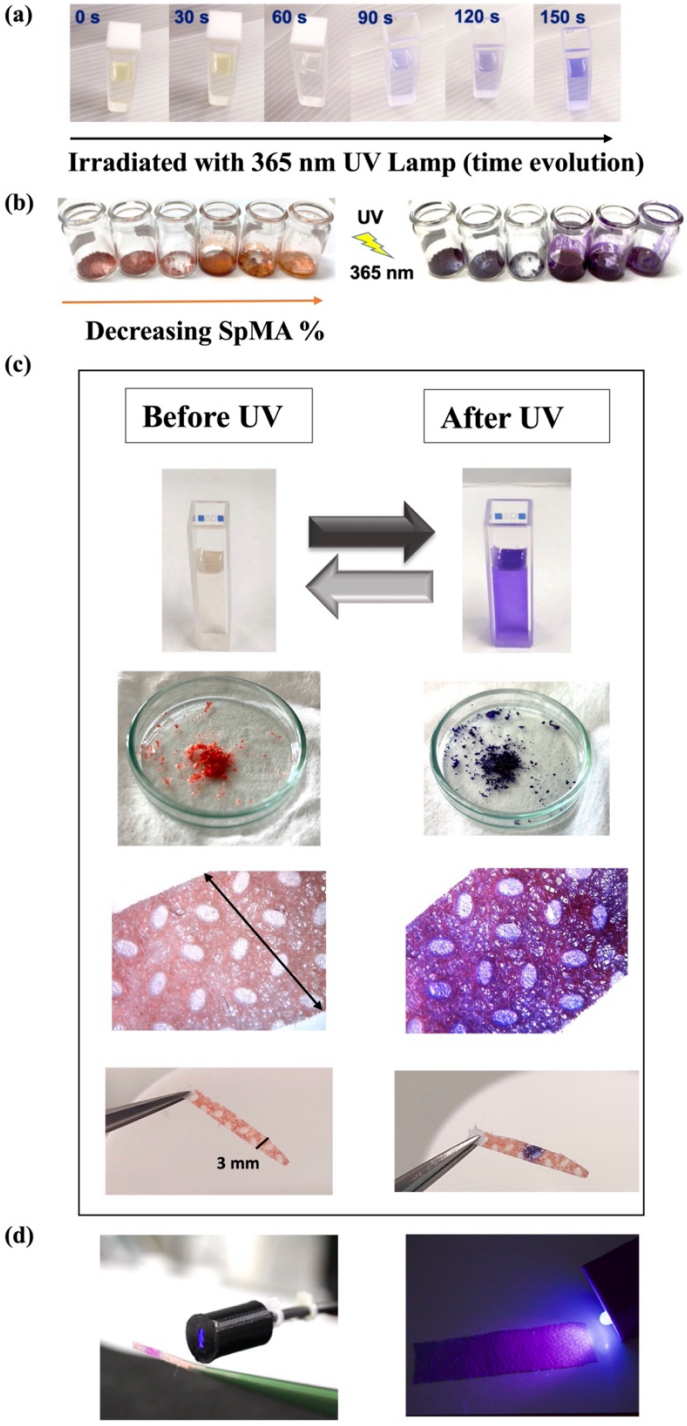

Figure 4.5 (a) Reversible photochromism in P(DEGMA-*co*-SpMA) (1%) copolymer solution with time evolution, (b) solid-state photochromism from SP form to MR form, (c) photochromism in different forms of P(DEGMA-*co*-SpMA) and coatings.

4.1.5 Thermal Analysis

For evaluating the thermal stability of the synthesized polymers, thermogravimetric analysis (TGA) was performed. The thermal stability of the polymer corresponds to its chemical and

microscopic structure and therefore, is of great information to evaluate its use for various applications. [237] As shown in **Figure 4.6 (a),** the thermal degradation of all synthesized SP-containing polymers started above 250 °C and the main mass loss was observed in the temperature range between 300 °C to 400 °C, indicative for their high thermal stability up to 300 °C. Noteworthy, the comparative PDEGMA homopolymer showed a lower degradation temperature of just above 200 °C. Further, while PDEGMA decomposed completely with no residue char left behind, the char residue of the copolymers in the TGA curve also increased with increasing SP content due to more aromatic structures.

Next, differential scanning calorimetry (DSC) measurements were performed for all synthesized polymers in order to assess their glass transition temperatures (**Figure 4.6 (b)**). In accordance with **Figure 4.7 (a),** it was observed that T_g of the P(DEGMA-*co*-SpMA) copolymers increased with an increase in the SP content in the polymers. The glass transition temperature was found to increase linearly from -28.2 °C for copolymer with 1% SpMA to 111.8 °C for copolymer with 70% SpMA content. On the other hand, the homopolymer P(DEGMA) with no SP in it, was found to have the T_g of -37.81 °C. The trend of the glass transition temperatures showed a slight deviation from a linear relation, which appeared indicative of specific interactions or breaking of the local flexible structure, as discussed in a recent study by the group of Liu. [238]

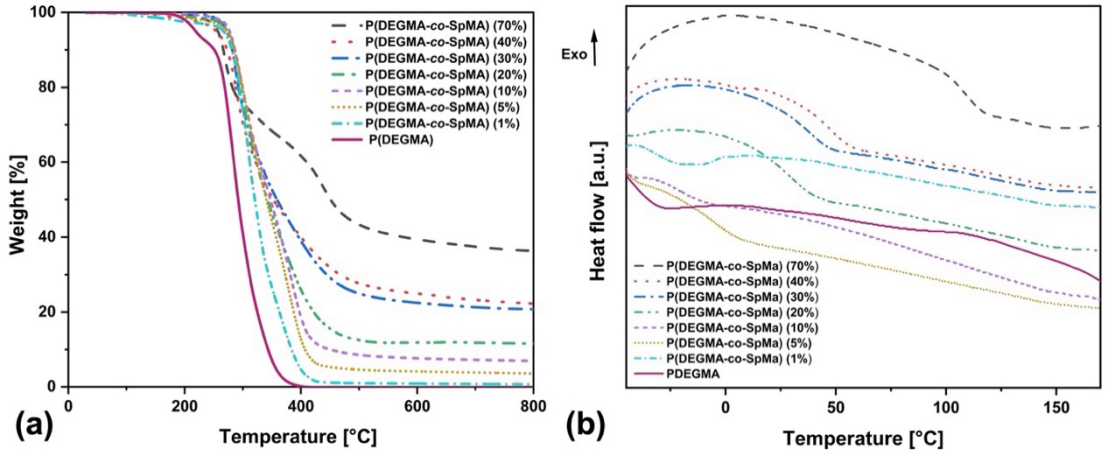

Figure 4.6 (a) TGA profiles and (b) DSC plots of synthesized P(DEGMA-*co*-SpMA) copolymers with different ratios of SpMA.

4.1.6 Photo-switchable Glass Transition Temperature

The glass transition temperature of a polymer can be impacted by different configurations (ring-opened or closed) in the polymer, due to changes in the volume, the stiffness of the

polymer chain, and also interchain cohesion of polymer chain. [88] Thus, it was expected that the photo-isomerization of SP would have an impact on the glass transition temperature. Therefore, differential scanning calorimetry (DSC) measurements were employed to measure the T_g before and after the UV irradiation with 365 nm for 2 minutes, directly on the dried finely powdered polymer samples. The photochromism in the solid polymer samples was visually observed as the orange-colored SP containing polymer changed its color to bright purple. It was found that the glass transition temperature (T_g) increased for all P(DEGMA-*co*-SPMA) copolymers after irradiation, as shown in **Figure 4.7 (b, c) and Table 4.1**.

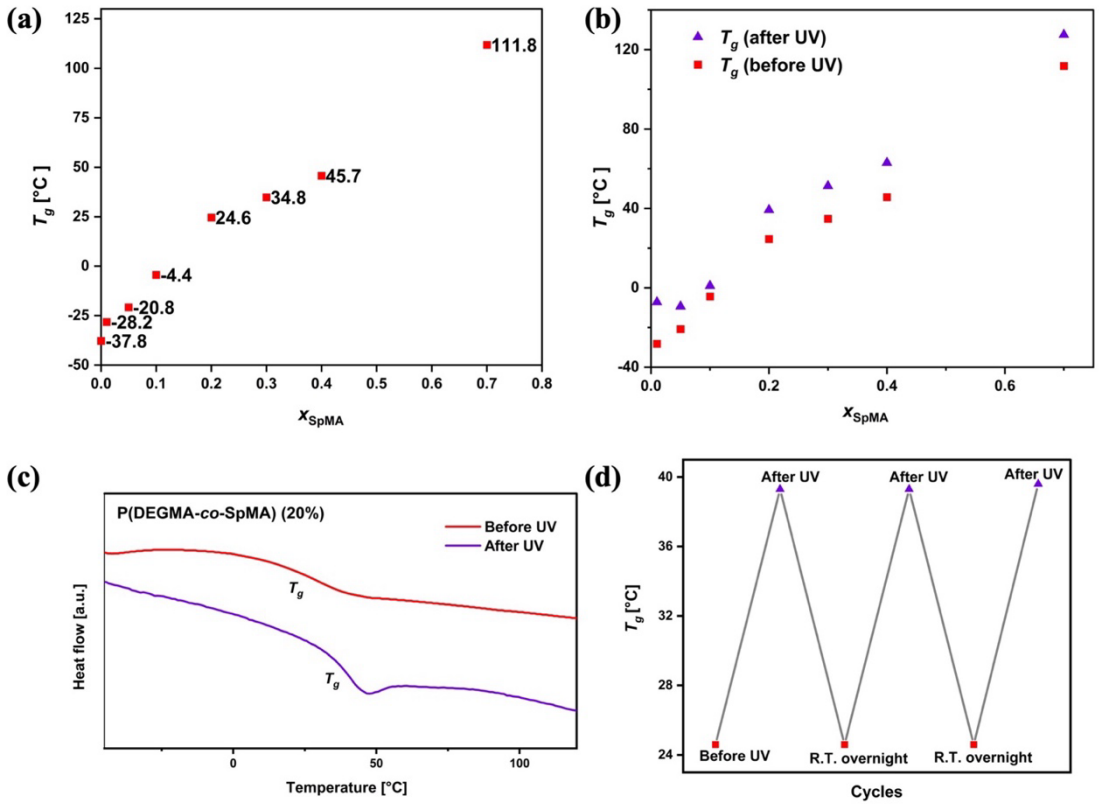

Figure 4.7 (a) Glass transition temperature (T_g) of synthesized P(DEGMA-*co*-SpMA) copolymers with different ratios of SpMA (determined using DSC), (b) Comparative trends of glass transition temperature (T_g) as a function of spiropyran content in the polymers, showing distinct behaviors before and after UV irradiation, (c) Exemplary DSC trace for a photo-switchable T_g before and after UV of P(DEGMA-*co*-SpMA) with 20% SpMA, (d) Graph representing reversibility in T_g with on/off cycles of UV irradiation on P(DEGMA-*co*-SpMA) with 20% SpMA.

Noteworthy, this trend of increasing T_g is exactly opposite to that of the Azo-containing polymer as reported previously. [88] Further, we observed that the ΔT change in T_g (i.e., difference in T_g before and after irradiation) depended very much on the SpMA content in the

polymer and did not follow a linear trend (**Figure 4.7 (b)**). While a rather dramatic change of $\Delta T \approx 20$ °C was observed for the copolymer with 1% SpMA, a minimum of $\Delta T \approx 5$ °C was detected for the copolymer with 10% SpMA.

One possible explanation for the rise in the T_g of the polymers under UV exposure is the increase in polarity of the polymer when SP photo-isomerizes to merocyanine. This increase in polarity can lead to an increase in the intermolecular forces between the polymer chains, making them more closely packed and ordered. This transition from a less-ordered state towards a more ordered state leads to a decrease in the entropy of the polymeric system.
Moreover, due to the viscoelastic nature of the polymers, the glass transition temperature (T_g) of the polymers directly influences their mechanical properties. Additionally, it was also visibly observed that as SP isomerized into MR, the polymers in viscous gel form (with high DEGMA content) become slightly harder, which is likely attributed to a rise in T_g. [239] This photo-induced visible shift in texture of the polymer, as a consequence of increasing T_g on UV irradiation, could also be attributed to the increasing interactions of highly polar merocyanine isomers with the polymeric chains, i.e., the chain mobility is restricted due to the dipole-dipole interaction between the merocyanine and the polymeric chain. [240]

It is worth noting that the exact mechanism behind the elevation in T_g on UV exposure could be complex and depends on several factors, such as specific polymer composition and the degree of SP incorporation.

Furthermore, to confirm the reversibility of the glass transition temperature, DSC measurements were conducted in a cyclic manner: initially before UV exposure, subsequently after UV exposure, and finally after the removal of light, allowing the polymer to rest at room temperature overnight between each cycle. As depicted in **Figure 4.7 (d)**, T_g demonstrated consistent readings throughout these cycles, thus substantiating the reversibility of the glass transition.

4.1.7 Recapitulation

In this chapter, different P(DEGMA-*co*-SpMA) copolymers with variable percentages of incorporated SP were successfully synthesized. All synthesized copolymers were found to undergo instant photo-isomerization in solid as well as solution phase, upon irradiation of UV light at 365 nm. The polymers featured a high thermal stability, with a decomposition temperature of over 250 °C. In addition, they also exhibit instant photochromism and

fluorescence when exposed to UV light. Such properties of SP could be useful for environmental detecting or biosensing. [241, 242] Moreover, a positive correlation was observed between the T_g and the SP content within the polymers, with T_g rising from -28.2 °C in copolymers containing 1% SpMA to 111.8 °C in those comprising 70% SpMA. Most importantly, as a consequence of an increase in polarity and a decrease in the overall entropy of the polymeric system when it switches from the ring-closed SP form to the ring-opened MC form, these copolymers showed an increase in T_g after exposure to UV. Interestingly, this pattern contrasts with the previously reported behavior of azobenzene-containing polymers, where the T_g demonstrated a reverse trend. [243] Additionally, this chapter highlighted that the change in T_g (ΔT), the difference between pre- and post-irradiation, was dependent on the SpMA content. However, this relationship did not exhibit a linear progression. For instance, the copolymer with 1% SpMA experienced a considerable ΔT change of approximately 20 °C, while the copolymer with 10% SpMA revealed a relatively minimal change of ΔT around 5 °C. The research conducted in this chapter provides a pathway for the manipulation of the T_g, thereby advancing our knowledge of T_g as well as broadening the range of applications of these polymeric materials. This unique property of polymers with a photo-tunable glass transition temperature (T_g) and tailored responsive behavior can be exploited for various potential applications like – smart windows [244], optical lenses [245], smart coatings and adhesives [243], etc. This could provide more dynamic control over optical properties. Development of polymers that can switch reversibly between higher and lower T_g forms is a very promising, yet novel approach for functional materials.

4.2 *pH*-responsive Interpenetrating Polymer Networks with *o*-nitrobenzyl Functionalized Polyelectrolyte Complex

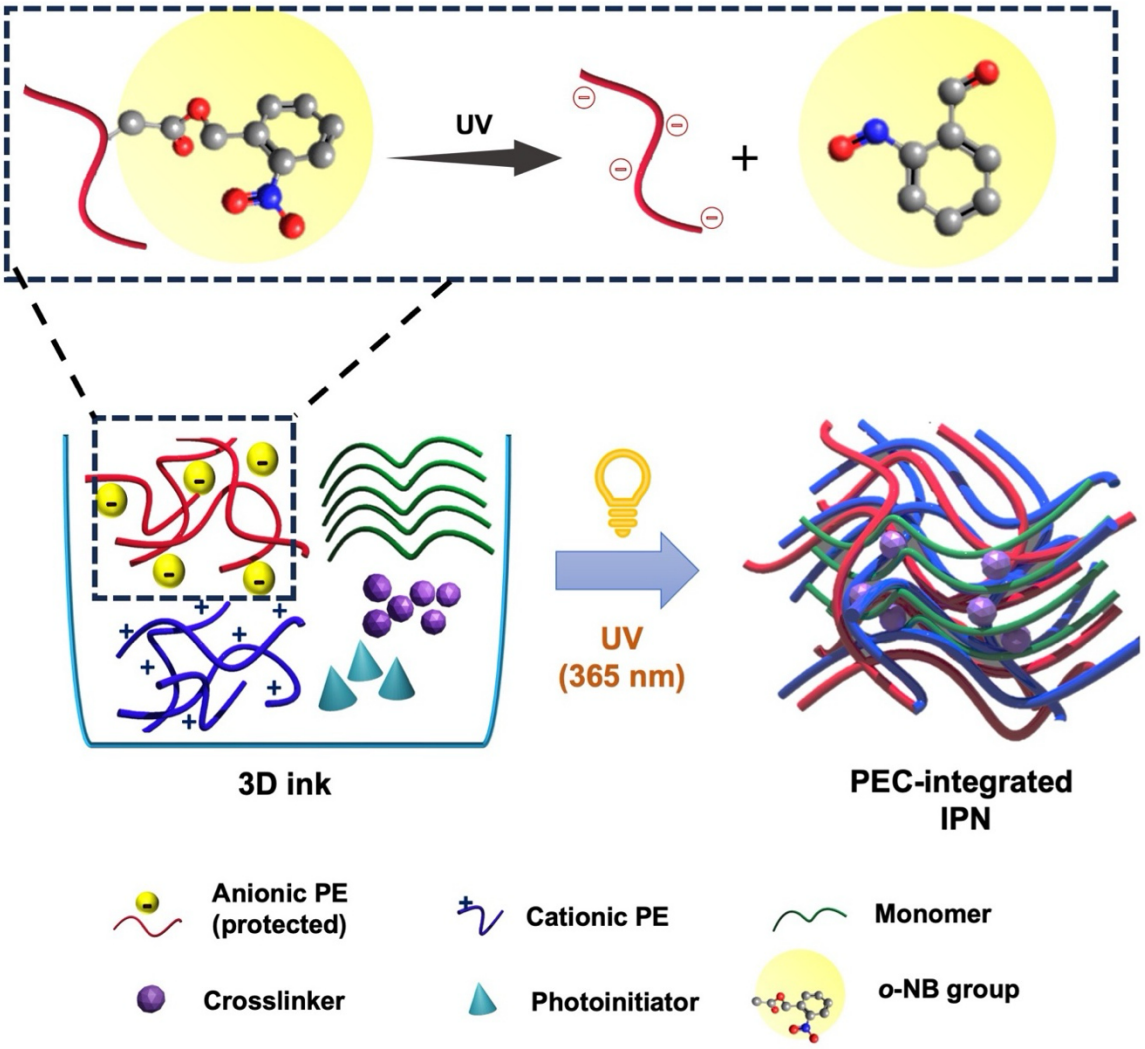

Parts of this chapter and the corresponding experimental section are submitted for publication as "V. Pruthi, V. Hirschberg, P. Théato. "3D Printable Polyelectrolyte Complex- integrated Interpenetrating Network Hydrogels with Customizable Mechanical Strength and *pH*-Responsiveness". Adv. Mater. Technol., 2024, 2400416. https://doi.org/10.1002/admt.202400416 and adapted with permission from Wiley, 2024.

4.2.1 Prologue

Among the photo-sensitive groups, *o*-nitrobenzyl (*o*-NB) derivatives have garnered significant attention due to their irreversible photolytic response to light stimuli. As discussed in **Chapter 2.4.3**, these derivatives are highly valued for their exceptional photolysis performance, ease of manufacturing, advantageous solubility characteristics, and the breadth of chemical functionalization methods available. [22] Exploiting the photo-labile characteristics of the *o*-NB group, this chapter presents an innovative methodology for fabricating *pH*-responsive interpenetrating polymer network (IPN) hydrogels through the utilization of advanced 3D printing technique. Moreover, as discussed in **Chapter 2.5.3,** the inclusion of Polyelectrolyte Complex (PEC) in IPN results in a cooperative enhancement of the mechanical characteristics of hydrogel networks. [191] This study advances the frontier by further investigating the sophisticated methodologies for 3D printing of PEC-embedded IPN structures.

Herein, IPNs have been deftly crafted by incorporating a PEC of HA and CS within a P(OEGMA-*co*-EGDEMA) matrix, with the carboxyl groups of HA modified by *o*-NB group to delay PEC formation during 3D ink development. The irradiation with UV subsequently leads to the simultaneous deprotection of HA and the crosslinking of the hydrogel, synthesizing a PEC-integrated IPN. A comprehensive suite of analytical methods, including mechanical testing and *pH*-responsive swelling analyses, have been utilized to assess the structural integrity and functional performance of the hydrogels.

4.2.2 Synthetic Strategy

For the fabrication of PEC-containing IPN hydrogels, the initial step is to prepare the photo-resin (3D ink) and optimize its composition. The strategy is to enable simultaneous photo-deprotection and photopolymerization in the photo-resin when exposed to UV light. **Figure 4.8** illustrates the method employed for the formulation of 3D ink.

To do so, naturally available, oppositely charged biopolymers - chitosan (CS) (a cationic polyelectrolyte) and hyaluronic acid (HA) (an anionic polyelectrolyte), were employed. Firstly, in order to avoid the PEC formation before printing, the carboxyl groups of HA were protected using an *ortho*-nitrobenzyl photo-labile protecting group (PPG). On exposure to UV light at 365 nm, the PPG is cleaved due to photo-induced deprotection and the COOH functionality is restored, which leads to the formation of PEC. Further, to induce photopolymerization in the 3D ink, oligo(ethylene glycol) methyl ether methacrylate (OEGMA), ethylene glycol

dimethylacrylate (EGDEMA) and lithium phenyl-2,4,6-trimethylbenzoylphosphinate (LAP) were used as a polymerizable vinyl monomer, crosslinker and water-soluble photoinitiator (PI), respectively. LAP is a suitable candidate for 3D inks to form hydrogels as it offers a balance between biocompatibility as well as photon absorption, along with a high polymerization rate at low concentrations. [203]

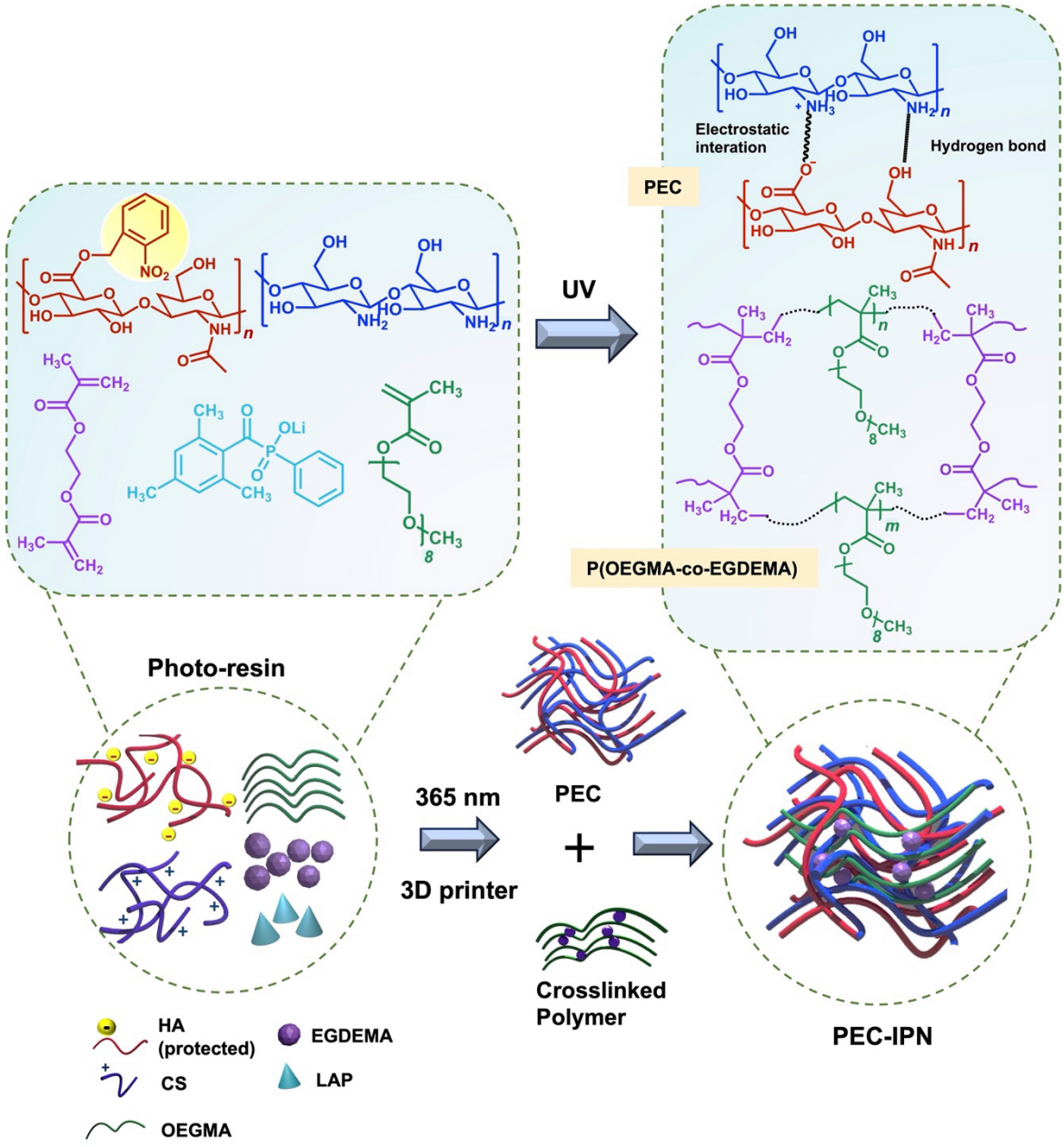

Figure 4.8 Conceptual diagram detailing the methodology for 3D ink formulation.

4.2.3 Protection and Deprotection of HA using Photo-labile *o*-NB Group

Protection:

The photo-labile protection of the carboxyl group on HA was achieved by grafting the *o*-NB groups onto carboxylic acid groups of HA chains through an ester linkage (**Scheme 4.2**). The HA salt was esterified with *ortho*-nitrobenzyl chloride, resulting in the formation of *o*-NB HA ester. By varying the amount of *ortho*-nitrobenzyl chloride added to the mixture, various *o*-NB grafted HA derivatives were obtained.

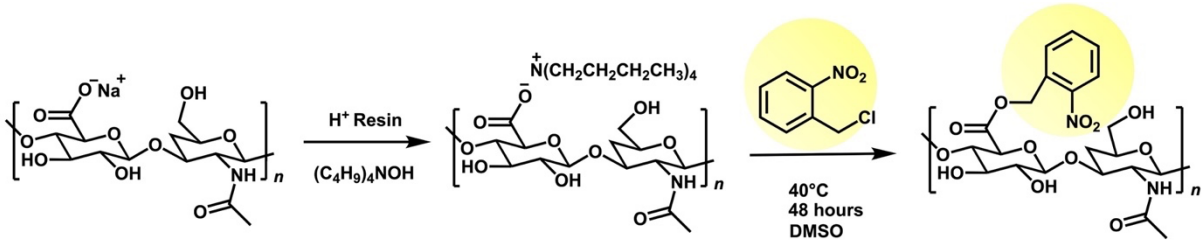

Scheme 4.2 Synthetic route for the protection of HA using *ortho*-nitrobenzyl photo-labile protecting group.

The esterification was confirmed using the ^{1}H NMR of HA-NB (**Figure 4.9 (a)**). ^{1}H NMR of the obtained *ortho*-nitrobenzyl ester of HA showed the characteristic shifts at 7.5 to 8.2 ppm for the aromatic (-C_6H_4-), along with the shifts at 3.1 to 4 ppm. The *o*-NB grafting degree was calculated by integrating the NMR signal from the aromatic protons in the *o*-NB group and the NMR signals from the anomeric protons of the disaccharide units in HA. The IR spectra of the product further validated the presence of the *ortho*-nitrobenzyl group (**Figure 4.9 (b)**). The characteristic bands of the -NO_2 group were observed at 1526 cm^{-1} and 1346 cm^{-1}, and the ester peak at 1750 cm^{-1}. Moreover, UV/vis spectroscopy was conducted for various HA-NBs with different grafting degrees, dissolved in water at a concentration of 0.2 mg/mL. The resulting spectra are depicted in **Figure 4.11 (a).**

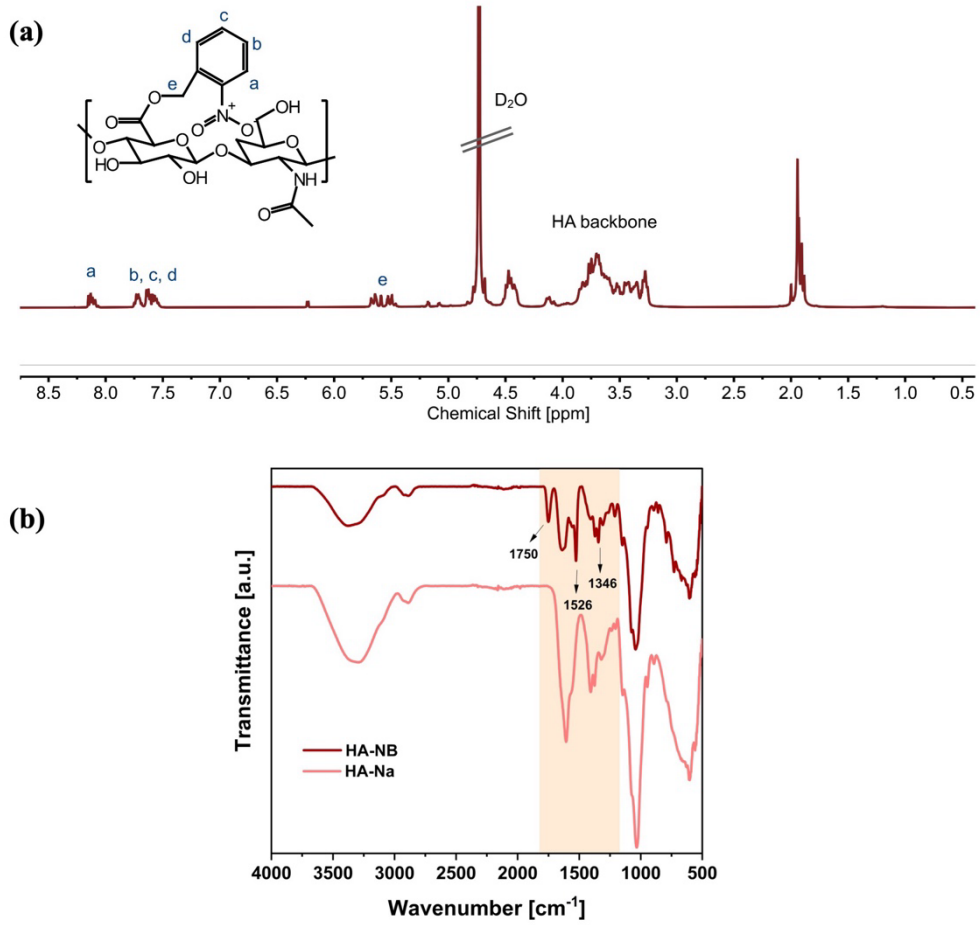

Figure 4.9 (a) ^{1}H NMR spectra of HA-NB in D_2O (400 MHz, 298 K), (b) IR spectra comparing HA-Na and HA-NB.

Photo-deprotection:

The *o*-NB protecting group can be easily cleaved when irradiated with UV light (365 nm), as shown in **Scheme 4.3.** Upon UV exposure, the *o*-NB ester linkage undergoes a photo-induced cleavage upon UV irradiation, resulting in the release of HA and the formation of a nitrosobenzaldehyde byproduct. This could be confirmed by the ^{1}HNMR spectra at different intervals of UV irradiation on HA-NB as shown in **Figure 4.10 (a).** The new peaks arising at 9.36 ppm and 10.25 ppm, representing the aldehyde CHO group in nitrosobenzaldehyde and the free COOH carboxylic acid group of HA, respectively, confirm the deprotection of HA-NB.

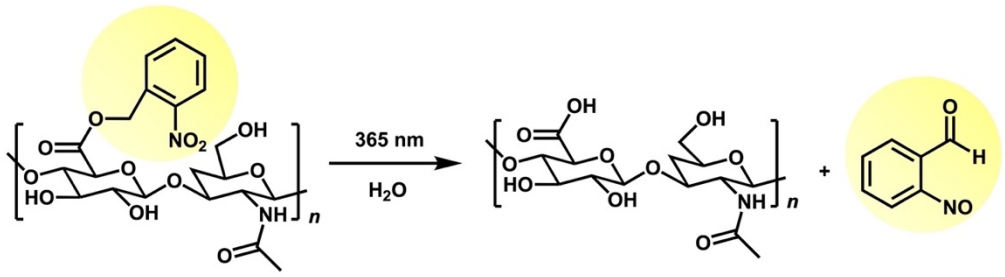

Scheme 4.3 Deprotection of *ortho*-nitrobenzyl ester of HA (HA-NB).

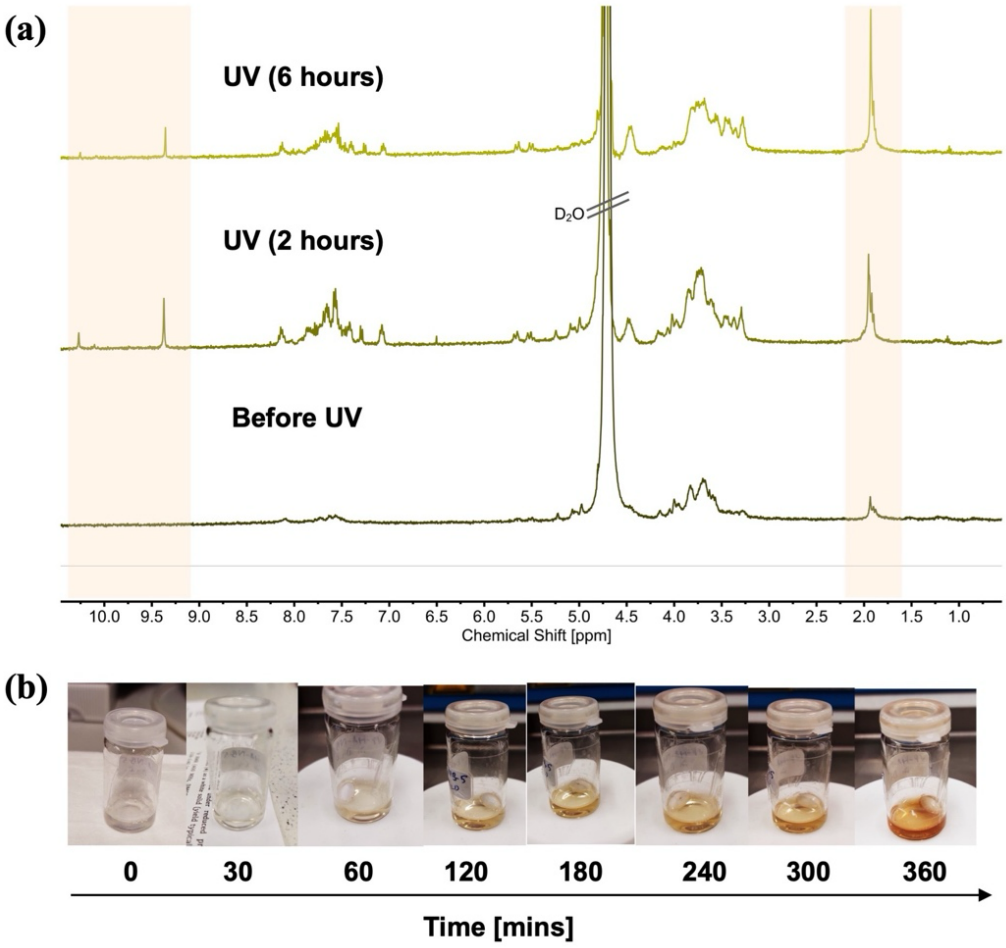

Figure 4.10 (a) ^{1}H NMR spectra (400 MHz, 298 K) presenting the deprotection process of HA-NB in D_2O at distinct photo-irradiation time intervals, (b) time-dependent colour transition in HA-NB solution under UV light exposure.

A change in the color of the HA-NB solution was noted when exposed to UV ($\lambda \sim 365$ nm) over a period of time, transitioning from a light yellow ($t = 0$ min) to a deeper yellow hue ($t =$ 360 mins) (**Figure 4.10 (b)**). The photo-deprotection of the HA-NB derivative was also studied using UV/vis spectroscopy (**Figure 4.11 (b)).** The time taken for photocleavage also depended on the intensity of light irradiated and the degree of NB grafting on HA. [163]

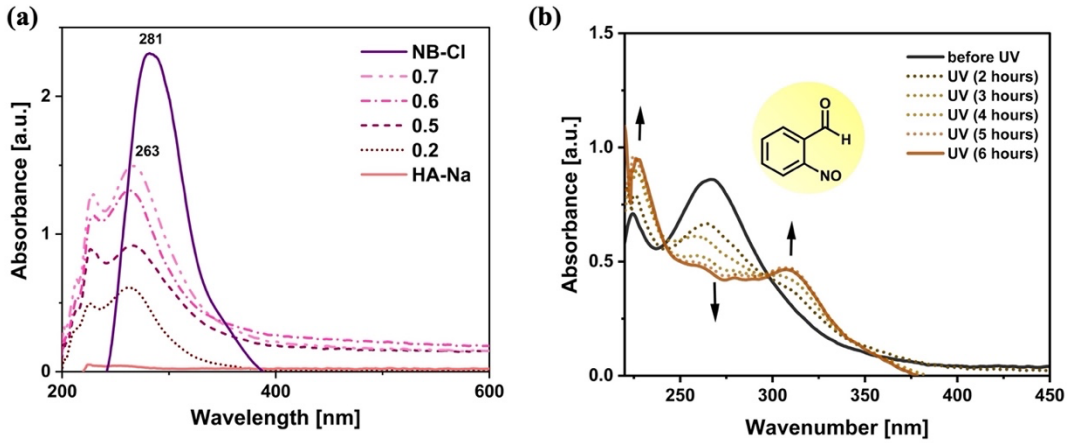

Figure 4.11 (a) UV-Vis absorption spectra of HA-NBs highlighting variations in grafting degrees, (b) UV/Vis absorption profiles demonstrating the deprotection of HA-NB upon UV exposure at various intervals (note: all spectra were acquired in D_2O at a concentration of 0.2 mg mL^{-1}).

4.2.4 Synthesis of Photopolymerized Hydrogels

All the photopolymers were first synthesized using the standard cast-mold technique, employing a UV lamp with a 365 nm wavelength as the illuminating source. The optimized compositions for the photo-induced syntheses of the hydrogels are detailed in **Table 4.2**.

Photo-crosslinkable P(OEGMA-*co*-EGDEMA) Hydrogel:

A variety of photopolymers were produced by adjusting the amounts and combinations of three components: OEGMA as the monomer, EGDEMA as a crosslinker, and LAP as the PI. The mixture was subjected to UV light (365 nm) for the fabrication of hydrogels. The crosslinker ratio was tuned to adjust the crosslinking density, with an excess potentially leading to brittleness. Also, the PI concentration was regulated to refine the speed and efficiency of curing. An optimal concentration range of 2- 4 mol% for EGDEMA and 1 wt % LAP was determined. The completion of crosslinking and photopolymerization was confirmed through the use of infrared (IR) spectroscopy. As depicted in the IR spectra (**Figure 4.13 (a)**), the C=C bonds in the methacrylate group (1637 cm^{-1}) of OEGMA and EGDEMA disappeared after photopolymerization and symmetric methylene stretching ($-CH_2$) at 2870 cm^{-1} remained as it does not participate in the polymerization.

PEC Hydrogel of HA-NB and CS:

PEC hydrogels were prepared by mixing different proportions of HA-NB and CS to optimize the ratio that would result in a stable hydrogel film. The hydrogel comprising HA-NB/ CS with

the ratio of 1:1 was found to be the most stable, probably as a result of maximum complexation due to the strongest ionic interaction. As shown in **Figure 4.12 (b)**, the IR spectra of dried PEC film was compared with that of HA-NB and CS. The IR spectra of PEC showed bands between 1560 cm^{-1} and 1650 cm^{-1} representing C=O, N-H and C-N vibrations. It confirms the ionic interaction between carboxylic acid group of HA and amine group of CS, hence the formation of PEC. Moreover, a slight shift in the position and changes in the intensity and shape of the O-H and N-H (~3200 to 3600 cm^{-1}) bands in PEC spectra also could be seen as a result of hydrogen bonding between HA and CS.

Semi-IPN Hydrogel containing Hyaluronic acid or Chitosan:

The formation of semi-IPNs comprised of either HA or CS involved dissolving them separately with a trio of OEGMA, EGDEMA, and LAP, and using UV light to induce gelation. The concentration of polyelectrolyte was varied in order to optimize the dissolution of the mixture and the stability of the hydrogel. **Figure 4.12 (c)** displays the IR spectra of semi-IPN containing HA, highlighting the distinctive bands of both HA and P(OEGMA-*co*-EGDEMA). Similarly, it presents the IR spectra for the semi-IPN with CS, emphasizing the characteristic bands of CS and P(OEGMA-*co*-EGDEMA).

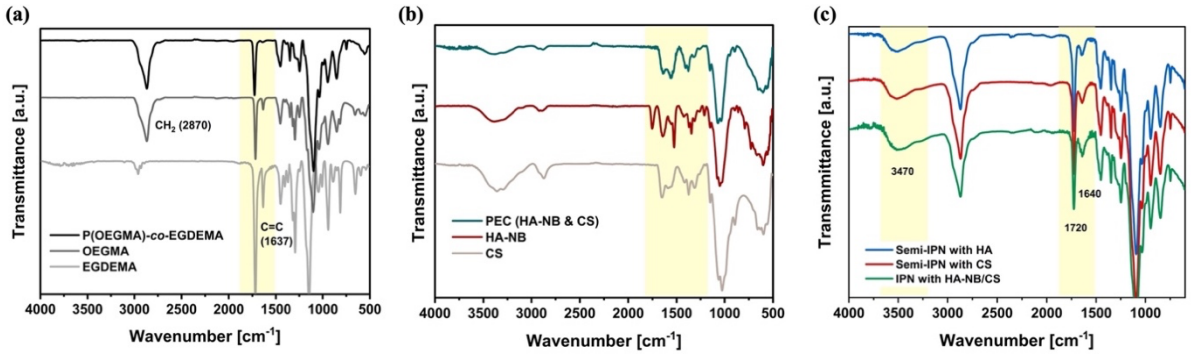

Figure 4.12 IR spectra of (a) P(OEGMA-*co*-EGDEMA) hydrogel alongside its individual components: OEGMA and EGDEMA, (b) PEC(HA-NB/CS) in comparison to HA-NB and CS, (c) Semi-IPNs and IPN hydrogels.

Polyelectrolyte Complex (PEC) containing IPN Hydrogel:

PEC-incorporated IPN hydrogels with varying properties were fabricated by using HA-NBs with different grafting degrees (0.2 to 0.7) and by adjusting the ratio of the HA-NB and CS components (i.e., 1:1, 1:2, 2:1) in the blend, containing OEGMA, EGDEMA and LAP. The proportions of polyelectrolytes were varied to investigate their effect on the degree of ionic interaction and complexation within the hydrogel. The simultaneous photopolymerization and

photocleavage of *o*-NB ester linkage was achieved by exposure to UV light (365 nm). The IR spectrum of IPN with PEC (HA-NB/CS) is shown in **Figure 4.12 (c)** which also displays the band at 1640 cm^{-1}, confirming the ionic interaction between HA and CS. **Figure 4.13 (a, b)** displays the IPN hydrogels produced using the invert-vial method, while **Figure 4.13 (c)** showcases the lyophilized hydrogel.

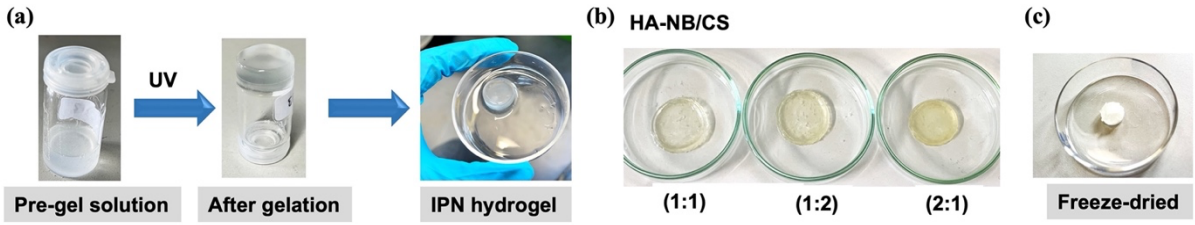

Figure 4.13 (a) Visualization of IPN (HA-NB/CS) hydrogel formation via the invert-vial technique, (b) IPNs with different proportions of HA-NB and CS, (c) lyophilized (freeze-dried) IPN hydrogel.

Table 4.2 Composition for the photo-induced synthesis of hydrogels.

Photopoymerized hydrogel	OEGMA (g)	EGDEMA (mol %)	LAP (wt %)	HA (mg)	HA-NB (mg)	CS (mg)	Gelling time [a)] (mins)	Elastic Modulus[b)] (kPa)
P(OEGMA-*co*-EGDEMA)	0.5	3	1	-	-	-	5	1
Semi-IPN with CS	0.5	3	1	-	-	2.5	5	4
Semi-IPN with HA	0.5	3	1	2.5	-	-	5	2
IPN (HA-$NB_{0.5}$/CS)1:1	0.5	3	1	-	2.5	2.5	15	8
IPN (HA-$NB_{0.5}$/CS)1:2	0.5	3	1	-	5.0	2.5	15	6.5
IPN (HA-$NB_{0.5}$/CS)2:1	0.5	3	1	-	2.5	5.0	15	7

[a)] Gelling time was calculated by measuring the time it takes for a liquid precursor to form a gel); [b)]Elastic modulus was determined through rheological assessments.

3D Hydrogel Ink Formulation:

To achieve the desired crosslinking density, mechanical properties, curing efficiency, and printability of the hydrogels, the photo-resin's optimized composition was established through

the synthesis methods mentioned earlier. It was scaled up in order to prepare sufficient ink (~10 mL) in the resin tank, to process the printing. A PEC-integrated IPN hydrogel ink was prepared by dissolving the solution of 50 mg HA-NB in water, 10 g OEGMA, 0.079 g EGDEMA (2 mol %) and 0.10 g LAP (1 wt%) solution in 3 mL water. Then, a solution of 50 mg CS in 1% AA was added to the mixture. The mixture was stirred for 15 mins to completely dissolve all the components. Once a homogenous mixture was obtained, it was then poured into the resin tank of the DLP 3D printer for printing.

4.2.5 3D Printing of Hydrogels

Figure 4.14 (a) displays a schematic representation of the protocol employed for the 3D printing of hydrogels using the 3D ink optimized in the previous step. In order to print the hydrogels, the components of the 3D ink were blended together to prepare a homogenous mixture and this ink was then transferred to the resin bath of a Digital Light Processing (DLP) printer.

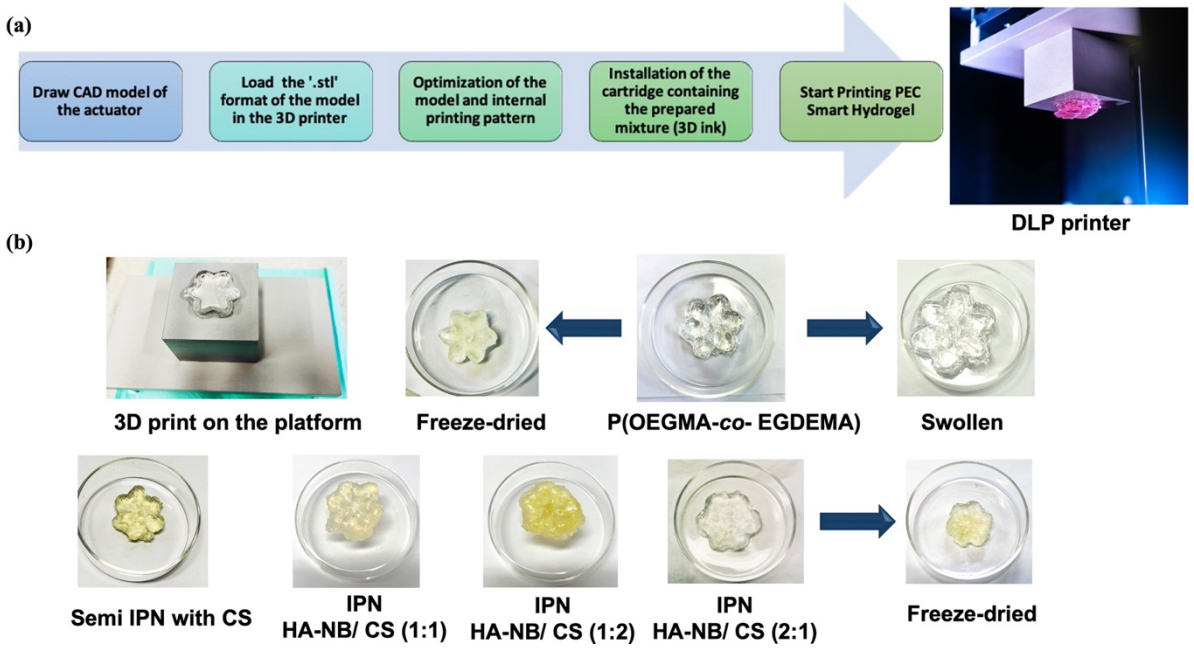

Figure 4.14 (a) Schematic representation of the protocol employed for 3D printing of hydrogels, (b) photographic captures of 3D printed hydrogels (printed using Miicraft Hyper 80x 3D printer with UV=365 nm).

When optimizing the 3D ink formulation, the interplay between the chemistry of the ink and the DLP printer settings was considered. The photo-resin was tuned to adjust the ink's viscosity (by varying the ratio of constituents) and curing depth (by modifying the PI composition). Additionally, the printing parameters such as- light intensity (365 nm), base curing exposure

time (50 s), layer thickness (20 µm)and printing speed (slow) were adjusted in order to refine the printed material. (More details are mentioned in **Experimental Section, Table 6.1).** PEC-based IPN hydrogels with variable compositions of HA-NB and CS were successfully printed as shown in **Figure 4.14 (b).**

4.2.6 Properties of Hydrogels

4.2.6.1 Swelling Properties

Swelling was measured in terms of the percentage increase in weight, indicating the amount of water the hydrogel had absorbed. The graph representing the comparison in the swelling percentage of all the hydrogels is depicted in **Figure 4.15 (a)**. The hydrogel pictures in **Figure 4.15 (b)** clearly show the remarkable difference in the size of the hydrogels when swollen till equilibrium.

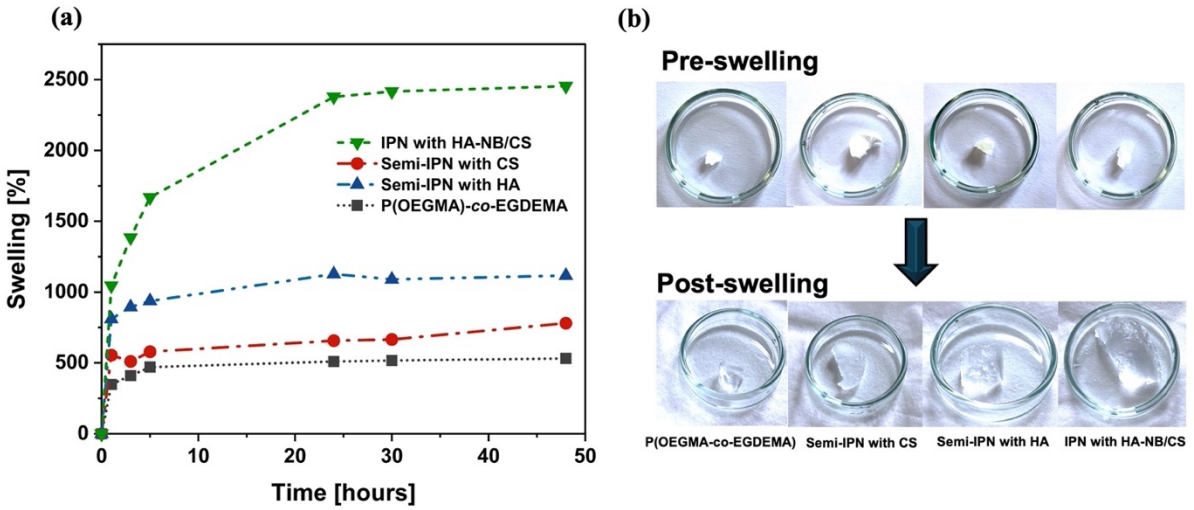

Figure 4.15 (a) Comparative analysis of swelling percentages among various hydrogels, (b) Representative images of hydrogels pre- and post-swelling.

The comparative trend observed in the swelling is as follows:

IPN hydrogels > Semi-IPN hydrogels > P(OEGMA-*co*-EGDEMA) hydrogel, with the equilibrium swelling percentages as follows: PEC-integrated IPN hydrogels at 2455%, Semi-IPN with HA at 1127%, semi-IPN with CS at 780%, and P(OEGMA-*co*-EGDEMA) hydrogel at 532%. The pronounced swelling ability of the polyelectrolyte IPN gels can be attributed to the electrostatic forces that drive the charged groups on the polymer chains apart. [246] Both HA and CS, being natural polysaccharides, possess hydrophilic characteristics, though they differ slightly in their water retention abilities.

4.2.6.2 *pH*- responsiveness

The swelling behavior of the synthesized hydrogels was also investigated at different *pH* values of *pH* 1, 3, 5, 7 and 11. As depicted in **Figure 4.16,** the IPN hydrogels exhibited maximum swelling at *pH*=3 and minimum at *pH*= 5. At *pH*=7, the swelling again increased and was observed to be higher at pH=11. This could be explained as PEC hydrogels are created through ionic interaction and the extent to which they swell is governed by the *pH*-responsive charge interactions of the two polymers. [247] Furthermore, they possessed a notable water content and high electric charge, facilitating the diffusion of water. [248] When *pH* changed, the charge balance as well as the degree of interaction between HA and CS also fluctuated. The lowest swelling occurred when pK_a(anionic)<*pH*<pK_a(cationic). [72] pK_a of HA and CS are 3 and 6.5, respectively. Therefore, at low *pH*, amino groups of CS are ionized and at *pH* >6.5, carboxyl groups of HA are ionized, resulting in higher swelling. The swelling ratio is least at *pH*=5, as a result of strong electrostatic interactions between the polyelectrolytes.

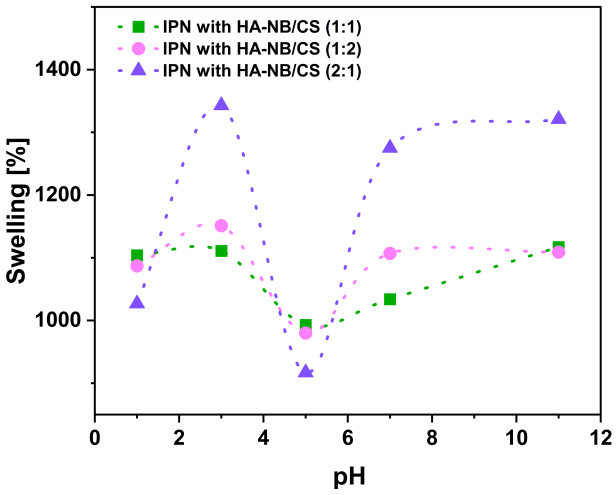

Figure 4.16 *pH*-responsive swelling behavior of IPN hydrogels with varying polyelectrolyte content. The connecting lines are merely for the visual guidance.

Additionally, swelling was also dependent on the relative proportion of polyelectrolytes in PEC as illustrated in **Figure 4.16.** This is attributed to the change in the degree of interaction and crosslinking density in the PEC. [248] Therefore, it is possible to modulate the properties of PEC-IPN hydrogel by tuning its composition. Hydrogels of this nature, characterized by *pH*-responsive swelling and adjustable attributes, hold immense potential across a wide array of applications, including drug delivery systems and the field of soft robotics.

4.2.6.3 Thermal Properties

Thermal characterization of the synthesized hydrogels was performed by employing Thermogravimetric Analysis (TGA) and Differential Scanning Calorimetry (DSC) techniques to provide a comprehensive understanding of their thermal stability and durability. **Figure 4.17 (a)** represents the comparative TGA curves for the freeze-dried hydrogels. All the fabricated hydrogels showed a high thermal decomposition temperature (T_d (5%)) ranging between 220 to 290 °C, indicating high thermal stability levels. Such resilience to heat ensures that these hydrogels can be employed across various applications where elevated temperatures are encountered, maintaining their integrity and functional performance without degradation. Furthermore, the DSC graphs of the swollen hydrogel samples are illustrated in **Figure 4.17 (b)**. DSC serves as a crucial method for identifying the physical state of water within the hydrophilic polymer. [249] The DSC of all hydrogels showed an endothermic peak at around 1 °C and 10 °C which is probably attributed to the melting of freezing bound water and freezing free water in the hydrogels, respectively. Additionally, the endothermic peak representing the vaporization of non-freezable bound water, varying from 107 °C in semi-IPNs, 110 °C in IPN and 114 °C in P(OEGMA-*co*-EGDEMA) can be observed. This variation could be associated with the changes in the degree of crosslinking, water-polymer interactions and hydrophilicity. [250] The interplay among the charged polymer chains present in HA and CS introduces a subtle shift in the peak and gives rise to an additional shoulder on the DSC curve.

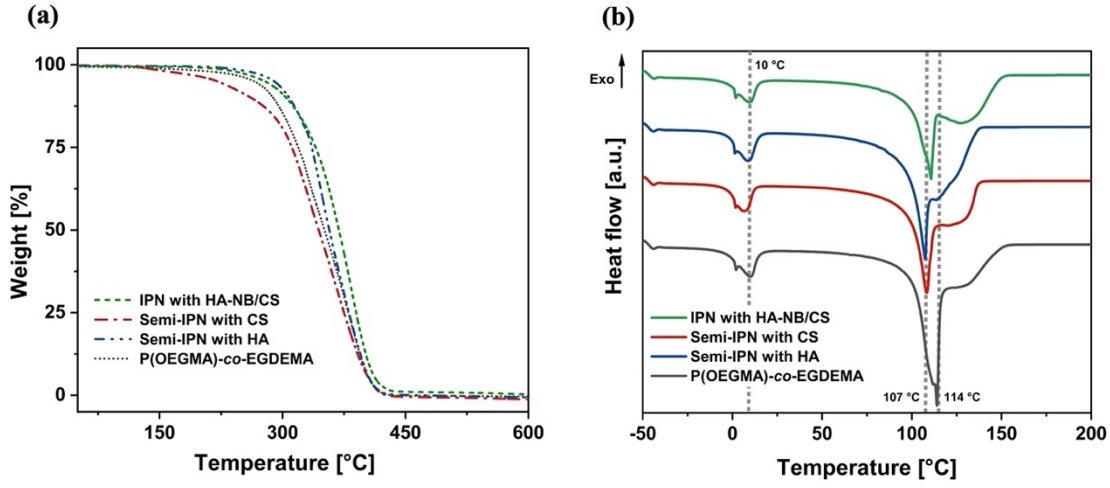

Figure 4.17 (a) TGA profiles and (b) DSC plots of P(OEGMA-*co*-EGDEMA), Semi-IPNs and IPN hydrogels.

4.2.6.4 Morphological Properties

Figure 4.18 shows scanning electron microscopy (SEM) images of freeze-dried P(OEGMA-*co*-EGDEMA), semi-IPN with CS, semi-IPN with HA and IPN with HA-NB/CS (1:1) hydrogels. The observed porosity in these hydrogels aligns well with the swelling percentage calculated for each hydrogel. This is due to the fact that the equilibrium water uptake of hydrogels notably rises with an increase in porosity. [251] Moreover, the different components in the semi-IPN and IPN structures had distinct effects on the porosity of the hydrogels. Introducing HA to the hydrogel resulted in a greater increase in porosity compared to adding CS. This could be due to their different interactions with the polymer matrix. Further, the combination of HA and CS in the IPN, containing P(OEGMA-*co*-EGDEMA) resulted in the largest pores, suggesting a potential synergistic effect or complexation between these components. This could be attributed to the entropy and strong electrostatic attraction between the oppositely charged polymers. [252]

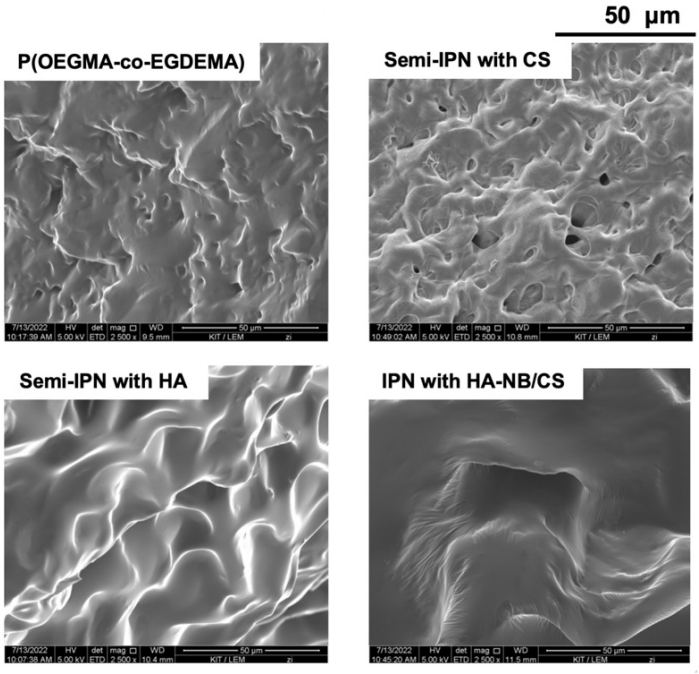

Figure 4.18 SEM micrographs of the synthesized hydrogels illustrating the differential porosity (Magnification =2500x).

4.2.6.5 Tunable Mechanical Properties

To analyze the mechanical behavior of the prepared hydrogels and to understand the influence of different components on their mechanical properties, strain and frequency-dependent shear rheology to study the flow behavior and uniaxial compression tests were conducted to measure

the storage modulus (elastic modulus, G') at room temperature (20 °C) and angular frequency ranging from 0.1 to 100 rad/s. [253, 254]

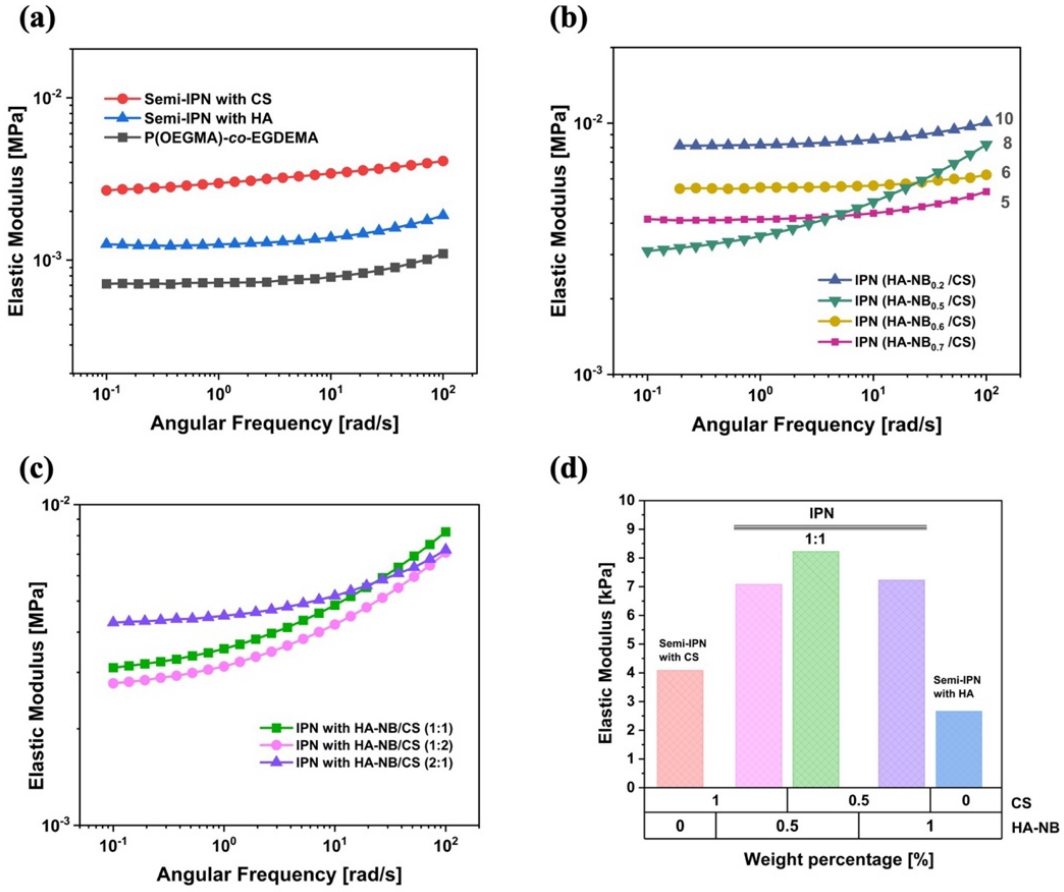

Figure 4.19 (a) Frequency sweep analyses demonstrating the viscoelastic properties via elastic modulus measurements for P(OEGMA-*co*-EGDEMA), Semi-IPNs, and IPN hydrogels, (b) viscoelastic evaluation of IPNs integrated with HA-NB of varied grafting degrees, (c) elastic modulus assessments of IPNs containing diverse ratios of polyelectrolytes, (d) relationship between elastic modulus and weight percentage of various polyelectrolytes at an angular frequency of 100 rad/s.

As illustrated in **Figure 4.19 (a)**, introducing a polyelectrolyte into the P(OEGMA-*co*-EGDEMA) hydrogel network increased G', thereby enhancing the hydrogel's stiffness. Furthermore, the Semi-IPN with CS integrated into P(OEGMA-*co*-EGDEMA) exhibited a stiffer network (G' ~4 kPa) compared to the Semi-IPN with integrated HA (G' ~2 kPa). IPNs that incorporated PEC (HA/CS) displayed even higher G' values (ranging from 5 to 10 kPa). This increase is attributed to heightened molecular interactions, complex formation, and higher crosslinking density due to the presence of two crosslinked networks within the IPN hydrogel system. Consequently, PEC-IPN hydrogels with different mechanical strengths were achieved

using HA-NB with varying grafting ratios of the *o*-NB group. **Figure 4.19 (b)** showcases how G' changed in relation to the grafting degree of NB. Notably, as the grafting degree of HA-NB decreased, G' increased. This phenomenon could be linked to a higher degree of complexation and a more compact network structure in IPN(HA-$NB_{0.2}$ /CS) (G'=10 kPa) with the least grafting degree of HA-NB. **Figure 4.19 (c)** further illustrates the impact of the ratios of HA-$NB_{0.5}$ and CS on G' of the PEC-integrated hydrogel. It is evident that by altering the structure and composition of networks, their mechanical properties can be tailored to suit specific application needs. Notably, the IPN with a (HA-$NB_{0.5}$/CS) ratio of 1:1 exhibited a higher G' (8 kPa) compared to the 1:2 and 2:1 HA-$NB_{0.5}$:CS ratios. **Figure 4.19 (d)** displays a bar graph that highlights the variations in the hydrogels' elastic modulus based on their different compositions. When HA-NB is integrated with CS in IPN, the resultant elastic moduli are higher than those in semi-IPNs consisting solely of HA and CS. This could be ascribed to the optimal synergy and strong electrostatic interaction in PEC, resulting in a more structurally cohesive and mechanically robust network. [191]

Compression Tests:

Moreover, compression tests were also performed for all the hydrogels for comparative analysis. As depicted in **Figure 4.20,** these hydrogels could endure substantial strain without breaking. The IPN hydrogel featured in **Figure 4.21 (a)** demonstrated its durability by resisting breakage even under intense compression at a strain of 80%. As illustrated in **Figure 4.21 (b)**, the IPN hydrogel was also subjected to a manual compression and recovery test, showing its ability to return to its initial state. Therefore, all the fabricated hydrogels demonstrated good mechanical properties, and outstanding compression properties, coupled with high flexibility and stretchability.

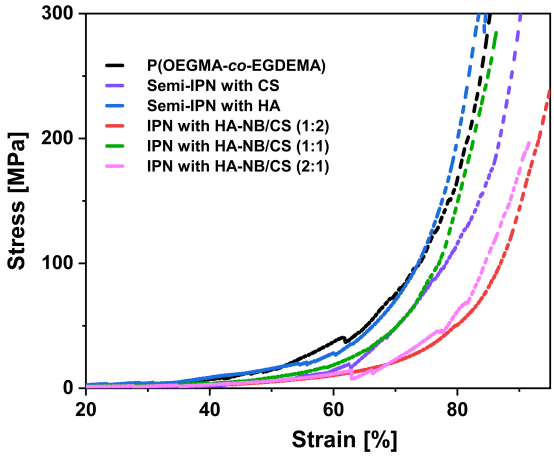

Figure 4.20 Stress-strain profiles derived from compressive testing of hydrogels.

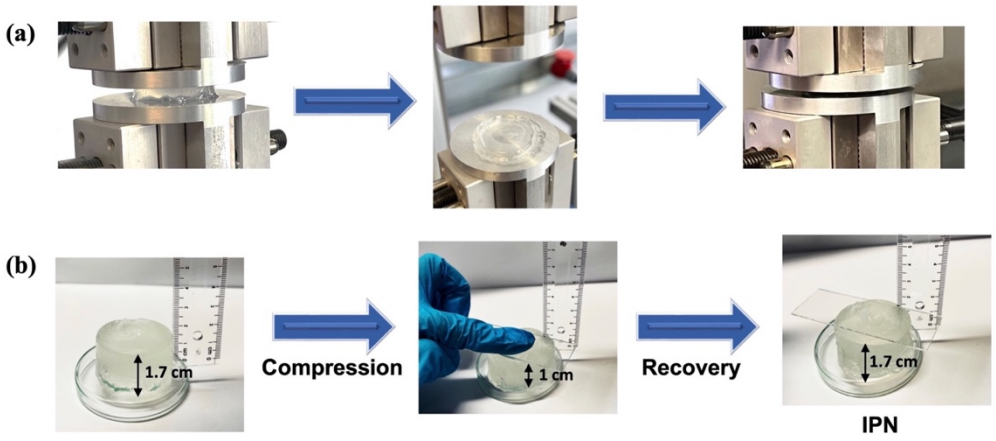

Figure 4.21 (a) Depiction of hydrogel resilience, maintaining integrity even under substantial compression at a strain of 80%, (b) visual demonstrations of hydrogels subjected to manual compression and subsequent recovery evaluations.

4.2.7 Recapitulation

In this chapter, a novel approach for the fabrication of IPN hydrogels is presented by skillfully combining the PEC of HA and CS with a photo-crosslinked network of P(OEGMA-*co*-EGDEMA) polymer. Firstly, the carboxyl group on HA is modified with a photo-labile *o*-NB group to avoid the early formation of the PEC during 3D ink development. This alteration culminated in a dynamic UV-mediated process, wherein the carboxyl group was photo-deprotected and the OEGMA hydrogel was crosslinked in a simultaneous action. In-depth characterizations of the hydrogels underscored their structural, morphological, and rheological properties. Additionally, their swelling dynamics as well as their *pH* sensitivity were evaluated. The IPNs with variable compositions were successfully printed using DLP. The fabricated IPN hydrogels created had mechanical attributes spanning 5 to 10 kPa, displaying significant flexibility, commendable compression resistance, and high strain tolerance. In conclusion, the research in this chapter presents a promising approach for the fabrication and 3D printing of PEC-integrated IPN hydrogels with regulated swelling and the maintenance of structural stability, mechanical robustness, and intrinsic functions within the hydrogels. Their *pH* sensitivity and excellent thermal resilience further solidify their potential. At its core, this strategy harmoniously melds the innate attributes of natural polyelectrolytes with contemporary 3D ink refinement techniques, offering a cost-efficient and dependable approach. The potential of this technique is vast, with promising implications for areas such as- biomimetics and soft robotics.

4.3 Dual Responsive Azobenzene-incorporated Polymer Networks

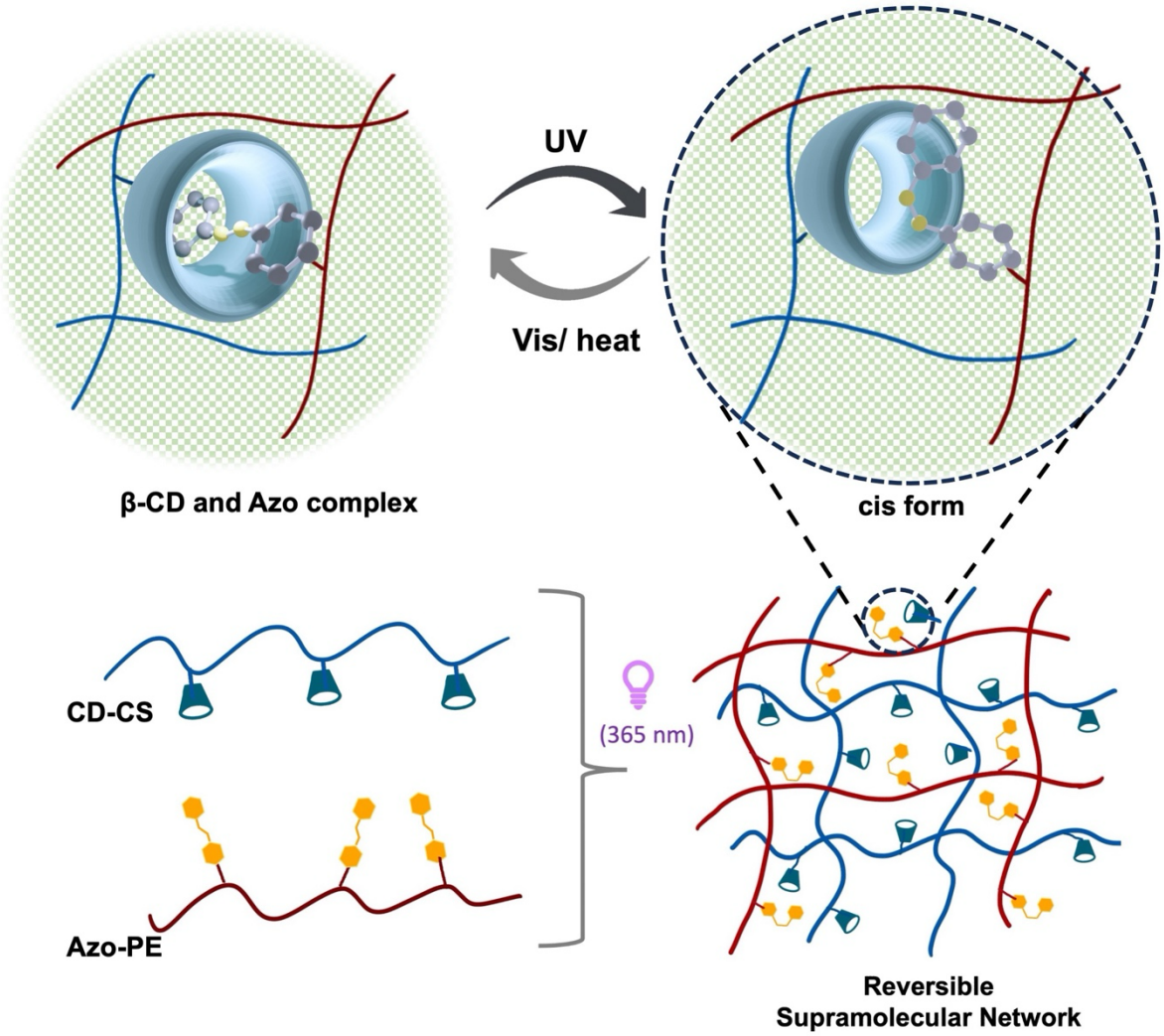

Parts of this chapter and the corresponding experimental section are submitted for publication as V. Pruthi, Y.F. Chen, P. Théato. "Azo-incorporated Complex Polymer Networks: Exploring Dual Responsiveness and 3D Printing Capabilities" 2024. In preparation.

4.3.1 Prologue

Building on the groundwork of **Chapter 4.2**, the current focus shifts towards the integration of photo-responsive elements into *pH*-responsive polyelectrolytes-integrated polymer networks, aiming to synthesize materials that are sensitive to both light and *pH* variations. This chapter reports the fabrication of three distinct polymer networks, each integrating an Azo-modified

polyelectrolyte and a β-cyclodextrin-functionalized polyelectrolyte into a P(OEGMA-*co*-EGDEMA) polymeric backbone.

Herein, a dual responsive PEC network hydrogel was designed, incorporating Azo functionalities that respond to light variations and polyionic commponents that exhibit sensitivity to pH. As discussed in **Section 2.4.2.4**, the molecular structure of Azo shows an inherent tendency to interact with the hydrophobic cavity of CD, forming a noncovalent host-guest complex. Such a complex is reversible and is susceptible to disassociation when Azo is photo-isomerized to its *cis* form upon UV irradiation. [155] Leveraging this reversible formation and disruption of an inclusion complex between CD and Azo, i.e., dynamic supramolecular bond, supramolecular hydrogels can be created. [160]

In the following sections, the synthesized Interpenetrating Polymer Networks (IPNs) and Supramolecular Polymer Networks (SPNs), their rigorous analysis to assess their physicochemical properties, encompassing their swelling capacity, thermal behavior, mechanical properties, and reactivity to light exposure and *pH* variations are discussed. The compatibility of these networks with 3D printing technologies has been thoroughly investigated as well.

4.3.2 Synthetic Strategy

The development of multifunctional polymer networks showcasing both light and *pH* sensitivity was achieved through a synthetic strategy that embeds dual key components: Azo-modified PEs and β-cyclodextrin-modified PE within the P(OEGMA-*co*-EGDEMA) polymer network, as shown in **Figure 4.22**. Initially, the Azo moiety, possessing a sulfonate (SO_3^-) group, was covalently linked to hyaluronic acid (HA) to form HA-Azo conjugates and also associated ionically with both CS and poly(diallyldimethylammonium chloride) (PDAC) to create corresponding supramolecular assemblies. In parallel, CS was chemically modified to incorporate β-CD forming CD-CS conjugate. The Azo-modified PE and CD-modified PE components are then incorporated into the photopolymerizable P(OEGMA-co-EGDEMA) matrix, facilitating the strategic assembly of interpenetrating or supramolecular polymeric network hydrogels. The integration of these modified PEs within the polymer framework results in a hydrogel that is capable of undergoing reversible expansion in response to light, a phenomenon underpinned by the reversible host-guest interactions between the Azo moieties and β-cyclodextrin (β-CD). The Azo component, in its thermodynamically favorable *trans* configuration, can be accommodated within the β-CD cavity, forming a stable inclusion

complex through hydrophobic interactions and van der Waals forces. Conversely, upon irradiation with UV light, the Azo moiety undergoes a *trans*-to-*cis* photo-isomerization, leading to a geometric alteration that disrupts its compatibility with the β-CD cavity, thereby inducing an expanded state of the hydrogel network.

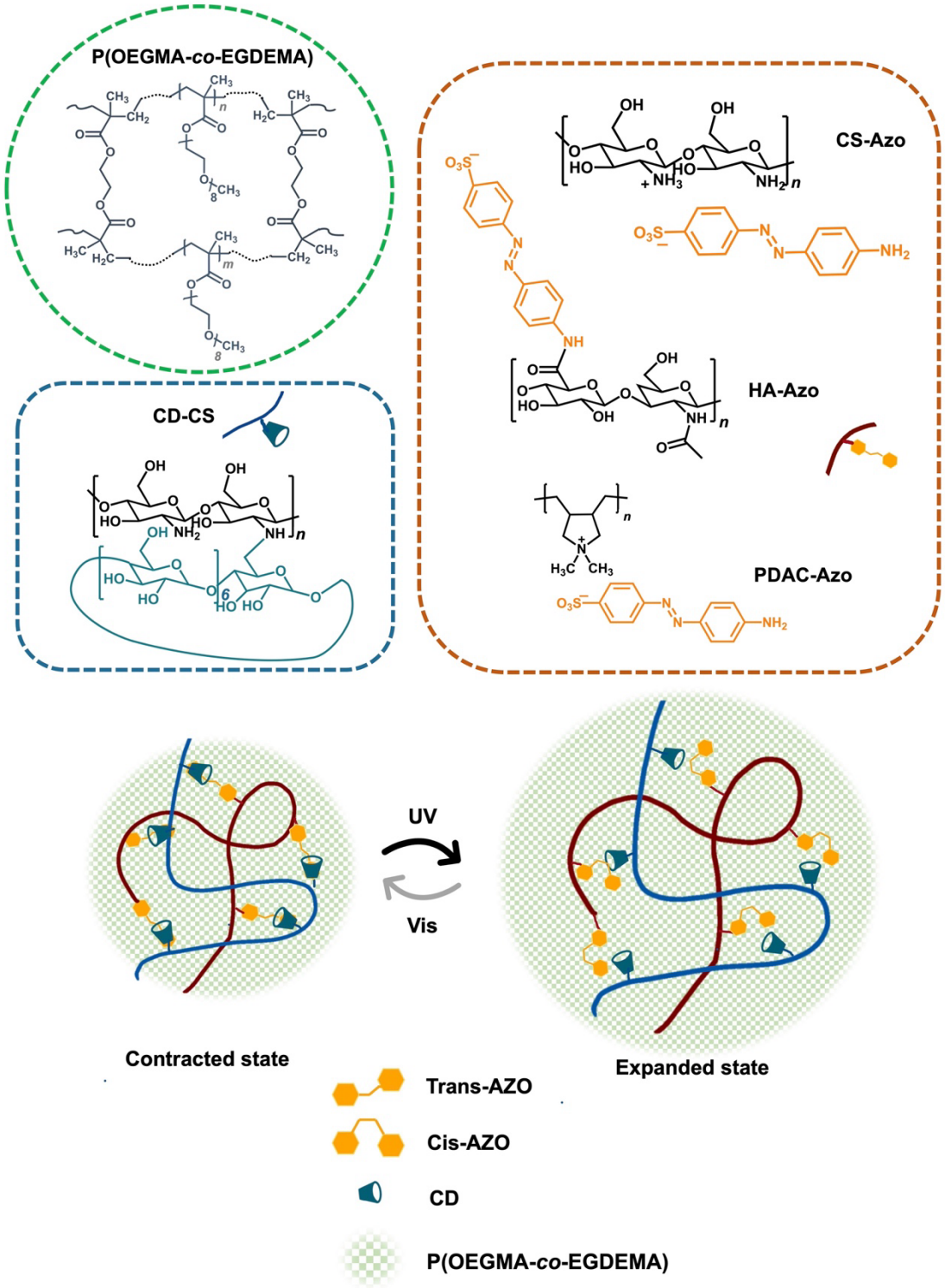

Figure 4.22 Schematic representation of the structure and strategic formation of the polymer network.

4.3.3 Incorporation of Azo and CD in Polyelectrolytes

Employing the subsequent methodology, the Azo group was integrated into the polyelectrolytes HA, CS, and PDAC, while CD was concurrently incorporated into CS.

Azo-modified Hyaluronic Acid:

HA-Azo was synthesized using a previously established methodology for the chemical modification of HA **(Scheme 4.4)**. [255, 256] The reaction involves the amidation of HA and sodium 4-aminoazobenzene-4'-sulfonate (Azo) facilitated by coupling agents EDC (1-ethyl-3-(3-dimethylaminopropyl) carbodiimide) and NHS (*N*-hydroxysuccinimide).

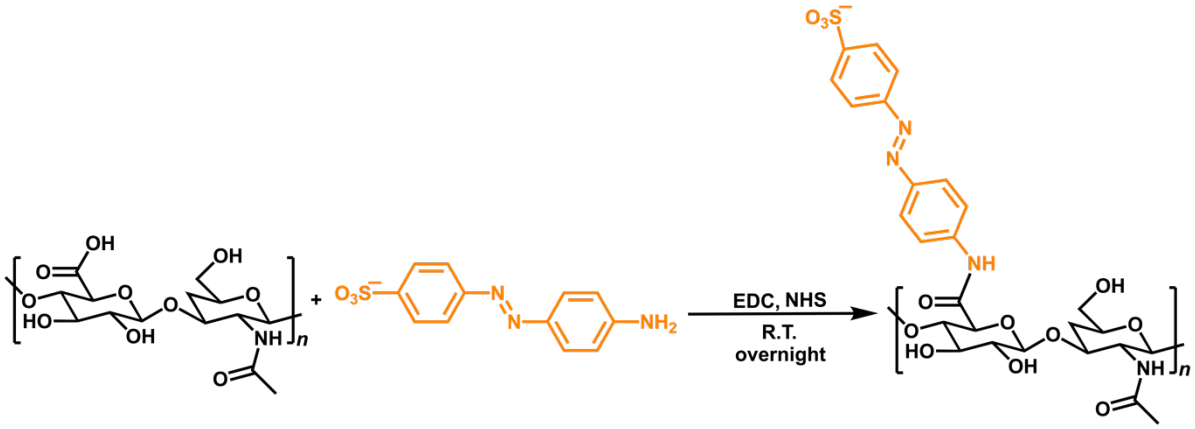

Scheme 4.4 Synthesis of Azo-modified hyaluronic acid (HA-Azo).

^{1}H NMR spectroscopy was conducted to confirm the formation of HA-Azo conjugates as shown in **Figure 4.23 (a).** The peaks (a) at δ = 8.00 ppm–7.00 ppm were assigned to the protons of the benzene rings of Azo and the peaks at δ= 3.00 ppm–4.00 ppm corresponding to the signals of the protons in the sugar rings which were all superimposed and difficult to assign each proton individually. The peak marked as (b) at 2.00 ppm was assigned to the – CH_3 protons of the *N*-acetyl group of HA. Moreover, the grafting percentages were quantified from the ratio of the peak area integration between (a, a′) and (b). HA-Azo conjugates with varying content of Azo, approximately ~ 13%, 6%, and 23 %, were synthesized. Further details on the synthesis are provided in the experimental section**, Chapter 6.5.1**.

Furthermore, IR spectroscopy provided verification of HA-Azo synthesis by identifying the characteristic absorptions: N–H stretching vibration at ~3290 cm^{-1}, =C–H stretching near 3100 cm^{-1}, N=N stretching of the Azo group at ~1550 cm^{-1}, and the C=O of the newly formed amide bond near cm^{-1} **(Figure 4.23 (b))**.

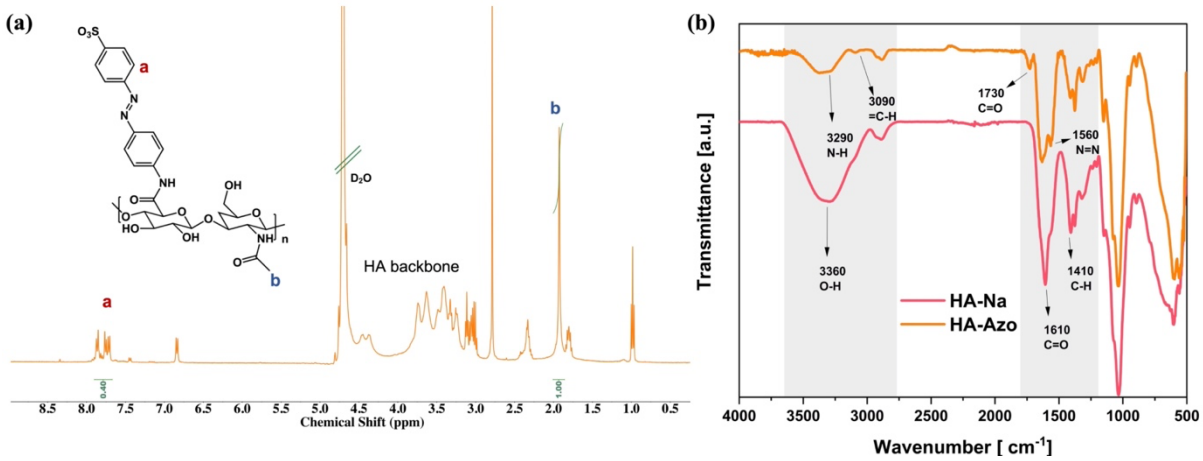

Figure 4.23 (a) ^{1}H NMR of HA-Azo in D_2O (400 MHz, 298 K), (b) IR spectra of HA-Na and HA-Azo.

β-Cyclodextrin-modified Chitosan:

The synthetic procedure for CD-CS commenced with the monotosylation of β-CD in an aqueous NaOH medium, as reported previously. [257] The resulting monotosylated cyclodextrin (CD-oTs) with reaction yield of 39% was confirmed using ^{1}H NMR (**Figure 4.24(a)**), with characteristic signals of β-CD and one tosyl group. Subsequently, CD-oTs was then engaged in a nucleophilic substitution reaction with the amino group of chitosan (CS) in an acetic acid solution (1% v/v in water), capitalizing on the tosyl group's proficiency as a leaving agent [156] **(Scheme 4.5)**.This resulted in the formation of β-CD-modified chitosan (CD-CS). The comprehensive synthesis methodology is detailed in the **experimental section, Chapter 6.5.2 and 6.5.3**.

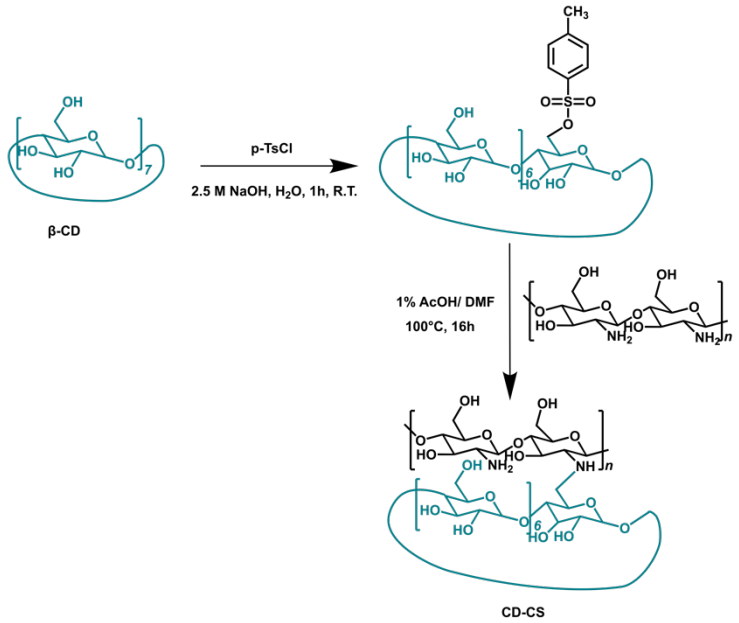

Scheme 4.5 Synthesis of β-Cyclodextrin-modified chitosan (CD-CS).

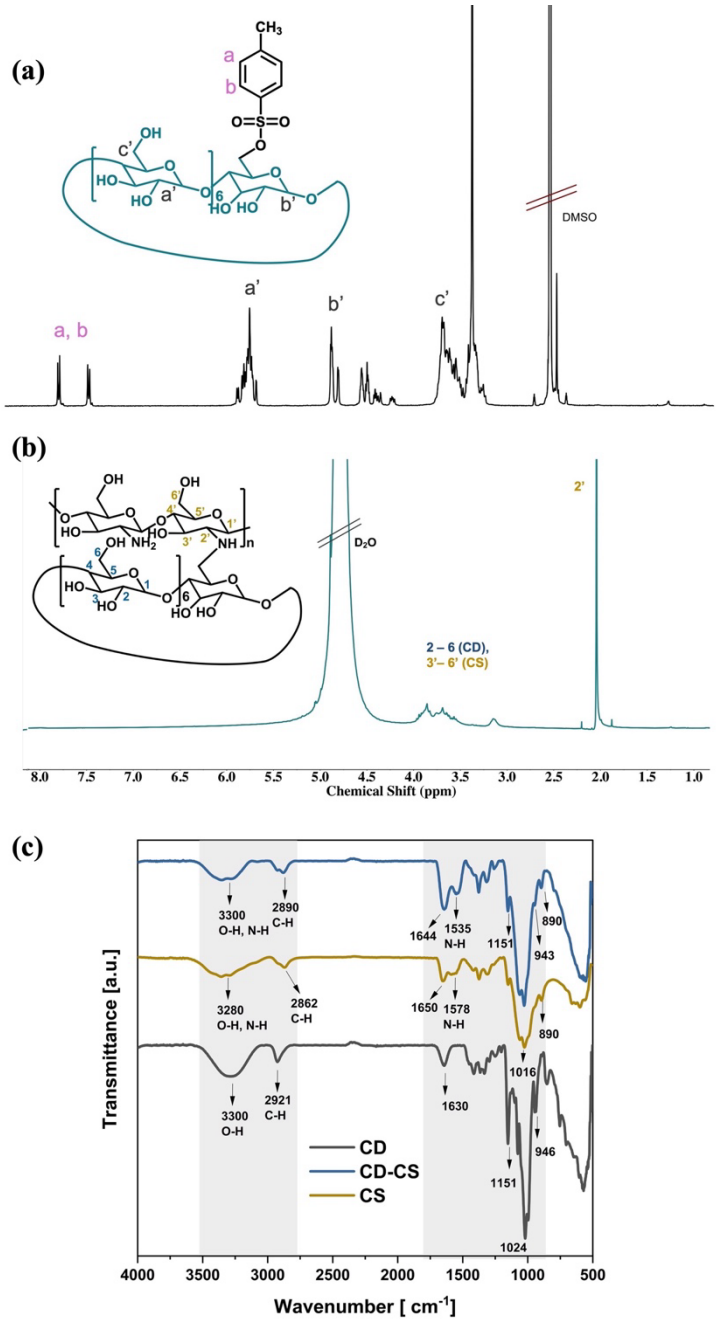

Figure 4.24 ^{1}H NMR of (a) CD-oTs in DMSO, (b) CD-CS in D_2O (400 MHz, 298 K), (c) IR spectra of CD, CS and CD-CS.

^{1}H NMR spectra typically reveal signals that are characteristic of both CD and CS moieties. As depicted in **Figure 4.24 (b),** multiple proton signals in the range of δ = 3 to 5 ppm window, which were attributable to H^2 –H^6 of CD and $H^{3'}$–$H^{6'}$ of CS protons. Conversely, the single signal at δ = 2 ppm was ascribed to the $H^{2'}$ proton of glucosamine. [258] Furthermore, IR spectral analysis of CD-CS revealed prominent absorptions at 3300 cm^{-1} for OH stretching and 1535 cm^{-1} for N-H stretching in the CS structure, as shown in **Figure 4.2.4 (c)**. Additionally, it

displayed notable peaks corresponding to the β-pyranyl vibrations in CS at 890 cm^{-1} and the α-pyranyl vibrations of β -CD at 943 cm^{-1}, confirming the modification of CS with β -CD.

PDAC-Azo Complex:

For the fabrication of the PDAC-Azo polymer complex, sodium 4-aminoazobenzene-4'-sulfonate (Azo) was incorporated into the solution of poly(diallyldimethylammonium chloride) (PDAC). The chemical structure of PDAC-Azo is shown in **Figure 4.22**. The electrostatic forces between the cationic PDAC and the sulfonic moieties of Azo lead to the development of a supramolecular assembly. [259] Infrared spectroscopy provided a methodological approach to identify and validate the intermolecular forces at play between Azo and PDAC. Relative to PDAC, PDAC-Azo exhibits distinct changes in its spectral profile, with the addition of N=N peak at 1598 cm^{-1} (**Figure 4.25**). The peaks at ~1110 and 1025 cm^{-1} are indicative of SO_3^- group from Azo. There is also a noticeable shift in ─C─H stretching vibration at ~ 2860 to 2950 cm^{-1} in PDAC-Azo, correlating to a change in the nitrogen atom's polarity in the dimethyl diallylammonium group of PDAC. Additionally, PDAC-Azo shows alterations in three characteristic peaks -N-H stretching and -CH_2 vibration at 3200 and 1470 cm^{-1}, confirming its assembly via electrostatic interactions. The proportion of Azo integrated into the complex was estimated through ^1H NMR spectroscopic analysis, which indicated that the Azo moiety accounted for an estimated 20% of the complex's composition **(refer to experimental section Chapter 6.5.5).**

Chitosan-Azo Complex:

Utilizing the established protocol for the PDAC-Azo complexation, the Chitosan-Azo (CS-Azo) variant was assembled in a similar fashion. Chitosan (CS), a biopolymer with reactive amino groups, was combined with sodium 4-aminoazobenzene-4'-sulfonate (Azo) under conditions that facilitate electrostatic binding between the anionic Azo sulfonate groups and the cationic amino groups of CS. This interaction promotes the formation of a supramolecular complex, analogous to the PDAC-Azo assembly. The molecular architecture of the CS-Azo complex was then elucidated using IR spectroscopy, confirming the presence of characteristic bonds indicative of the successful complex formation (**Figure 4.25**). The distinctive peaks include the N=N peak and -SO_3^- group of Azo at 1598 cm^{-1} and ~1100 cm^{-1} respectively and -OH stretching of CS at 3360 cm^{-1}. The resultant complex is illustrated in **Figure 4.22.** ^1H NMR spectroscopy was utilized to ascertain the Azo incorporation in the complex, revealing an Azo content of roughly 2%, showing low complexation (refer experimental section **Chapter 6.5.4**).

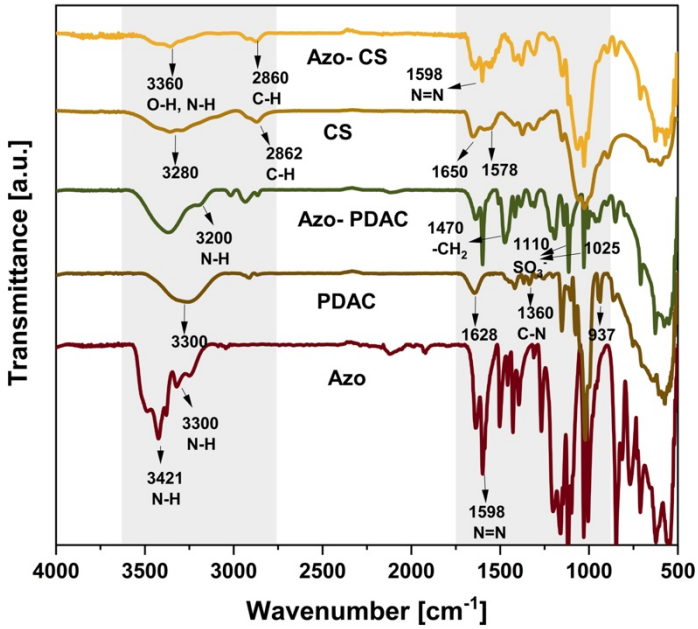

Figure 4.25 IR spectra chitosan-Azo complex (CS-Azo) and PDAC-Azo complex (PDAC-Azo), alongside their individual components: Azo, CS and PDAC.

4.3.4 Azo-containing IPN and SPN Hydrogels

A series of intricate IPNs and SPNs with photo-responsive properties were fabricated (**Table 4.3**). These hydrogels incorporate Azo-integrated PEs and CD-integrated PEs, following the detailed methods outlined further on. Despite their differences, all hydrogels share the same polymer framework, which includes OEGMA as the building block, EGDEMA as the cross-linker, and LAP as the PI. All the complex hydrogels were fabricated by free-radical photopolymerization in the presence of UV of 365 nm.

IPN with HA-Azo/CD-CS:

IPN hydrogels, encompassing a polyelectrolyte matrix with variable compositions of Azo-functionalized HA and CD-modified CS in the molar ratios of 1:1 and 1:2, were synthesized. Individual PE solutions were systematically prepared and subsequently integrated into a foundational precursor solution comprised of OEGMA, EGDEMA, and LAP (refer to Experimental section, **Chapter 6.5.6, Table 4.4**). Then, the exposure to UV light for 15 mins with a wavelength of 365 nm triggers both physical and chemical crosslinking pathways, facilitating the creation of complex orange-colored hydrogels (**Figure 4.2.6 (b)).** In the synthesized hydrogel, a PEC involving HA and CS groups was embedded within a covalently cross-linked structure produced by the photopolymerization of P(OEGMA-*co*-EGDEMA), forming an IPN. The IR spectrum shown in **Figure 4.2.6 (a)** depicts the characteristic band of

-N=N- at 1560 cm^{-1} Accompanying this, the spectrum shows distinct bands corresponding to the -OH stretching at 3360 cm^{-1}, -CH_2- stretching at 2860 cm^{-1}, and the amide -C=O stretching at 1760 cm^{-1}, integrally associated with the polymer P(OEGMA-*co*-EGDEMA) and its constituent groups HA-Azo and CD-CS.

SPN with CS-Azo/ CD-CS:

In a similar experimental approach, CS-Azo and CD-CS were integrated into the precursor solution, resulting in the formation of complex SPN hydrogels. The PE components were combined in equal molar ratios. Refer to **Chapter 6.5.6** in the experimental section for detailed methodologies. The IR spectroscopic analysis indicated a displacement of the CS characteristic -OH stretching frequency to approximately 3400 cm^{-1}, suggesting complexation within the hydrogel framework. Furthermore, due to substantial spectral overlap, individual absorption bands of the polyelectrolytes were indistinguishable.

SPN with PDAC-Azo/ CD-CS:

By replicating the established protocol, a balanced mixture of PDAC-Azo and CD-CS was used to create an SPN hydrogel, ensuring an equivalency of the polymer components. The specific ratios and components of the solutions prepared prior to photopolymerization are detailed in **Table 4.4.** The IR spectrum, shown in **Figure 4.26** displays characteristic absorption peaks corresponding to both PDAC-Azo and CD-CS, with significant overlapping of the absorption bands.

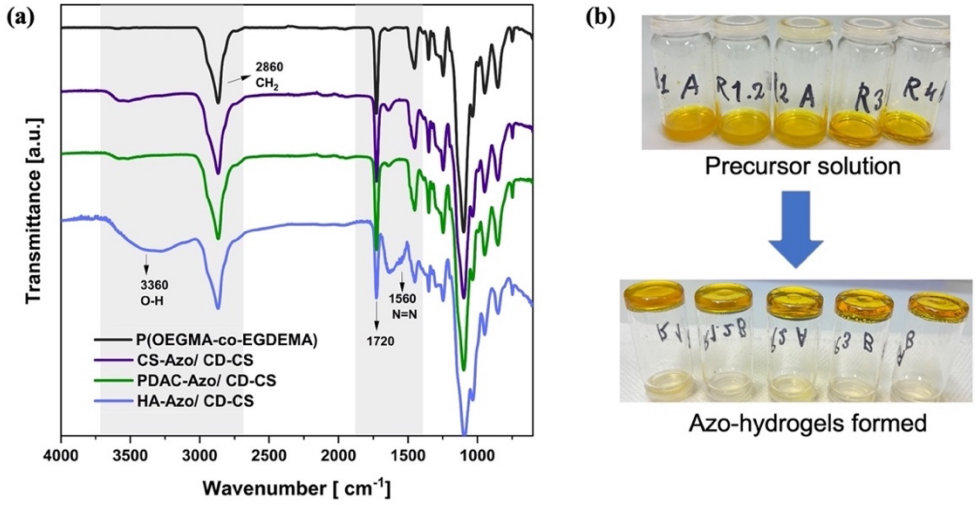

Figure 4.26 (a) IR spectra of IPN (HA-Azo/CD-CS) and SPN (CS-Azo/CD-CS, PDAC-Azo/CD-CS) hydrogels alongside P(OEGMA-*co*-EGDEMA), (b) visualization of pre-gel solutions and hydrogel formation using the invert-vial technique.

4.3.5 Properties of Hydrogels

4.3.5.1 Swelling Properties

The swelling capacity of each hydrogel was determined by the percentage change in weight, which serves as an indicator of water absorption. The hydrogels were initially weighed dry, then submerged in deionized water, and after removing excess surface moisture with filter paper, the weights of the swollen samples were recorded at different time intervals, until equilibrium was achieved. The swelling ratios were then computed based on these weights using the following equation.

$$\boldsymbol{Swelling}\ (\%) = \frac{W_S - W_d}{W_d} \times \mathbf{100}$$

where W_s is the weight of the swollen hydrogel and W_d is the initial weight of the dry hydrogel. The graphical representation of swelling percentages among the different hydrogels can be found in **Figure 4.27**.

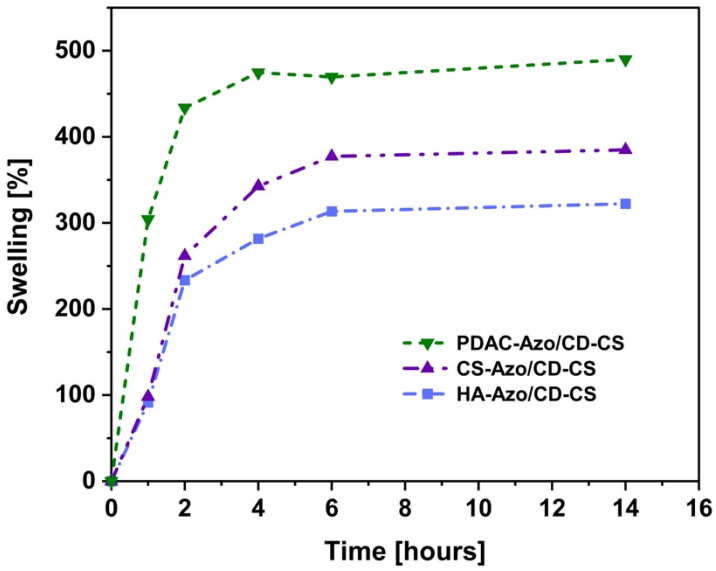

Figure 4.27 Swelling behavior comparison across different Azo-Integrated Hydrogels.

The observed pattern in swelling can be summarized as follows:

PDAC-Azo/CD-CS > CS-Azo/CD-CS > HA-Azo$_{0.23}$/CD-CS[1:1] > HA-Azo$_{0.23}$/CD-CS [1:2]

The swelling capacity of each polymer network is influenced by its composition and the interactions between its components. Factors such as the ionic charge of the polymers, the presence of hydrophilic groups, and the network structure all play critical roles in determining how much water the hydrogel can absorb. Moreover, the range in swelling percentages across different hydrogels may reflect the diversity in their crosslinking densities.

In the synthesized IPN matrix integrating HA-Azo$_{0.23}$ with CD-CS, there is a pronounced formation of a strong polyelectrolyte complex due to the intense electrostatic interactions between the HA and CS chains. This is further augmented by the formation of an inclusion complex between Azo and CD, which collectively imparts the hydrogel with the highest degree of crosslinking density among the prepared series. Therefore, these hydrogels show lowest swelling ability.

Conversely, CS, as a natural polycation, displays moderate water affinity, resulting in moderate swelling in the SPN hydrogel incorporated with CS-Azo and CD-CS. Meanwhile, the SPN with PDAC-Azo and CD-CS experiences the most substantial swelling, a consequence of PDAC's high charge density and its strong hydrophilic properties.

Table 4.3 Composition of fabricated polymer networks and their properties

Polymer Network	Azo-PE (mol %)	Azo content in PE (%)	CD-CS (mol %)	Swelling %[a]	T_d (5%) [b]	Storage Modulus [c] (kPa)
IPN with HA-Azo/ CD-CS	1	23	1	322	266	14
SPN with CS-Azo/ CD-CS	1	2	1	384	260	10
SPN with PDAC-Azo/ CD-CS	1	19	1	490	276	6

[a)] Swelling % is calculated as the percentage increase in weight, comparing the initial dry weight of the hydrogel to its weight upon reaching swelling equilibrium, [b)] decomposition temperature T_d (5%) determined by TGA analysis, [c)] storage modulus determined through rheological assessments.

4.3.5.2 *pH*-responsiveness

The swelling patterns of the synthesized hydrogels, which highlighted their varying capacities to absorb water were analyzed across a range of *pH* values- 3, 5, 7, and 11. As depicted in **Figure 4.28,** the complex hydrogels exhibited varying degrees of swelling at different *pH* levels. This could be attributed to the ionic interactions within their structure, with the degree of swelling being modulated by the *pH*-dependent charge dynamics between the constituent polymers. [247]

As previously mentioned in **Chapter 2.5.2**, the charge balance as well as the degree of interaction between the PEs change with a change in *pH* of the surrounding solution. Minimal swelling is observed in the *pH* range where the anionic pK_a is less than the ambient *pH* but

below the cationic pK_a. [72] With the pK_a values for HA at 3 and CS at 6.5, amines on CS are protonated at low *pH*, while carboxyl acids on HA ionize at *pH* above 6.5, enhancing swelling. Furthermore, PDAC, as a cationic polyelectrolyte with strong water solubility, undergoes dissociation, releasing chloride anions as counterions and maintaining its quaternary ammonium functionality along the polymer chain across the entire *pH* spectrum. [260] Notably, the synthesized IPN and SPN hydrogels showed the lowest swelling percentage at *pH* 5 due to pronounced electrostatic interactions between the charged polymer components. [252]

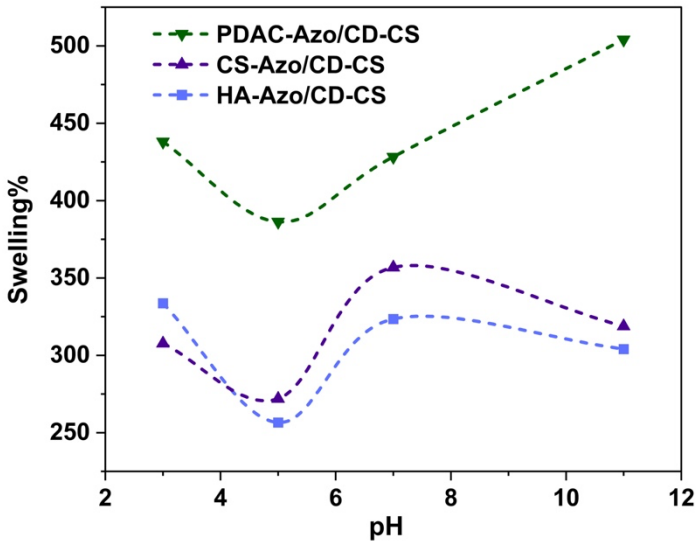

Figure 4.28 *pH*-responsive swelling behavior of Azo-integrated IPN and SPN hydrogels. The connecting lines are merelly for the visual guidance.

pH-responsiveness in bilayer hydrogels:

Three distinct bilayer configurations were assembled, with a uniform polymer matrix of P(OEGMA-*co*-EGDEMA) in each layer. To begin with, different pre-gel solutions were prepared, each incorporating a different PE yet employing the same polymeric base, which consisted of OEGMA as the monomer, EGDEMA as crosslinker, and LAP as the initiator for photopolymerization (refer to the experimental section **Chapter 6.5.8**, **Table 6.4** for further details). The bilayer structure was engineered with an initial formation of a layer with Azo-modified PE (either HA-Azo, CS-Azo, or PDAC-Azo), succeeded by a layer with a PE with a counterionic charge (CD-CS or HA), which was selected based on the composition of the precursor layer. For the first configuration (BL1), HA-Azo is integrated in the first layer and CD-CS in the second; the second configuration (BL2) comprised a first layer incorporated with CS-Azo and a second layer with HA; and the third configuration (BL3) consisted of a first layer integrated with PDAC-Azo followed by a second layer with HA.

Figure 4.29 shows in detail the stepwise procedure followed for the fabrication of bilayer hydrogels. Initially, the precursor solution for the first layer, enriched with Azo-modified PEs, was deposited into a Petri dish and subjected to UV to induce photopolymerization. After the curing of this layer, the solution for the second layer was applied atop and irradiated with UV light. This process yielded a bilayer hydrogel system, where the presence of Azo was exclusive to one layer. The adhesion between the two layers was significantly reinforced by the electrostatic interactions occurring at the interface, due to the opposing charges of the PEs in each layer.

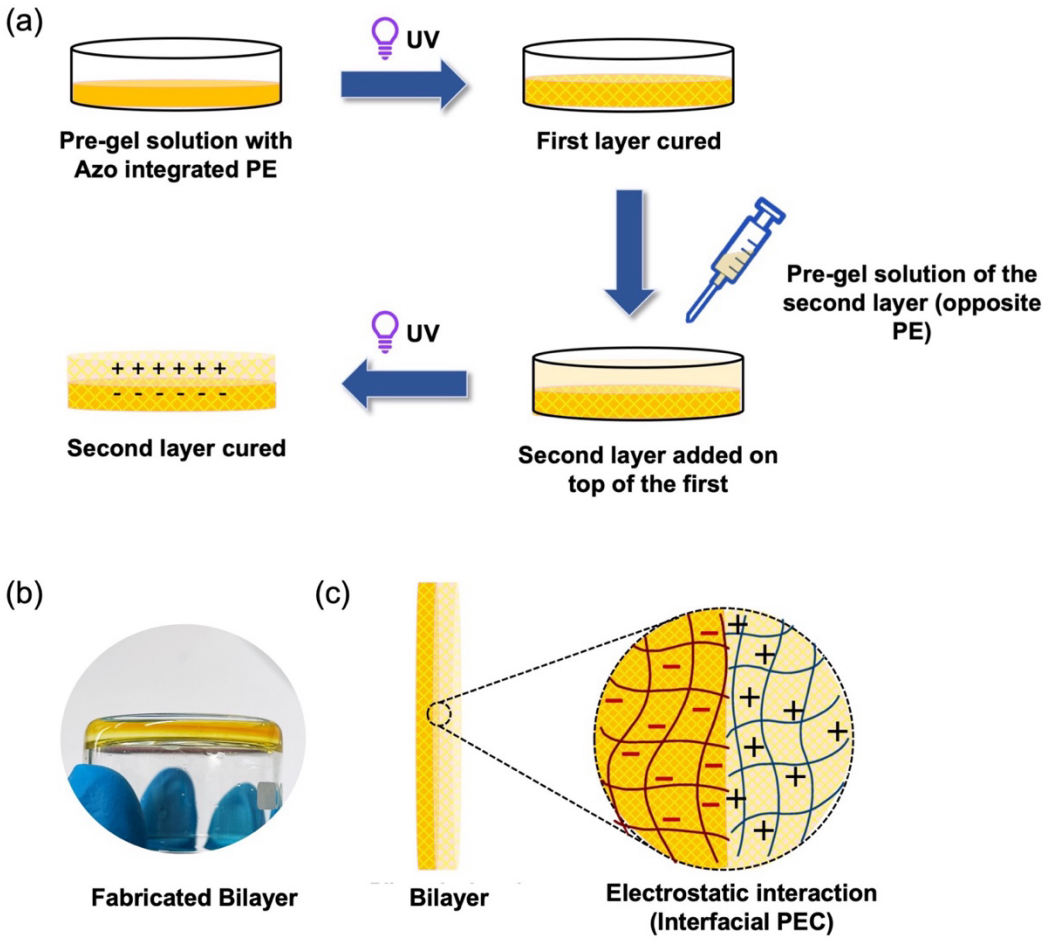

Figure 4.29 (a) Stepwise fabrication of bilayer hydrogel: protocol initiates with UV polymerization of Azo-incorporated base layer (bright yellow), followed by the addition and curing of a second layer containing oppositely charged PE (pale yellow), (b) image of the fabricated bilayer hydrogel and (c) graphic illustration of the bilayer interface, adhered by electrostatic interaction between oppositely charged PEs.

Subsequently, the bilayer hydrogels were sliced into elongated strips and immersed in buffer solutions of varying *pH* values (3, 5, 7, and 11) to assess their sensitivity to *pH* alterations. The

layer incorporated with Azo-modified *PE* exhibited a bright yellow hue, whereas the layer devoid of this modification displayed a faint yellowish tint.

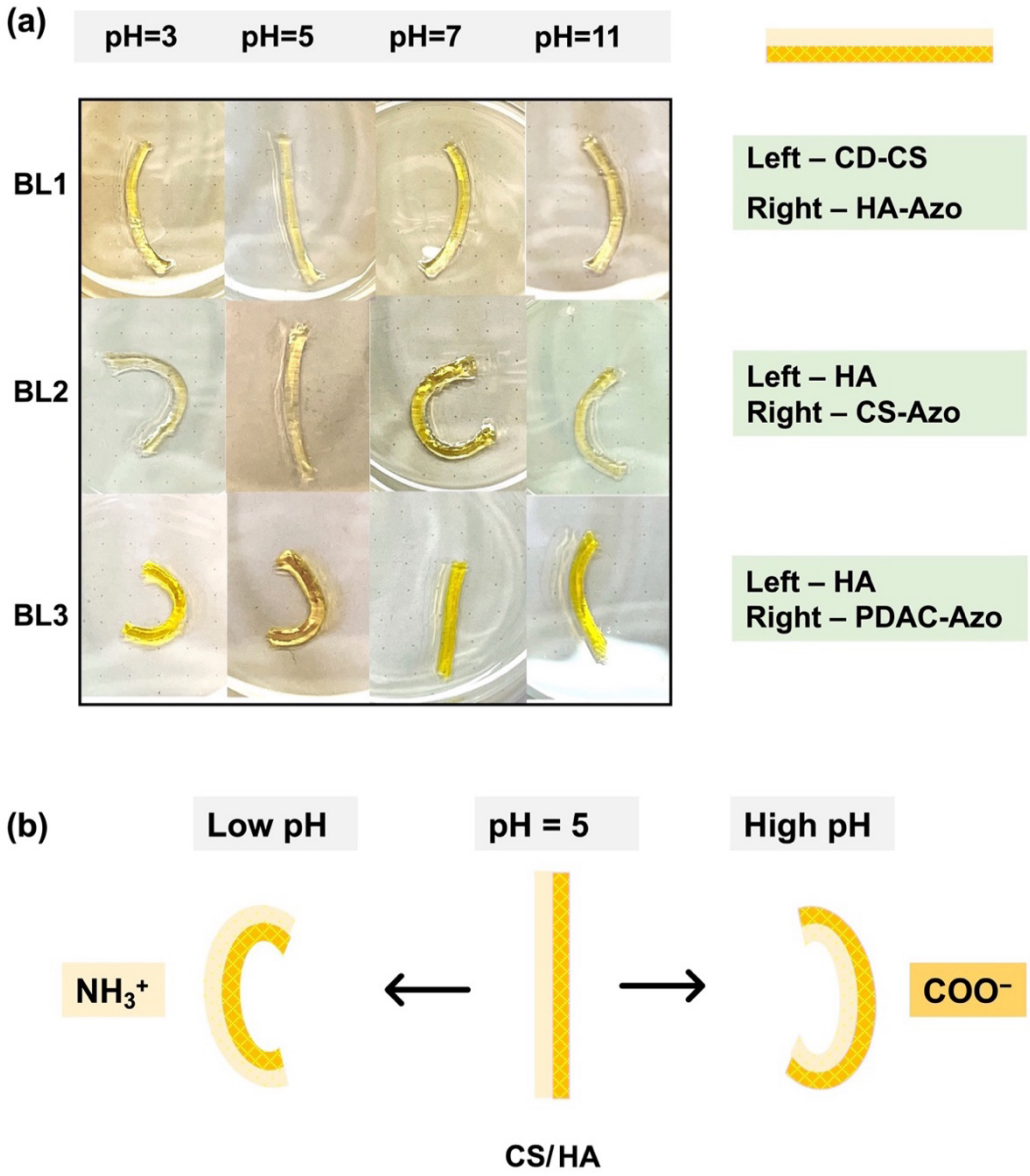

Figure 4.30 (a) Demonstration of *pH* sensitivity in bilayer hydrogels, (b) A graphic elucidation of bending behavior in bilayer BL1.

When the bilayer is exposed to different *pH* environments, each layer responds according to the *pH*-sensitivity of the respective polymer as shown in **Figure 4.30.** Differential expansion of the layers drives the bilayer to bend towards the more extensively swelling layer. As delineated in **Section 4.2.6.2**, CS layer experiences higher swelling at low *pH* due to the ionization of amino groups, while HA layers exhibit minimal swelling as the acidic conditions inhibit carboxyl group ionization. Consequently, at *pH* = 3, the bilayer inclines towards the HA side in both BL1 and BL2 configurations. In contrast, at a *pH* nearly 7 or

higher, the ionization of HA's carboxyl groups leads to increased swelling, inverting the bilayer's curvature towards the CS side as the swelling capacity of CS diminishes. Notably, at a *pH* of 5, BL1 and BL2 bilayers maintain a nearly linear form, indicating a balanced swelling effect between the HA and CS hydrogel layers.

Furthermore, the charge of PDAC remains relatively stable across a spectrum of *pH* levels, thus in the BL3 system, the curvature of the bilayer is predominantly influenced by the swelling behavior of the HA layer when exposed to varying *pH* conditions. Consequently, at a *pH* of 3 and 5, where HA experiences limited swelling, the bilayer tends to bend toward the HA layer. In contrast, at *pH* values close to 7 and higher, the bilayer inclines toward the side opposite the HA layer due to its increased swelling.

4.3.5.3 Photo-responsiveness

To elucidate the photo-responsive behavior, UV-vis spectroscopic analysis was conducted for Azo-modified PEs, dissolved in water with a concentration of 0.3 mg/mL. **Figure 4.31 (a)** depicts the UV spectra comparing the absorbance of HA-Azo, CS-Azo, and PDAC-Azo, differentiated by their Azo compositions. Each of them showed a strong absorption peak at around 400 nm, which is a characterstic of the azo group (–N=N–) chromophore present in them. The intense absorbance region extending from 380 nm to 450 nm is ascribed to the π→π* electronic transitions associated with the azo moiety. The presence of the amino substituents on the azo group induces a bathochromic shift of the π→π* absorption maxima, which diminishes the energy gap to the n→π* transition, effectively camouflaging the latter in the spectral data for these Azo-conjugated polymers due to significant overlapping.

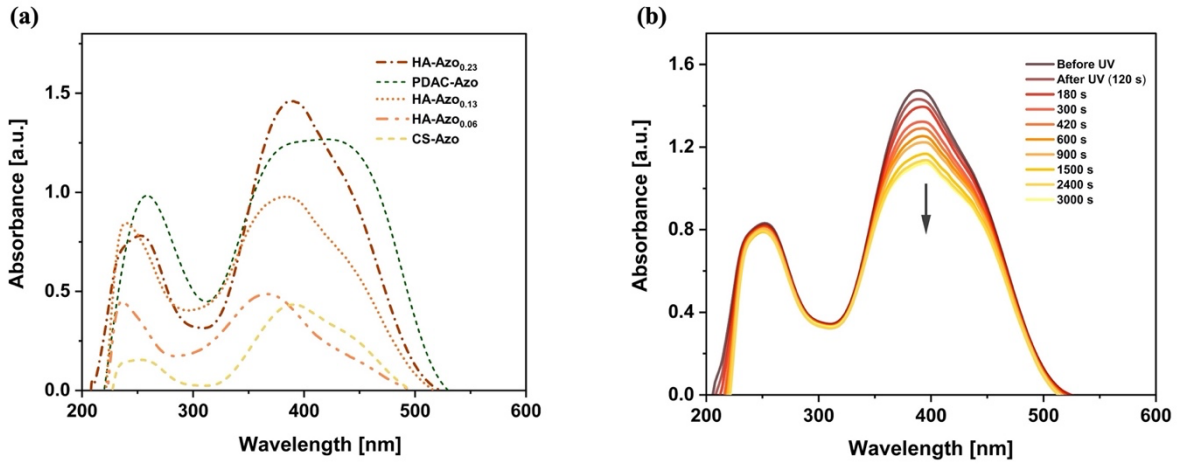

Figure 4.31 (a) Comparative UV absorption spectra for Azo-modified PEs, (b) time evolution UV spectra of HA-$Azo_{0.23}$ when irradiated with UV at room temperature.

Moreover, the data reveal that HA-Azo possesses the highest absorbance, presumably owing to its elevated percentage of Azo. In contrast, CS-Azo, characterized by the least amount of Azo, exhibited minimal absorbance. As depicted in **Figure 4.31 (b),** the time-resolved UV spectra of HA-Azo indicate a diminishing absorbance near 400 nm with prolonged exposure to 365 nm UV light. This phenomenon is consistent with the progressive photo-isomerization of Azo, leading to a transition from its predominant *trans* form to the *cis* form. [259]

Additionally, UV spectroscopic evaluation was carried out to study the photo-responsive behavior of the Azo-incorporated complex hydrogels in their solid form. Disc-shaped samples of the IPN and SPN hydrogels were prepared following the protocol described in **Section 4.3.4**. Each of them showed a gradual decline in absorbance at around 400 nm on UV exposure, as depicted in **Figure 4.32.** This observation is ascribed to the photo-isomerisation of the Azo moiety present within the hydrogel, which shifts from the *trans* to the *cis* configuration upon UV exposure.

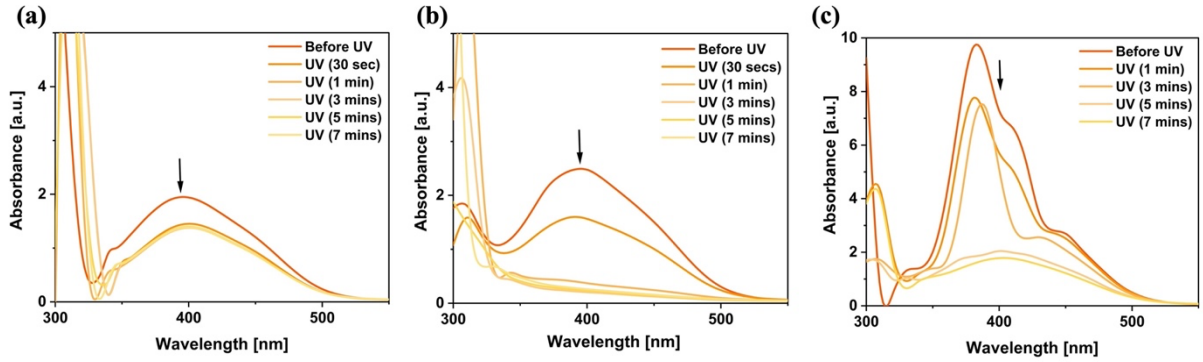

Figure 4.32 Time evolution UV absorption spectra of hydrogels with (a) HA-Azo$_{0.23}$/CD-CS, (b) CS-Azo/CD-CS and (c)PDAC-Azo/CD-CS when irradiated with UV at room temperature.

Photo-responsive dynamics in Azo Hydrogels

The photoreactive expansion-contraction dynamics of hydrogels that incorporate Azo and β-CD functionalities were studied. Circular hydrogel disks designated as HA-Azo/CD-CS, CS-Azo/CD-CS, and PDAC-Azo/CD-CS, with a standard diameter of approximately 25 mm were prepared and swollen in water. Initial weight of the swollen hydrogel samples were recorded. The samples were then exposed to UV light while immersed in an aqueous medium for one hour. Post-irradiation, the hydrogels were retrieved and re-weighed to ascertain any change in weight. Upon irradiation with 365 nm UV light, a *trans* to *cis* transformation of the Azo units is induced, whereas exposure to 450 nm visible light facilitates the reverse isomerization. [126] **Figure 4.33** illustrates the variation in weight of the hydrogels in response to the respective

light treatments. The light source employed for the irradiation was UV (λ= 365 nm) and Vis ((λ= 450 nm). It was observed that UV exposure increased the weight of the hydrogel, while prolonged Vis light exposure reduces the weight, reverting it to its near-original state.

This behavior can be attributed to the photo-responsive Azo groups within the hydrogel, which undergo a configuration change from *trans* to *cis* under UV light. This change affects the Azo group's structural fit within the β-CD cavity, leading to hydrogel expansion. The inverse process occurs under visible light, where the Azo reverts to its *trans* configuration, which interacts more favorably with the β-CD cavity via hydrophobic forces and van der Waals interactions.

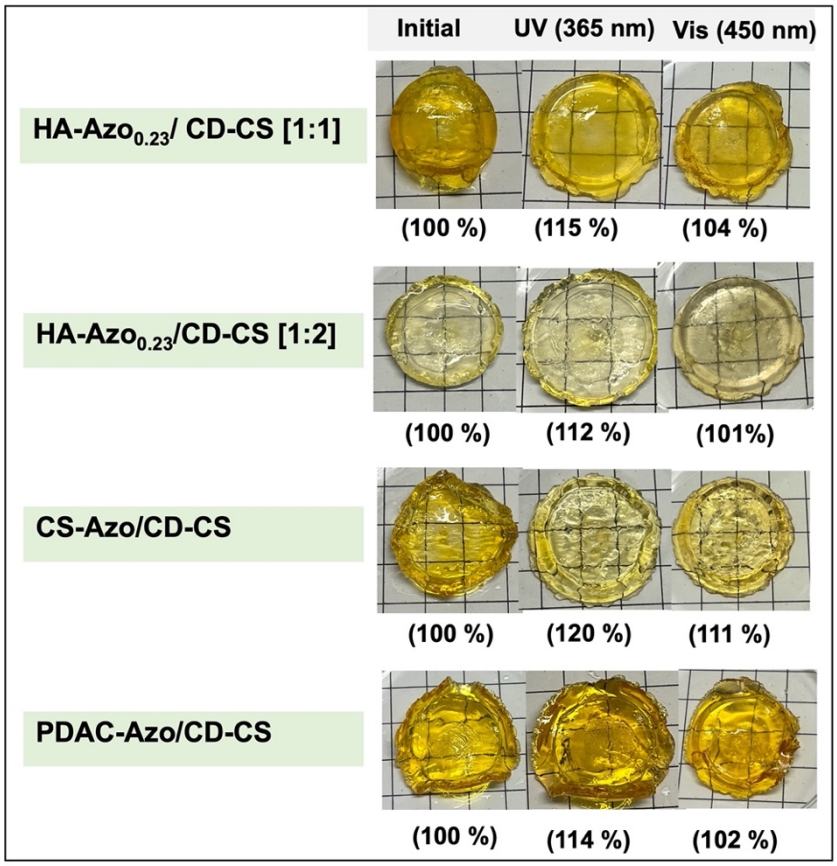

Figure 4.33 Photo-responsive dynaimcs in Azo-integrated IPN and SPN hydrogels.

Light-triggered expansion and contraction in these hydrogels are a result of dynamic host-guest interactions, where the β-CD displays a higher binding affinity for the *trans* form of Azo.[160] Visible light irradiation induces isomerization of Azo compounds, favoring the formation of the trans configuration, as evidenced by UV/vis spectroscopic analysis. This isomerization is expected to enhance the generation of Azo-cyclodextrin (Azo-CD) complexes, which are challenging to quantify directly. The presumed rise in complex formation is indicative of

increased cross-linking density, which is typically associated with a reduction in hydrogel swelling. In contrast, UV light exposure facilitates the cis isomerization of Azo, which would decrease cross-linking density and thus, increase swelling.

4.3.5.4 Thermal Properties

The thermal properties of the engineered hydrogels were rigorously assessed utilizing thermogravimetric analysis (TGA) to study their thermal stability. Depicted in **Figure 4.34** are the relative TGA thermograms of the lyophilized hydrogels. Notably, all dried networks demonstrated a significant onset of thermal degradation (T_d (5%)) within the range of 240 to 275 °C, reflective of their pronounced thermal stability. This thermal robustness confers upon the dried networks the capacity to withstand operation in environments characterized by elevated temperatures, thereby preserving both their structural coherence and functional attributes without succumbing to thermal degradation.

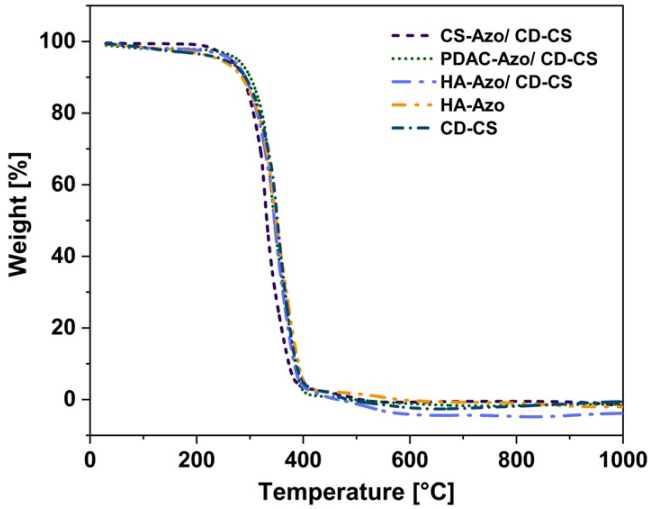

Figure 4.34 Comparative TGA traces of diverse hydrogel compositions.

Moreover, differential scanning calorimetry (DSC) was conducted to provide insights into the polymer network interactions and crosslinking density, critically assessing the state of water within the hydrophilic matrix. [249] Thermal analysis via DSC demonstrated that all hydrogels exhibit an endothermic peak around 8 °C to 10 °C, which is presumably due to the transition of free water. The observed peak for the vaporization of non-freezing water at temperatures of 110 to 115 °C for the Azo-integrated IPN and SPN hydrogels as shown in **Figure 4.35 (a).** Moreover, a shift in the endothermic peak is observed in IPN (HA-Azo/CD-CS) at 109 °C when both HA-Azo and CD-CS were incorporated, compared to the hydrogels composed of HA-Azo or CD-CS independently at 105 °C and 120 °C respectively (**Figure 4.35 (b)**). This

could be attributed to enhanced crosslinking within the IPN arising due to the complexation between HA-Azo and CD-CS. Additionally, the presence and alteration of the shoulder peak reinforce the existence of a complex and the overlapping thermal transitions of the contrasting polyelectrolytes.

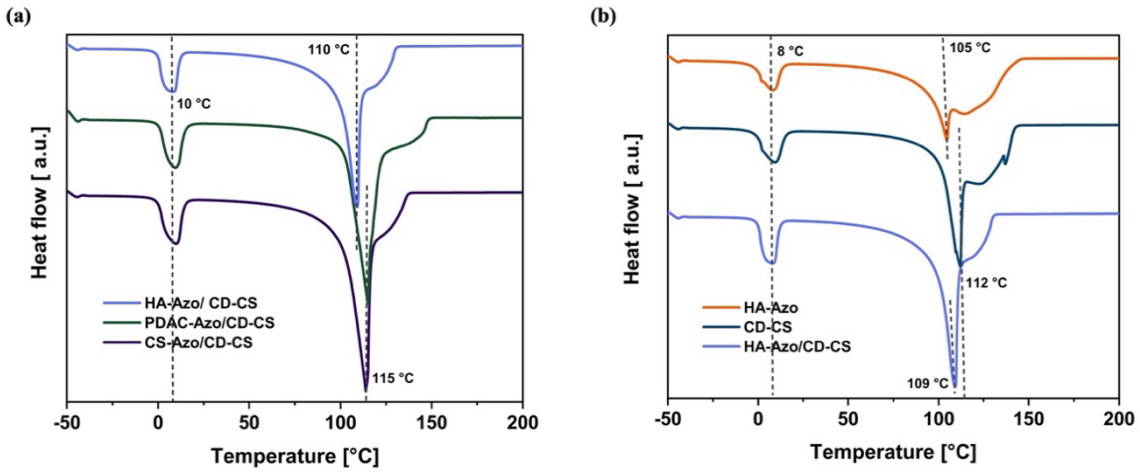

Figure 4.35 DSC thermograms illustrating: (a) the thermal behavior of IPN and SPN hydrogels, (b) the thermal characteristics of IPN (HA-Azo/CD-CS) v/s hydrogels composed of HA-Azo or CD-CS alone.

4.3.5.5 Mechanical Properties

The mechanical properties of the synthesized hydrogels were evaluated through strain and frequency-dependent shear rheological assessments to investigate their viscous and elastic behavior, alongside determining the storage modulus at ambient temperature (20 °C) across an angular frequency spectrum of 0.1 to 100 rad/s (**Figure 4.36 (a)**).

Figure 4.36 (b) depicts the results of the shear rheology tests conducted on the IPN and SPN hydrogels formulated with Azo-modified polyelectrolytes (PEs) and cyclodextrin-modified PEs with opposite charges, highlighting a comparison of the storage moduli. It was observed that the PDAC-Azo/CD-CS hydrogel presented a storage modulus (G') of 6 kPa. The CS-Azo/CD-CS variant displayed a greater G' value of 10 kPa, with the HA-Azo/CD-CS hydrogel surpassing both, exhibiting the greatest G' at 14 kPa. This can be explained by the formation of a strong polyelectrolyte complex between HA and CS in the IPN hydrogel containing HA-Azo and CD-CS. This results in a mechanically stronger network in comparison to the SPN which is formed in case of CS-Azo/CD-CS and PDAC-Azo/CD-CS.

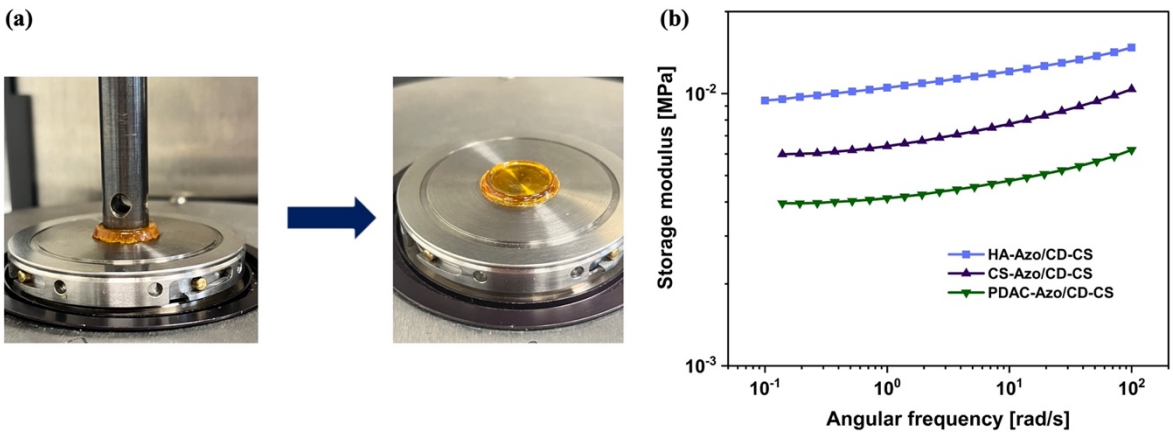

Figure 4.36 (a) Demonstration of hydrogel resilience to shear forces during rheological assessment, (b) frequency-dependent viscoelastic characterization of Azo-integrated IPN and SPN hydrogels via storage modulus evaluation.

4.3.6 3D Printing of IPN and SPN Hydrogels

The pre-gel solution composed of OEGMA, EGDEMA and LAP for the polymer matrix and integrated with an Azo-integrated PE and a CD-integrated PE, was scaled up to create three distinct 3D printable inks (refer to experimental section, **Chapter 6.5.7, Table 6.3**). Employing the DLP method, this ink facilitated the production of the floral-shaped print of the IPN hydrogel HA-Azo/CD-CS, as well as the SPN hydrogels CS-Azo/CD-CS and PDAC-Azo/CD-CS. The same protocol was followed as mentioned in **Section 4.3.4** to successfully achieve the prints, illustrated in **Figure 4.37 (a) and (b).** In the printing procedure, the operational parameters were carefully selected as follows: the light intensity was determined to be 365 nm, the base curing exposure time was tuned to 50 s, the layer thickness was accurately set at 20 µm, and a slow printing speed was maintained.

Furthermore, the pre-gel solutions exhibited an orange tint which transformed to bright yellow upon 3D printing, and this coloration further altered after the structures were left in the dark, as shown in **Figure 4.37 (b).** These variations in coloration are presumably due to the photo-isomerization of the Azo groups embedded in the hydrogel networks. Initially in its stable *trans* form in the pre-gel solution, the Azo groups convert to the *cis* form during UV-mediated 3D printing, followed by a spontaneous isomerization back to the *trans* conformation when kept in dark overnight.

Figure 4.37 (c) illustrates the reversible morphological adaptation of the PDAC-Azo/CD-CS hydrogel upon one hour of 365 nm UV irradiation in an aqueous environment. The initial shape

of the hydrogel is reestablished after two hours of illumination with 450 nm visible light, indicative of the Azo groups within the hydrogel undergoing reversible photo-isomerization.

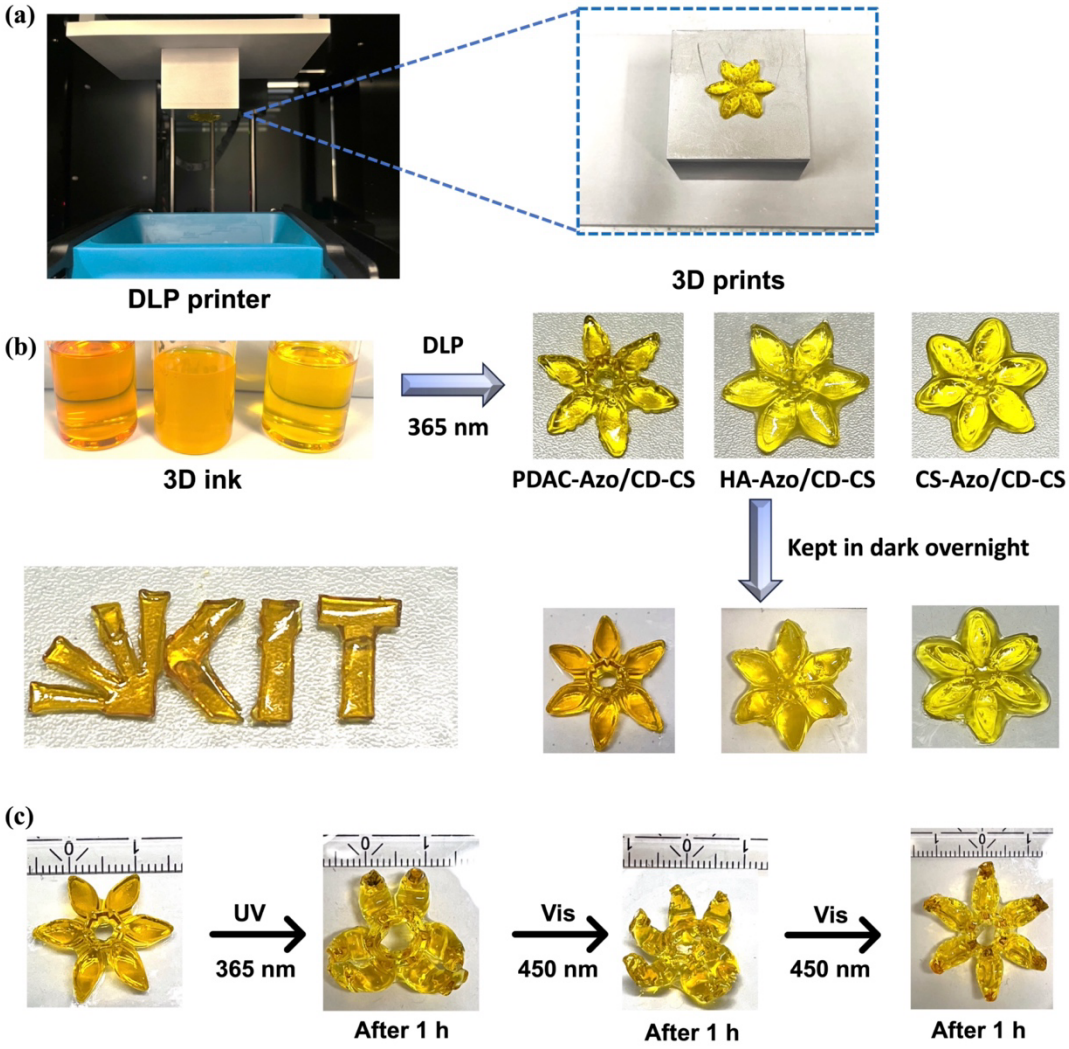

Figure 4.37 (a) 3D printing apparatus with completed print affixed to the platform, (b) illustration of the 3D inks and the corresponding floral printed hydrogels and KIT logo produced, alongside reversible color changes observed when kept in dark overnight, (c) captured photo-responsive deformations in shape and size upon alternating UV and visible light irradiation.

The reversible photo-deformation in the hydrogel network on alternate UV and Vis light irradiation is driven by the dynamic supramolecular interactions between the Azo and β-CD constituents within the matrix. In the presence of visible light, the Azo moiety adopts its trans configuration, which has the affinity to form an inclusion complex with β-CD, resulting in a higher crosslink density and a consequent contracted state of hydrogel. Upon UV irradiation, the Azo moiety undergoes isomerization to its cis conformation, which doesn't structurally fit

within the β-CD cavity, thereby reducing crosslinking density and facilitating the hydrogel's expansion. This is observed as a deformation in the shape of the hydrogel. The deformation is reversible upon the subsequent application of visible light for a duration of two hours.

The hydrogel exhibits preferential bending towards the source of light irradiation, observed to be from the top in this instance (**Figure 4.37 (c)**). This indicates a spatially inhomogeneous photonic interaction within the hydrogel. The diminished transmission of light into the deeper layers of the hydrogel creates an intensity gradient, with the uppermost layer receiving a higher dose of irradiation. This results in an upward bending motion, attributable to the variances in the photo-induced mechanical stresses across the hydrogel's cross-section.

4.3.7 Recapitulation

In this chapter, the development of three novel polymer networks is elucidated, each embedding an Azo-modified PE and a β-CD-functionalized PE within a P(OEGMA-*co*-EGDEMA) backbone. The design of these networks endows them with dual responsiveness to both light and *pH* fluctuations, attributed to the Azo groups and polyionic elements, respectively. Comprehensive characterizations of the synthesized IPN and SPNs have been carried out to study their structural, morphological and mechanical properties. The rheological assessment of hydrogel networks has established that IPN hydrogels integrated with HA-$Azo_{0.23}$/CD-CS [1:1] within the P(OEGMA-*co*-EGDEMA) matrixs have a markedly higher storage modulus (G') of 14 kPa compared to their SPN counterparts containing CS-Azo/CD-CS [1:1] and PDAC-Azo/CD-CS [1:1], with respective G' values of 10 kPa and 6 kPa. This distinction in mechanical robustness is credited to the formation of strong PEC between HA and CS and the supramolecular bindings between CD and Azo groups within the IPN hydrogel. In contrast, the SPNs exhibit mechanical properties supported exclusively by supramolecular interactions.

Moreover, the three polymer networks exhibit differential swelling capacities when immersed in solutions of varying *pH*. This phenomenon is attributable to the unique ionization properties of the polymeric components within each network under differing *pH* conditions. In addition, the *pH*-dependent behavior of the system was further investigated using three distinct bilayer configurations, where each bilayer was composed of countercharged polyelectrolytes. Differential bending responses were observed among the constructs when subjected to solutions of different *pH* values. Further investigation using UV spectroscopy demonstrated the photo-responsive properties of the Azo-modified polyelectrolytes, as well as the Azo-

containing IPNs and SPNs. The integration of these polymer networks with advanced DLP technique was also evaluated and successful 3D prints of these polymers into intricate floral geometries were accomplished.

Conclusively, the chapter details the development of three innovative polymer networks that are both dual-responsive and 3D printable, demonstrating substantial mechanical integrity. The potential of these hydrogel networks is particularly high in the realms of biomimetic constructs and soft robotic applications.

5. Conclusion and Outlook

This dissertation systematically investigated the creation of advanced polymeric materials which are distinguished by their distinctive physicochemical characteristics and versatile functionality. It casts light on the strategic synthesis of polymers with tunable properties, exploiting the synergistic effects of their molecular composition, structural design, and synthetic methodologies.

Firstly, the research commenced with a detailed account of the successful synthesis and analytical characterization of P(DEGMA-*co*-SpMA) copolymers, emphasizing the controlled variability in the incorporation of SP. These copolymers exhibit remarkable thermal stability and instant photo-isomerization capabilities. A direct relationship was established between the copolymer's glass transition temperature (T_g) and the percentage of SpMA, with the T_g notably increasing with higher SpMA content. Moreover, the research identifies a pivotal increase in the copolymers' glass transition temperature in response to UV light, which is fundamentally linked to an escalation in molecular polarity and a reduction in system entropy during the conversion from the SP's ring-closed form to the MR's ring-opened form. This study advances the understanding of polymers with photo-tunable T_g and custom-tailored responsiveness, offering innovative possibilities for their incorporation into smart materials applications, including but not limited to adaptive optical technologies and responsive coatings. Such advancements herald a new era of polymers that can reversibly transition between distinct T_g states, embodying a revolutionary approach in functional materials design.

The second investigation unveiled an innovative method for crafting *pH*-responsive IPN hydrogels, employing a refined 3D printing process that exploits the photodegradable *o*-NB groups. This synthetic route ingeniously embeds a polyelectrolyte complexation of HA and CS within a photo-crosslinkable P(OEGMA-*co*-EGDEMA) matrix. Comprehensive analyses of the hydrogels highlighted their structural, morphological, and viscoelastic properties. Their responsive swelling behavior and *pH* sensitivity were also methodically assessed. Utilizing DLP technology, IPNs with diverse compositions were effectively fabricated, yielding hydrogels with mechanical properties ranging from 5 to 10 kPa, marked by notable flexibility, robust compressive strength, and excellent strain resilience. The work showcased the seamless convergence of PEC with state-of-the-art 3D printing techniques.

Conclusion and Outlook

Expanding upon the foundational work of the preceding project, the third study introduced the synthesis of hybrid polymer networks adept in dual responsiveness to light and *pH* stimuli. It presented the fabrication of three differentiated polymer networks, each embedding an Azo-modified and a β-CD-functionalized PE within a P(OEGMA-*co*-EGDEMA) scaffold. These novel IPNs and SPNs were subjected to a rigorous analysis of their physicochemical properties, swelling and thermal behaviors, mechanical integrity, and reactivity to light and *pH*. The IPN hydrogels with HA-Azo/CD-CS stood out, exhibiting a storage modulus of 14 kPa reflecting their superior mechanical properties due to polymer entanglement and supramolecular interactions, unlike the SPNs which showed reduced moduli due to their dependence on non-covalent forces. Additionally, their *pH*-reactive bending capacities were probed through bilayer systems, revealing their adaptability. The integration of these polymers with DLP technology facilitated the fabrication of precise, complex 3D forms, indicating significant potential for these hydrogel networks in futuristic biomimetic constructs and soft robotics applications.

In summary, this thesis delivers a noteworthy contribution to polymer science, delivering pioneering materials characterized by their responsiveness to light and *pH*, and heralding new applications in advanced technology and robotics. It constructs a substantial groundwork for the development of polymers with exceptional physicochemical versatility and applicability in cutting-edge technological advancements. From the precise synthesis of photo-tunable SP-based copolymers to the innovative creation of IPN hydrogels and dual-responsive polymer networks, this research has not only expanded the current understanding of polymeric behavior under various stimuli but has also highlighted the critical role of modern fabrication techniques in material design. Looking ahead, the implications of this research extend beyond the laboratory, offering the potential to revolutionize multiple industries with materials that can intelligently interact with their environment.

6. Experimental Section

Within this section, a comprehensive overview of the instruments utilized for characterization purposes, the materials applied in the context of this thesis, alongside the experimental protocols and their analytical outcomes are presented. The procedural aspects of the projects mentioned previously are elaborated upon in the relevant subchapters.

6.1 Instrumentation and General Procedure

6.1.1 Nuclear Magnetic Resonance (NMR) Spectroscopy

^{1}H NMR (400 MHz) spectra were recorded on a Bruker Ascend 400 NMR spectrometer at ambient temperature. All samples were dissolved in deuterated solvents; chemical shifts are reported relative to the residual solvent signals.

6.1.2 Infrared (IR) Spectroscopy

Attenuated Total Reflection (ATR) Fourier-Transform (FT) Infrared (IR) Spectroscopy (ATR FT-IR) spectra were recorded on a Bruker Vertex 80 from 500 - 4000 cm^{-1} at 25 °C.

6.1.3 UV/Vis Spectroscopy

UV/Vis absorption spectra were recorded using an Ocean optics spectrometer. Spectra for the SP-based copolymers were recorded in $CHCl_3$ at 20 °C. The spectra for all modified-polyelectrolytes (HA-NB, HA-Azo, CS-Azo and PDAC-Azo) were performed in D_2O at 20 °C.

Time-evolved UV absorption spectra of the Azo-containing hydrogels in Chapter 4.3 were obtained on a Hitachi U4100 ultraviolet-visible (UV-vis) spectrometer to record the isomerization of AZO molecules.

6.1.4 Fluorescence Spectroscopy

Cary Eclipse fluorescence spectrophotometer was employed for recording fluorescence spectra.

6.1.5 Gel Permeation Chromatography (GPC)

Gel permeation chromatography (GPC) of SP-based copolymers was carried out in THF and at room temperature on a Tosoh Bioscience HLC-8320GPC EcoSEC system equipped with 3 PSS SDV columns, 5 μm (100, 1000, 100 000 Å) (8 Å~ 300 mm^2), and a UV and a differential refractive index (RI) detector.

6.1.6 Scanning Electron Microscopy (SEM)

SEM images of freeze-dried hydrogels were taken with a Zeiss LEO 1530 microscope operating at 5 kV. Samples were sputtered with gold (thickness 5 nm) prior to measurement.

6.1.7 Differential Scanning Calorimetry (DSC)

Differential scanning calorimetry was conducted using a DSC Q200 (TA Instruments) ranging from −50 °C to 200 °C with a scan rate of 10 K min^{-1} for all spiropyran polymers and from -70 °C to 180 °C after UV irradiation.

For all the swollen hydrogels in Chapter 4.2 and 4.3 , DSC measurements were performed in temperatures ranging from -50 °C to 200 °C with a scan rate of 10 Kmin^{-1}.

6.1.8 Thermal Gravimetric Analysis (TGA)

For thermal studies, thermal gravimetric analysis (TGA) was carried out using a TGA 5500 (TA Instruments) at a heating rate of 10 K min^{-1} under a nitrogen atmosphere up to 1000 °C.

6.1.9 Rheological Measurements

For the rheological measurements, disc-shaped hydrogels (25 mm diameter and 4 mm height) were prepared. The shear tests were performed at 20 °C. Rheology of as prepared hydrogels was tested at 20 °C using a shear rheometer (ARES-G2, TA-Instruments) with a Peltier (thermoelectric cooling) unit to keep the temperature constant. Further, compression tests of hydrogels (swollen in water for 15 minutes) were performed using a Universal Testing Machine “Inspect Table 10 kN”, Hegewald & Peschke at room temperature equipped with a 1.5 kN force cell. Before the measurements, the dimensions of the samples were measured using a vernier caliper.

6.1.10 3D Printing Technique

First of all, the CAD model of the print was created using Fusion 360 software and ".stl" format of the model was sliced using Miicraft Utility software. Then, the hydrogels were printed using Miicraft Hyper 80X 3D printer that employs a UV source of 365 nm wavelength. The parameters set for printing included a layer thickness of 20 μm, a power ratio of 100%, UV exposure at a wavelength of 365 nm, a base curing time of 50 s and curing time of 5 s for each layer. The printing parameters (power ratio, layer thickness and curing time for each layer) were further adjusted.

6.1.11 Swelling Measurements

To determine the swelling percentage of hydrogels, the initial and swollen sample weights were recorded at different time intervals. The process involved taking pre-weighed dry samples and submerging them in deionized water. After removing the excess surface water with filter paper, the swollen samples were weighed at different time frames.

6.2 Materials

2,3,3-Trimethyl-3H-indole (TCI), 2-bromoethanol (TCI), 2-hydroxy-5-nitrobenzaldehyde (abcr), methacryloyl chloride (Alfa Aesar), azobisisobutyronitrile(AIBN) (Sigma Aldrich), potassium hydroxide (Carl Roth), sodium hyaluronate (M_w ~10^6 Da, Alfa Aesar) and chitosan ((M_w =50,000-190,000 Da, Sigma Aldrich), lithium phenyl-2,4,6-trimethylbenzoylphosphinate (LAP, Sigma Aldrich), 2-nitrobenzyl chloride (Sigma Aldrich), and tetrabutylammonium hydroxide (Sigma Aldrich), cationic-exchange resin (Amberlite IRN-77, H^+ form), sodium 4-aminoazobenzene-4'-sulfonate (TCI), 1-ethyl-3-(3-dimethylaminopropyl) carbodiimide hydrochloride (EDC, Carl Roth), *N*-hydroxysuccinimide (NHS, Fischer Scientific), phosphate-buffered saline (PBS, *pH* =7.4, Fischer Scientific, hydrochloric acid (HCl, Carl Roth), *p*-toluenesulfonyl chloride (TCI), β-Cyclodextrin (β-CD, Acros Organics), *N,N*-dimethylformamide (DMF, Carl Roth), dimethyl sulfoxide (DMSO, Carl Roth) poly(diallyldimethylammonium chloride (PDAC, M_w =100-200 kDa, Sigma Aldrich), buffer solutions (*pH* =3, 5, 7, 11, Carl Roth), acetic acid (100%, Carl Roth), sodium hydroxide (NaOH, >98%, Carl Roth), sodium chloride (NaCl, Carl Roth), magnesium sulfate ($MgSO_4$, ≥99%, Carl Roth) were used as received.

Di(ethylene glycol)methyl ether methacrylate (DEGMA, Sigma Aldrich, 95%), oligo(ethylene glycol) methyl ether methacrylate (OEGMA, M_w = 500, Sigma Aldrich), ethylene glycol dimethacrylate (EGDEMA, Sigma Aldrich) were passed through basic alumina oxide before use.

All other solvents were of analytical grade or higher and were used without further purification. Ultrapure MilliQ water with a resistivity of 18 MΩ cm was employed.

6.3 Procedures for "Photo-responsive Spiropyran and DEGMA-based Copolymers"

6.3.1 Synthesis of SpMA

The SP derivative (SpMA) was synthesized in four different steps, starting from the commercially available compound- 2,3,3-trimethyl-3H-indole. [112, 261]

Preparation of bromide salt by alkylation of 2,3,3-trimethyl-3H-indole

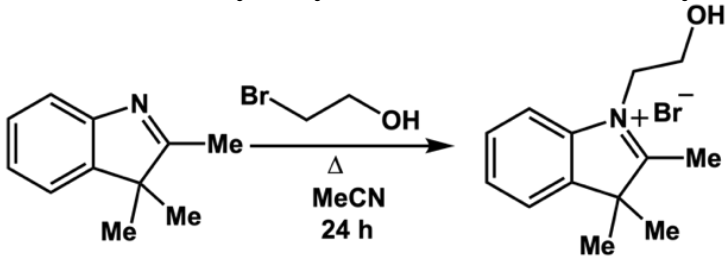

16 mmoles (2.61 g) of 2,3,3-trimethyl-3H-indole and 20 mmoles (2.46 g) of 2-Bromoethanol were mixed in acetonitrile (20 mL). The solution was heated for 24 hours at 85 °C under reflux and N_2. Then, it was cooled down to room temperature, following which the solvent was distilled off under reduced pressure. Subsequently, the residue was suspended in hexane (25 mL). It was then, sonicated and filtered. The final stage involved crystallisation using chloroform, yielding 1-(2-hydroxyethyl)-2,3,3-trimethyl-3H-indolium bromide (a pink solid weighing 2.95 g, 64.9%).

^{1}H NMR (400 MHz, CD3CN) δ/ ppm = 7.83 (m, 1H), 7.78 – 7.58 (m, 3H), 4.72 (t, J = 6.3 Hz, 1H), 4.62 – 4.55 (m, 2H), 4.07 – 3.98 (m, 2H), 2.85 (s, 3H), 2.23 (s, 7H), 1.61 (s, 6H).

^{13}C NMR (101 MHz, CD_3CN) δ/ ppm = 142.91, 130.68, 129.98, 124.27, 118.26, 116.45, 58.79, 55.60, 51.70, 22.83, 15.47.

Synthesis of oxazole derivative by reacting bromide salt with KOH

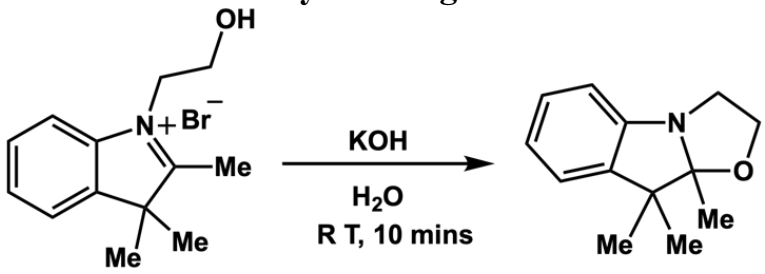

A solution of 10 mmoles (2.93 g) of the obtained bromide salt and 16 mmoles (0.92 g) of KOH in 50 mL H_2O was stirred at ambient temperature for 10 min. It was then extracted with diethyl ether. Later, the organic phase was concentrated under reduced pressure to give the oxazole derivative (yellow oil, 1.84 g, 88%).

^{1}H NMR (400 MHz, $CDCl_3$) δ/ ppm = 7.06 (m, 1H), 7.00 (m, 1H), 6.85 (m, 1H), 6.69 (m, 1H), 3.81 – 3.72 (m, 1H), 3.65 (m, 1H), 3.56 – 3.36 (m, 2H), 1.33 (d, 6H), 1.11 (s, 3H).

^{13}C NMR (101 MHz, $CDCl_3$) δ/ ppm = 150.64, 140.11, 127.60, 122.51, 121.80, 112.08, 109.08, 63.09, 50.19, 47.06, 28.20, 24.59, 20.91, 17.69.

Synthesis of SP-OH derivative by reaction with 2-hydroxy-5-nitrobenzaldehyde

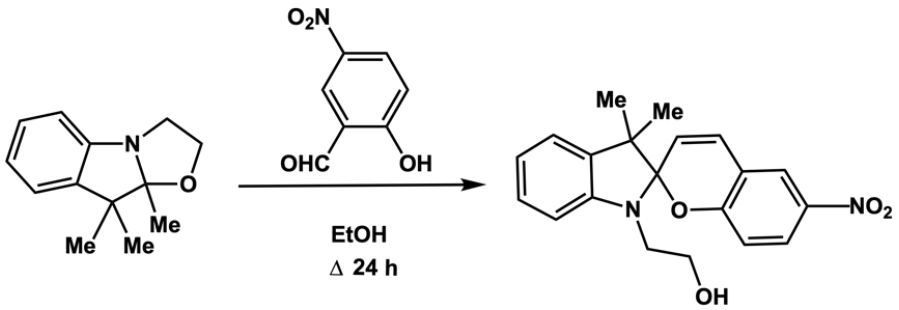

A solution of 2-hydroxy-5-nitrobenzaldehyde (7.5 mmoles, 1.2534 g) and the oxazole derivative (5 mmoles, 1.0875 g) in ethanol (10 mL) was heated for 24 hours under reflux and N_2. After cooling down to ambient temperature, the solvent was distilled off under reduced pressure to afford SP-OH as a purple solid (1.3049 g, 74 %).

^{1}H NMR (400 MHz, $CDCl_3$) δ/ ppm = 7.99 – 7.90 (m, 2H), 7.13 (m, 1H), 7.03 (m, 1H), 6.88 – 6.78 (m, 2H), 6.69 (d, 1H), 6.60 (d, 1H), 5.81 (d, 1H), 3.79 – 3.70 (m, 1H), 3.65 (q, 2H), 3.39 (m, 1H), 3.27 (m, 1H), 1.50 (s, 1H), 1.22 (s, 3H), 1.21 – 1.10 (m, 6H).

^{13}C NMR (101 MHz, $CDCl_3$) δ/ ppm = 159.44, 147.11, 141.32, 135.97, 128.41, 128.00, 126.13, 122.91, 122.08, 122.05, 120.15, 118.68, 115.67, 107.06, 106.87, 61.02, 52.98, 46.26, 26.05, 20.17.

Synthesis of Spiropyran methacrylate from SP-OH derivative

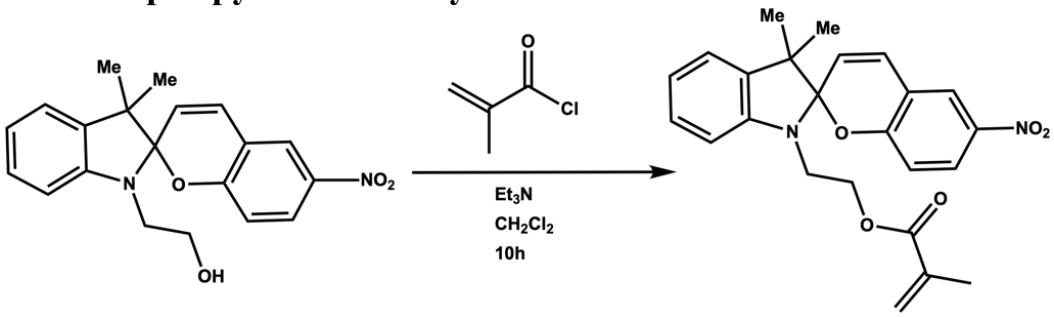

SP-OH (3 mmol, 1.05 g), methacryloyl chloride (7.5 mmole, 0.784 g) and Et_3N (7.5 mmole, 0.758 g) were added into 40 ml CH_2Cl_2 at 0 °C. Then, the mixture was stirred for 10 hours. The resulting solution was filtered and extracted by saturated sodium bicarbonate solution and water (1:1). The organic layer was then dried by $MgSO_4$, and concentrated under vacuum. A purple solid was obtained. Further purification was done using column chromatography (Ethyl acetate:Hexane, 1:1) and crystallization (using 95% ethanol). The purified yellow solid was obtained (yield= 45 %).

^{1}H NMR (400 MHz, $CDCl_3$) δ/ ppm = 7.98 – 7.90 (m, 3H), 7.18 – 7.07 (m, 2H), 7.07 – 6.98 (m, 2H), 6.93 – 6.78 (m, 4H), 6.76 – 6.57 (m, 3H), 6.48 – 6.31 (m, 1H), 6.00 (m, 1H), 5.84 – 5.77 (m, 1H), 5.49 (m, 1H), 4.29 – 4.13 (m, 3H), 3.72 – 3.26 (m, 5H), 1.93 (m, 6H), 1.76 – 1.53 (m, 4H), 1.42 – 1.34 (m, 3H), 1.34 – 1.16 (m, 7H), 1.09 (d, 5H).

^{13}C NMR (101 MHz, CDCl3) δ/ ppm = 167.22, 159.42, 146.68, 141.12, 136.07, 135.72, 128.81, 128.44, 128.32, 128.27, 127.87, 127.71, 125.99, 125.95, 125.92, 122.79, 122.14, 122.01, 121.83, 121.81, 120.08, 119.95, 118.44, 115.58, 106.84, 106.78, 62.65, 52.90, 42.45, 25.87, 19.86, 18.37.

6.4 Procedures for "*pH*-responsive IPN with *o*-NB Functionalized PEC"

6.4.1 Synthesis of HA-NB Derivative

The sodium salt of HA was converted into its acidic form by draining it through a cationic-exchange resin (Amberlite IRN-77, H^+ form), which was then neutralized by tetrabutylammonium hydroxide $(C_4H_9)_4N^+OH^-$ to *pH* 7. [262] The tetrabutylammonium salt of HA was obtained after freeze-drying for two days. 0.1242 g of HA-TBA salt was then dissolved in dried DMSO at 40 °C. Subsequently, a solution of *ortho*-nitrobenzyl chloride (0.0343 g) in 1 mL DMSO was slowly introduced into it, and the reaction was continued at 40 °C on a magnetic stirrer for 48 hours. To the resultant *o*-NB-grafted HA solution, a concentrated aqueous solution of NaCl (10 % w/w) was added to convert it into sodium salt, which was then precipitated in acetone and filtered. Thereafter, it was washed thoroughly with acetone and dried. The obtained *o*-NB HA ester was purified extensively by dialysis against Milli-Q water for a week and then freeze-dried (Yield= 25 %).

6.4.2 Synthesis of Photo-crosslinkable P(OEGMA-*co*-EGDEMA) Hydrogel

A pre-gel mixture was developed by combining OEGMA and EGDEMA in a water-based solution containing LAP. This solution was subsequently exposed to UV light at a wavelength of 365 nm, leading to the formation of a hydrogel within 5 minutes of exposure. The successful creation of the hydrogel was validated using the inverse-vial technique, a standard method in the field.

6.4.3 Synthesis of PEC of HA-NB and CS

To synthesize a PEC, a solution of HA-NB in de-ionized water and a solution of CS in water with a few drops of 1 vol% acetic acid (AA) were prepared separately by stirring overnight. Then, a mixture was prepared by dissolving equal proportions of HA-NB and CS solutions. The mixture was stirred overnight under UV for deprotection and for the formation of PEC. The prepared solution was then poured into petri dishes and was dried in the oven at 40 °C for

48 h. Further, the obtained product was washed with water to remove any unreacted compounds. The formed PEC films were dried in a vacuum oven for a week.

6.4.4 Synthesis of Semi-IPN containing HA or CS

To synthesize semi-IPNs featuring either hyaluronic acid or chitosan, the following procedure was employed. Firstly, HA was thoroughly dissolved in the least possible volume of water to form a solution. Subsequently, this solution was combined with a reaction mixture in water, which comprised OEGMA, EGDEMA, and LAP. On the other hand, to create a semi-IPN containing CS, CS was dissolved in a mixture of water and 1 vol% AA to form a solution. Later, this solution was then integrated into a similar reaction mixture. These pre-gel solutions were then irradiated with UV (365 nm) for 5 mins, resulting in the formation of semi-IPN hydrogels.

6.4.5 Synthesis of PEC-integrated IPN Hydrogel

For obtaining PEC-incorporated IPN hydrogel, two separate solutions of HA-NB and CS were initially prepared. The HA-NB was dissolved in water, while the CS solution was prepared in a blend of water and 1% AA. These two solutions were subsequently mixed with an aqueous solution, containing OEGMA, EGDEMA and LAP. The final mixed solution exhibited a *pH* of approximately 4.5. To form the hydrogel, this mixture was then subjected to UV light (365 nm) for 15 mins.

6.4.6 3D Printing of IPN Hydrogels

Table 6.1 provides a comprehensive breakdown of the 3D ink formulation alongside the calibrated printing parameters of the 3D printer employed in the fabrication of IPN hydrogels.

Table 6.1 Optimized composition of 3D ink and parameters of 3D printer.

3D Print	OEGMA (g)	EGDEMA (mol %)	LAP (wt %)	HA-NB (mg)	CS (g)	Layer thickness (μm)	Print time (mins)	Curing time (s)	Base curing time (s)	Power ratio
P(OEGMA-*co*-EGDEMA)	10	2	1	-	-	20	90	5	50	100
Semi-IPN with CS	10	2	1	-	0.10	20	90	5	50	100
IPN (HA-$NB_{0.5}$/CS)1:1	10	2	1	0.05	0.05	20	90	5	50	100
IPN (HA-$NB_{0.5}$/CS)1:2	10	3	1	0.02	0.04	20	90	5	50	100
IPN (HA-$NB_{0.5}$/CS)2:1	10	3	1	0.04	0.02	20	90	5	50	100

6.5 Procedures for "Dual Responsive Azo-incorporated Polymer Networks"

6.5.1 Synthesis of HA-Azo Conjugates

To synthesize HA-Azo, HA (0.1 g) was initially dissolved in a PBS buffer (*pH* 6.2), to which EDC (0.3 g) and NHS (0.12 g) were added and the mixture was stirred for 15 mins at ambient conditions. The solution's *pH* was then calibrated to 7.3 before the addition of Azo (2.22 g) with continuous agitation for 48 h, and the resulting HA-Azo was purified through dialysis against deionized water and freeze-drying (22% yield). The molar ratio of HA and Azo was varied to obtain different degrees of substitution of Azo (~ 13%, 6%, and 23 %,), which was then calculated using ^{1}H NMR spectroscopy.

The calculation for Degree of substitution:

$$Degree\ of\ grafting = \frac{Integral\ of\ aromatic\ protons\ of\ Azo\ group}{Integral\ of\ anomeric\ proton\ of\ HA}$$

6.5.2 Synthesis of Monotosylated Cyclodextrin (CD-oTs)

β-CD (10 g, 8.8 mmol) was dissolved in Milli-Q water (90 mL), followed by the addition of 2.5 M NaOH solution (35.2 mL). Subsequently, *p*-toluenesulfonyl chloride (*p*-TsCl) (2.6 g,

13.4 mmol, 1.5 equivalent) was incrementally introduced into the mixture, which was then stirred at ambient temperature for 1 hour. After filtration and washing of the residue with water, the filtrate (*pH*~10) was treated with cation-exchange resin (Amberlite IRN-77, H^+ form) preconditioned with 6 M HCl. The reaction proceeded until the *pH* reached 2–3, inducing the precipitation of the product. The mixture was initially passed through a 300 μm sieve to remove the resin beads, and the resultant precipitate was further filtered using a sintered glass funnel. The final product, a white solid (4.43 g, 39% yield), was obtained after washing and freeze-drying. ^{1}H NMR (400 MHz, DMSO) δ / ppm = 7.74 (d, 1H), 7.42 (d, 1H), 5.86 — 5.61 (m, 6H), 4.86 – 4.79 (m, 2H), 4.76 (d, 1H), 4.53 – 4.48 (m, 1H), 4.44 (m, 1H), 4.40 – 4.28 (m, 1H), 3.67 – 3.62 (m, 1H), 3.65 – 3.54 (m, 1H), 3.54 – 3.40 (m, 1H), 3.34 (s, 2H), 3.29 (s, 3H), 3.29 – 3.16 (m, 1H), 2.42 (s, 1H).

6.5.3 Synthesis of CD-modified CS

The synthesis of β-CD- functionalized CS was carried out using a previously reported method. Initially, CS (1.4 g, 8.85 mmol of repeating units) was dissolved in 115 mL of 1% AA (v/v). To this, a solution of 6-OTs-βCD 1 (5.0 g, 3.85 mmol, 0.4 equivalent) in dimethylformamide (60 mL) was added. The combined mixture was then refluxed at 100 °C for 16 hours. Post-reflux, the mixture underwent partial distillation to reduce solvent volume, followed by dialysis using a 3500 Da MWCO membrane for 2 days, first against a 0.1 M NaCl aqueous solution and subsequently against ultrapure water. The final step involved freeze-drying the solution to yield CD-CS as a white solid (yield= 26%).

6.5.4 Synthesis of CS-Azo Complex

Initially, a solution of CS was formulated in 1% acetic acid (AA), and concurrently, an equivalent ratio of sodium 4-aminoazo benzene-4'-sulfonate was solubilized in water. The two solutions were then combined and agitated continuously for an overnight period at ambient temperature. After the stirring process, dialysis was employed against de-ionized water to eliminate any residual CS and Azo. The resultant mixture was subjected to lyophilization, forming a solid yellow powder, referred to as the CS-Azo complex (yield= 30 %).

6.5.5 Synthesis of PDAC-Azo Complex

To synthesize the PDAC-Azo complex, distinct solutions containing equal molar ratios of PDAC and sodium 4-aminoazo benzene-4'-sulfonate were initially dissolved in water. The

PDAC solution was slowly merged into the Azo solution, ensuring constant stirring. This mixture was agitated for an entire day at room temperature. Subsequent to that, NaCl was removed through dialysis, and the final step involved freeze-drying the solution to yield an orange solid, designated as PDAC-Azo (yield= 54 %).

6.5.6 Synthesis of Azo-containing IPN and SPN Hydrogels

The construction of the IPN hydrogel incorporating HA-Azo/CD-CS, as well as the SPNs containing CS-Azo/CD-CS and PDAC-Azo/CD-CS, was achieved using the specific constituent concentrations outlined in **Table 6.2.** For each formulation, the HA-Azo and PDAC-Azo were separately prepared in aqueous solutions, while CD-CS and CS-Azo were solubilized in a 1% acetic acid (AA) solution prior to their combination into the pre-gel mixtures. Finally, the mixtures were irradiated with UV light (365 nm) for 15 mins to form the IPN and SPN hydrogels.

Table 6.2 Pre-gel formulation for the synthesis of IPN and SPN hydrogels.

Hydrogels	OEGMA (g)	EGDEMA (mol%)	LAP (wt%)	HA-Azo (mol %)	CS-Azo (mol %)	PDAC-Azo (mol %)	CD-CS (mol %)
IPN with HA-Azo/ CD-CS (1:1)	0.5	3	1	1	-	-	1
IPN with HA-Azo/ CD-CS (1:2)	0.5	3	1	0.5	-	-	1
SPN with CS-Azo/ CD-CS	0.5	3	1	-	1	-	1
SPN with PDAC-Azo/ CD-CS	0.5	3	1	-	-	1	1

6.5.7 3D Printing of Azo-incorporated IPN and SPN Hydrogels

Table 6.3 offers an in-depth delineation of the formulation of the 3D printable ink and the operational parameters of the 3D printing device applied in the fabrication of the Azo-containing IPN and SPN hydrogels interpenetrating polymer network hydrogels.

Table 6.3 3D ink composition for printing Azo-incorporated IPN and SPN hydrogels.

3D Print	OEGMA (g)	EGDEMA (mol%)	LAP (wt%)	Azo-PE (mg)	CD-CS (mg)	Layer thickness (μm)	Print time (mins)	Curing time (s)	Base curing time (s)	Power ratio
IPN with HA-Azo/ CD-CS	10	2	1	20	40	20	90	5	50	100
SPN with CS-Azo/ CD-CS	10	2	1	25	25	20	90	5	50	100
SPN with PDAC-Azo/ CD-CS	10	3	1	50	50	20	90	5	50	100

6.5.8 Synthesis of Bilayer

In the synthesis of bilayer hydrogel assemblies, the initial step involved the separate formulation of pre-gel solutions for each layer, with the concentrations of the components involved listed in **Table 6.4**. The bilayer systems were devised in three variations: the initial system BL1 featured an HA-Azo first layer with a CD/CS second layer; the subsequent system BL2 included a CS-Azo first layer and an HA second layer; and the final system BL3 was formed with a PDAC-Azo first layer topped by an HA second layer.

Table 6.4 Composition of individual layers in the bilayer hydrogel systems.

Hydrogels	OEGMA (g)	EGDEMA (mol%)	LAP (wt%)	HA-Azo or HA (mol %)	CS-Azo (mol %)	PDAC-Azo (mol %)	CD-CS (mol %)
HA-Azo	0.5	3	1	1	-	-	-
CD-CS	0.5	3	1	-	-	-	1
CS-Azo	0.5	3	1	-	1	-	-
PDAC-Azo	0.5	3	1	-	-	1	-
HA	0.5	3	1	1	-	-	-

Bibliography

[1] L. Zhai, *Chem. Soc. Rev.* **2013**, *42*, 7148.

[2] R. Narayanaswamy, V. P. Torchilin, *Molecules* **2019**, *24*, 603.

[3] A. K. Bajpai, S. K. Shukla, S. Bhanu, S. Kankane, *Prog. Polym. Sci.* **2008**, *33*, 1088.

[4] D. Buenger, F. Topuz, J. Groll, *Prog. Polym. Sci.* **2012**, *37*, 1678.

[5] J. Tavakoli, Y. Tang, *Polymers* **2017**, *9*, 364.

[6] S. Maiz-Fernandez, L. Perez-Alvarez, U. Silvan, J. L. Vilas-Vilela, S. Lanceros-Mendez, *Polymers* **2022**, *14*, 650.

[7] Q. Shi, H. Liu, D. Tang, Y. Li, X. Li, F. Xu, *NPG Asia Mater.* **2019**, *11*, 64

[8] R. Brighenti, Y. Li, F. J. Vernerey, *Front. Mater.* **2020**, *7*, 196

[9] H. Banerjee, M. Suhail, H. Ren, *Biomimetics* **2018**, *3*, 15.

[10] P. Schattling, F. D. Jochum, P. Theato, *Polym. Chem.* **2014**, *5*, 25.

[11] T. H. Lee, J. Y. Jho, *Macromol. Res.* **2018**, *26*, 659.

[12] Z. Han, P. Wang, G. Mao, T. Yin, D. Zhong, B. Yiming, X. Hu, Z. Jia, G. Nian, S. Qu, W. Yang, *ACS Appl. Mater. Interfaces* **2020**, *12*, 12010.

[13] C. J. Barrett, J.-i. Mamiya, K. G. Yager, T. Ikeda, *Soft Matter* **2007**, *3,* 15.

[14] M. C. García, "Ionic-strength-responsive polymers for drug delivery applications", in *Stimuli Responsive Polymeric Nanocarriers for Drug Delivery Applications*, Woodhead Publishing, **2019**, 393.

[15] I. Carayon, A. Gaubert, Y. Mousli, B. Philippe, *Biomater. Sci.* **2020**, *8*, 5589.

[16] J. Thevenot, H. Oliveira, O. Sandre, S. Lecommandoux, *Chem. Soc. Rev.* **2013**, *42*, 7099.

[17] F. Ercole, T. P. Davis, R. A. Evans, *Polym. Chem.* **2010**, *1*, 37.

[18] S. L. Oscurato, M. Salvatore, P. Maddalena, A. Ambrosio, *Nanophotonics* **2018**, *7*, 1387.

[19] J. Shang, S. Lin, P. Theato, *Polym. Chem.* **2018**, *9*, 3232.

[20] R. Klajn, *Chem. Soc. Rev.* **2014**, *43*, 148.

[21] C. Zong, M. Hu, U. Azhar, X. Chen, Y. Zhang, S. Zhang, C. Lu, *ACS Appl. Mater. Interfaces* **2019**, *11*, 25436.

[22] T. Liu, B. Bao, Y. Li, Q. Lin, L. Zhu, *Prog. Polym. Sci.* **2023**, *146,* 101741.

[23] A. Berradi, F. Aziz, M. E. Achaby, N. Ouazzani, L. Mandi, *Polymers* **2023**, *15,* 2908.

[24] A. Mora-Boza, E. Lopez-Ruiz, M. L. Lopez-Donaire, G. Jimenez, M. R. Aguilar, J. A. Marchal, J. L. Pedraz, B. Vazquez-Lasa, J. S. Roman, P. Galvez-Martin, *Polymers* **2020**, *12*, 2661.

[25] J. Li, C. Wu, P. K. Chu, M. Gelinsky, *Mater. Sci. Eng. R. Rep.* **2020**, *140*, 100543.

[26] J.-F. Xing, M.-L. Zheng, X.-M. Duan, *Chem. Soc. Rev.* **2015**, *44*, 5031.

[27] T.-S. Jang, H.-D. Jung, H. M. Pan, W. T. Han, S. Chen, J. Song, *Int J Bioprint*, **2018**, *4,* 126.

[28] J. Jia, D. J. Richards, S. Pollard, Y. Tan, J. Rodriguez, R. P. Visconti, T. C. Trusk, M. J. Yost, H. Yao, R. R. Markwald, Y. Mei, *Acta biomater.* **2014**, *10*, 4323.

[29] L. Yang, X. Fan, J. Zhang, J. Ju, *Polymers* **2020**, *12,* 389.

[30] L. He, S. Vibhagool, H. Zhao, V. Hoven, P. Theato, *Macromol. Chem. Phys.* **2018**, 219.

[31] G. Stoychev, A. Kirillova, L. Ionov, *Adv. Opt. Mater.* **2019**, *7,* 1900067.

[32] S. Dai, P. Ravi, K. C. Tam, *Soft Matter* **2008**, *4*, 435.

[33] M. Bansal, A. Dravid, Z. Aqrawe, J. Montgomery, Z. Wu, D. Svirskis, *J. Controlled Release* **2020**, *328*, 192.

[34] E. Yarali, M. Baniasadi, A. Zolfagharian, M. Chavoshi, F. Arefi, M. Hossain, A. Bastola, M. Ansari, A. Foyouzat, A. Dabbagh, M. Ebrahimi, M. J. Mirzaali, M. Bodaghi, *Appl. Mater. Today* **2022**, *26*, 101306.

[35] J. Zhang, X. Jiang, X. Wen, Q. Xu, H. Zeng, Y. Zhao, M. Liu, Z. Wang, X. Hu, Y. Wang, *J. Phys. Mater.* **2019**, *2,* 032004.

[36] Y. L. Colson, M. W. Grinstaff, *Adv. Mater.* **2012**, *24*, 3878.

[37] M. Wei, Y. Gao, X. Li, M. J. Serpe, *Polym. Chem.* **2017**, *8*, 127.

[38] J. Hu, S. Liu, *Macromolecules* **2010**, *43*, 8315.

[39] M. Vigata, C. Meinert, D. W. Hutmacher, N. Bock, *Pharmaceutics* **2020**, *12,* 1188.

[40] D. Parasuraman, M. J. Serpe, *ACS Appl. Mater. Interfaces* **2011**, *3*, 2732.

[41] R. Kempaiah, Z. Nie, *J. Mater. Chem. B* **2014**, *2*, 2357.

[42] Q. Zhao, Y. Chang, Z. Yu, Y. Liang, L. Ren, L. Ren, *J. Mater. Chem. B* **2020**, *8*, 9362.

[43] X. Sun, S. Agate, K. S. Salem, L. Lucia, L. Pal, *ACS Appl. Bio. Mater.* **2021**, *4*, 140.

[44] L. M. Randolph, M.-P. Chien, N. C. Gianneschi, *Chem. Sci.* **2012**, *3*, 1363.

[45] E. Gil, S. Hudson, *Prog. Polym. Sci.* **2004**, *29*, 1173.

[46] A. D. Jenkins, P. Kratochvíl, R. F. T. Stepto, U. W. Suter, *Pure Appl. Chem.* **1996**, *68*, 2287.

[47] E. Blasco, M. Wegener, C. Barner-Kowollik, *Adv. Mater.* **2017**, *29,* 1604005.

[48] Y. Gu, J. Zhao, J. A. Johnson, *Angew. Chem. Int. Ed. Engl.* **2020**, *59*, 5022.

[49] *Br. Med. J.* **1914**, *1*, 284.

[50] J. Millar, *J. Chem. Soc.* **1960**, 1, 1311.

[51] A. K. Nayak, M. S. Hasnain, *Advanced biopolymeric systems for drug delivery*, Springer, **2020**.

[52] E. S. Dragan, *Chem. Eng. J.* **2014**, *243*, 572.

[53] M. Shivashankar, B. K. Mandal, *Int. J. Pharm. Pharm. Sci.* **2012**, *4*, 1.

[54] R. Bai, H. Zhang, X. Yang, J. Zhao, Y. Wang, Z. Zhang, X. Yan, *Polym. Chem.* **2022**, *13*, 1253.

[55] Z. Qi, C. A. Schalley, *Acc. Chem. Res.* **2014**, *47*, 2222.

[56] D. W. Balkenende, C. A. Monnier, G. L. Fiore, C. Weder, *Nat. Commun.* **2016**, *7*, 10995.

[57] R. Dong, Y. Pang, Y. Su, X. Zhu, *Biomater. Sci.* **2015**, *3*, 937.

[58] L. Wang, L. Cheng, G. Li, K. Liu, Z. Zhang, P. Li, S. Dong, W. Yu, F. Huang, X. Yan, *J. Am. Chem. Soc.* **2020**, *142*, 2051.

[59] S. Konishi, Y. Kashiwagi, G. Watanabe, M. Osaki, T. Katashima, O. Urakawa, T. Inoue, H. Yamaguchi, A. Harada, Y. Takashima, *Polym. Chem.* **2020**, *11*, 6811.

[60] X. Yan, F. Wang, B. Zheng, F. Huang, *Chem. Soc. Rev.* **2012**, *41*, 6042.

[61] G. Zhang, Q. Zhao, W. Zou, Y. Luo, T. Xie, *Adv. Funct. Mater.* **2016**, *26*, 931.

[62] E. M. Ahmed, *J. Adv. Res.* **2015**, *6*, 105.

[63] B. S. Kaith, A. Singh, A. K. Sharma, D. Sud, *J. Polym. Environ.* **2021**, *29*, 3827.

[64] S. Trombino, C. Servidio, F. Curcio, R. Cassano, *Pharmaceutics* **2019**, *11,* 407.

[65] S. Lankalapalli, V. Kolapalli, *Indian J. Pharm. Sci.* **2009**, *71*, 481.

[66] J. L. Drury, D. J. Mooney, *Biomaterials* **2003**, *24*, 4337.

[67] S. Yue, H. He, B. Li, T. Hou, *Nanomaterials* **2020**, *10,* 1511.

[68] Q. Rong, W. Lei, M. Liu, *Chemistry* **2018**, *24*, 16930.

[69] J. Liu, S. Qu, Z. Suo, W. Yang, *Natl. Sci. Rev.* **2021**, *8*, nwaa254.

[70] C. Lei, Y. Guo, W. Guan, H. Lu, W. Shi, G. Yu, *Angew. Chem. Int. Ed. Engl.* **2022**, *61*, e202200271.

[71] P. Jiang, P. Lin, C. Yang, H. Qin, X. Wang, F. Zhou, *Chem. Mater.* **2020**, *32*, 9983.

[72] M. Gierszewska, J. Ostrowska-Czubenko, E. Chrzanowska, *Eur. Polym. J.* **2018**, *101*, 282.

[73] P. Wei, X. Yan, F. Huang, *Chem. Soc. Rev.* **2015**, *44*, 815.

[74] F. D. Jochum, F. R. Forst, P. Theato, *Macromol. Rapid Commun.* **2010**, *31*, 1456.

[75] J. Qiao, Q. Ma, C. Cheng, L. Qi, *Chem. Asian J.* **2023**, *18*, e202300285.

[76] H. Fu, D. M. Policarpio, J. D. Batteas, D. E. Bergbreiter, *Polym. Chem.* **2010**, *1,* 631.

[77] S. Uchiyama, N. Kawai, A. P. de Silva, K. Iwai, *J. Am. Chem. Soc.* **2004**, *126*, 3032.

[78] O. Bertrand, J.-F. Gohy, *Polym. Chem.* **2017**, *8*, 52.

[79] A. Saneja, R. Kumar, D. Arora, S. Kumar, A. K. Panda, S. Jaglan, *Drug Discovery Today* **2018**, *23*, 1115.

[80] A. Raza, U. Hayat, T. Rasheed, M. Bilal, H. M. N. Iqbal, *J. Mater. Res. Technol.* **2019**, *8*, 1497.

[81] H. Chen, Y. Zhao, *ACS Appl. Mater. Interfaces* **2018**, *10*, 21021.

[82] G. Kocak, C. Tuncer, V. Bütün, *Polym. Chem.* **2017**, *8*, 144.

[83] L. Li, J. M. Scheiger, P. A. Levkin, *Adv. Mater.* **2019**, *31*, e1807333.

[84] J. Li, X. Zhou, Z. Liu, *Adv. Opt. Mater.* **2020**, *8*, 2000886.

[85] M. Pilz da Cunha, M. G. Debije, A. Schenning, *Chem. Soc. Rev.* **2020**, *49*, 6568.

[86] K. M. Al-Aribe, G. K. Knopf, A. S. Bassi, *Sens. Actuators, B* **2013**, *176*, 1056.

[87] M.-J. Lee, D.-H. Jung, Y.-K. Han, *Mol. Cryst. Liq. Cryst.* **2006**, *444*, 41.

[88] B. Seefeldt, R. Kasper, M. Beining, J. Mattay, J. Arden-Jacob, N. Kemnitzer, K. H. Drexhage, M. Heilemann, M. Sauer, *Photochem. Photobiol. Sci.* **2010**, *9*, 213.

[89] Y. Hao, J. Meng, S. Wang, *Chin. Chem. Lett.* **2017**, *28*, 2085.

[90] K. Mishra, J. P. Fuenzalida-Werner, F. Pennacchietti, R. Janowski, A. Chmyrov, Y. Huang, C. Zakian, U. Klemm, I. Testa, D. Niessing, V. Ntziachristos, A. C. Stiel, *Nat. Biotechnol.* **2022**, *40*, 598.

[91] Y. Wang, Z. Chen, N. Li, H. Zhang, J. Wei, *Eur. Polym. J.* **2022**, *166*, 111025.

[92] Y. Wang, C.-L. Sun, L.-Y. Niu, L.-Z. Wu, C.-H. Tung, Y.-Z. Chen, Q.-Z. Yang, *Polym. Chem.* **2017**, *8*, 3596.

[93] S. Menon, R. Thekkayil, S. Varghese, S. Das, *J. Polym. Sci., Part A: Polym. Chem.* **2011**, *49*, 5063.

[94] V. Pruthi, Y. Akae, P. Theato, *Macromol. Rapid Commun.* **2023**, *44*, 2300270.

[95] Y. Yu, T. Maeda, J. Mamiya, T. Ikeda, *Angew. Chem. Int. Ed. Engl.* **2007**, *46*, 881.

[96] J. Fritzsche, *J. prakt. Chem.* **1866**, *97*, 290.

[97] O. Grimm, F. Wendler, F. H. Schacher, *Polymers* **2017**, *9,* 396.

[98] W. Szymanski, J. M. Beierle, H. A. Kistemaker, W. A. Velema, B. L. Feringa, *Chem. Rev.* **2013**, *113*, 6114.

[99] F. A. Jerca, V. V. Jerca, R. Hoogenboom, *Nat. Rev. Chem.* **2022**, *6*, 51.

[100] P. Klan, T. Solomek, C. G. Bochet, A. Blanc, R. Givens, M. Rubina, V. Popik, A. Kostikov, J. Wirz, *Chem. Rev.* **2013**, *113*, 119.

[101] J. Keyvan Rad, Z. Balzade, A. R. Mahdavian, *J. Photochem. Photobiol., C* **2022**, *51,* 100487.

[102] E. Fischer, Y. Hirshberg, *J. Chem. Soc.*, **1952**, 4522.

[103] L. Kortekaas, W. R. Browne, *Chem. Soc. Rev.* **2019**, *48*, 3406.

[104] J. Xie, J. Zhang, Y. Ma, Y. Han, J. Li, M. Zhu, *J. Mater. Chem. C* **2022**, *10*, 7154.

[105] F. Jiang, S. Chen, Z. Cao, G. Wang, *Polymer* **2016**, *83*, 85.

[106] Y. Yang, H. Zhao, Y. Li, Y. Chen, Z. Wang, W. Wu, L. Hu, J. Zhu, *ACS Omega* **2023**, *8*, 16459.

[107] K. Y. Shinpei Kado, Tomoo Murakami, and Keiichi Kimura, *J. Am. Chem. Soc.* **2005**, *127*, 3026.

[108] O. Kovalenko, Y. Lopatkin, P. Kondratenko, D. Belous, *Eur. Phys. J. D.* **2018**, *72*, 20.

[109] H. Görner, *Phys. Chem. Chem. Phys.* **2001**, *3*, 416.

[110] S. Swansburg, E. Buncel, R. P. Lemieux, *J. Am. Chem. Soc.* **2000**, *122*, 6594.

[111] M. Li, Q. Zhang, Y.-N. Zhou, S. Zhu, *Prog. Polym. Sci.* **2018**, *79*, 26.

[112] F. M. Raymo, S. Giordani, *J. Am. Chem. Soc.* **2001**, *123*, 4651.

[113] L. Florea, D. Diamond, F. Benito-Lopez, *Macromol. Mater. Eng.* **2012**, *297*, 1148.

[114] Y. Bardavid, I. Goykhman, D. Nozaki, G. Cuniberti, S. Yitzchaik, *J. Phys. Chem. C* **2011**, *115*, 3123.

[115] L. Hauser, A.-C. Knall, M. Roth, G. Trimmel, M. Edler, T. Griesser, W. Kern, *Monatsch. Chem.* **2012**, *143*, 1551.

[116] S.-R. Keum, S.-M. Ahn, S.-J. Roh, S.-Y. Ma, *Dyes Pigm.* **2010**, *86*, 74.

[117] B. B. Mistry, R. G. Patel, V. S. Patel, *J. Appl. Polym. Sci.* **1997**, *64*, 841.

[118] J. Verborgt, G. Smets, *J. Polym. Sci., Polym. Chem. Ed.* **1974**, *12*, 2511.

[119] S. A. Ahmed, R. M. Okasha, K. S. Khairou, T. H. Afifi, A.-A. H. Mohamed, A. S. Abd-El-Aziz, *Polymers* **2017**, *9*, 630.

[120] R. Nakao, N. Ueda, Y. Abe, T. Horii, H. Inoue, *Polym. Adv. Technol.* **1995**, *6*, 243.

[121] D. S. Achilleos, M. Vamvakaki, *Macromolecules* **2010**, *43*, 7073.

[122] C.-Q. Huang, Y. Wang, C.-Y. Hong, C.-Y. Pan, *Macromol. Rapid Commun.* **2011**, *32*, 1174.

[123] Y. S. Park, Y. Ito, Y. Imanishi, *Macromolecules* **1998**, *31*, 2606.

[124] T. Wu, G. Zou, J. Hu, S. Liu, *Chem. Mater.* **2009**, *21*, 3788.

[125] E. Mitscherlich, *Ann. Phys.* **1834**, *108*, 225.

[126] A. Bafana, S. S. Devi, T. Chakrabarti, *Environ. Rev.* **2011**, *19*, 350.

[127] G. S. Hartley, *Nature* **1937**, *140*, 281.

[128] A. A. Beharry, G. A. Woolley, *Chem. Soc. Rev.* **2011**, *40*, 4422.

[129] J. Van Hoorick, H. Ottevaere, H. Thienpont, P. Dubruel, S. Van Vlierberghe, *Polymer and photonic materials towards biomedical breakthroughs*, Springer, **2018**.

[130] A. Gimenez-Gomez, L. Magson, B. Peñin, N. Sanosa, J. Soilán, R. Losantos, D. Sampedro, *Photochem* **2022**, *2*, 694.

[131] E. Wagner-Wysiecka, N. Lukasik, J. F. Biernat, E. Luboch, *J. Incl. Phenom. Macrocycl. Chem.* **2018**, *90*, 189.

[132] M. Baroncini, J. Groppi, S. Corra, S. Silvi, A. Credi, *Adv. Opt. Mater.* **2019**, *7*, 1900392.

[133] T. Fujino, S. Y. Arzhantsev, T. Tahara, *J. Phys. Chem. A* **2001**, *105*, 8123.

[134] N. Tamai, H. Miyasaka, *Chem. Rev.* **2000**, *100*, 1875.

[135] J. Casellas, M. J. Bearpark, M. Reguero, *ChemPhysChem* **2016**, *17*, 3068.

[136] S. Samanta, T. M. McCormick, S. K. Schmidt, D. S. Seferos, G. A. Woolley, *Chem. Commun.*, **2013**, *49*, 10314.

[137] P. Griefs, *Justus Liebigs Ann. Chem.* **1858**, *106*, 123.

[138] C. Mills, *J. Chem. Soc., Trans.* **1895**, *67*, 925.

[139] R. O. Hutchins, D. W. Lamson, L. Rua, C. Milewski, B. Maryanoff, *J. Org. Chem.* **1971**, *36*, 803.

[140] B. Ortiz, P. Villanueva, F. Walls, *J. Org. Chem.* **1972**, *37*, 2748.

[141] O. Wallach, L. Belli, *Ber. Dtsch. Chem. Ges.* **1880**, *13*, 525.

[142] Z. Zhang, Z. Xie, C. Nie, S. Wu, *Polymer* **2022**, *256,* 125166.

[143] S. Wu, S. Duan, Z. Lei, W. Su, Z. Zhang, K. Wang, Q. Zhang, *J. Mater. Chem.* **2010**, *20*, 5202.

[144] A. Priimagi, A. Shevchenko, *J. Polym. Sci., Part B: Polym. Phys.* **2014**, *52*, 163.

[145] Y. Yu, M. Nakano, T. Ikeda, *Nature* **2003**, *425*, 145.

[146] L. Zhang, H. Liang, J. Jacob, P. Naumov, *Nat. Commun.* **2015**, *6*, 7429.

[147] T. Eom, W. Yoo, S. Kim, A. Khan, *Biomaterials* **2018**, *185*, 333.

[148] A. Kravchenko, A. Shevchenko, V. Ovchinnikov, A. Priimagi, M. Kaivola, *Adv. Mater.* **2011**, *23*, 4174.

[149] S. Wu, H. J. Butt, *Macromol. Rapid Commun.* **2020**, *41*, 1900413.

[150] L. Dong, Y. Feng, L. Wang, W. Feng, *Chem. Soc. Rev.* **2018**, *47*, 7339.

[151] P. Theato, *Angew. Chem. Int. Ed.* **2011**, *50*, 5804.

[152] X. Peng, H. Wang, *J. Polym. Sci., Part B: Polym. Phys.* **2018**, *56*, 1314.

[153] P. F. Luo, S. L. Xiang, C. Li, M. Q. Zhu, *J. Polym. Sci.* **2021**, *59*, 2246.

[154] I. Tomatsu, K. Peng, A. Kros, *Adv. Drug Delivery Rev.* **2011**, *63*, 1257.

[155] A. M. Rosales, C. B. Rodell, M. H. Chen, M. G. Morrow, K. S. Anseth, J. A. Burdick, *Bioconjugate Chem.* **2018**, *29*, 905.

[156] A. Hardy, C. Seguin, A. Brion, P. Lavalle, P. Schaaf, S. Fournel, L. Bourel-Bonnet, B. Frisch, M. De Giorgi, *ACS Appl. Mater. Interfaces* **2018**, *10*, 29347.

[157] G. Crini, *Chem. Rev.* **2014**, *114*, 10940.

[158] M. Arslan, R. Sanyal, A. Sanyal, "Cyclodextrin-Containing Hydrogel Networks", in *Encyclopedia of Biomedical Polymers and Polymeric Biomaterials*, **2016**, 2243.

[159] A. Harada, Y. Takashima, M. Nakahata, *Acc. Chem. Res.* **2014**, *47*, 2128.

[160] Y. Takashima, S. Hatanaka, M. Otsubo, M. Nakahata, T. Kakuta, A. Hashidzume, H. Yamaguchi, A. Harada, *Nat. Commun.* **2012**, *3*, 1270.

[161] A. Romano, I. Roppolo, E. Rossegger, S. Schlogl, M. Sangermano, *Materials* **2020**, *13,* 2777.

[162] J. A. Barltrop, P. J. Plant, P. Schofield, *Chem. Commun. (London)* **1966**, 22, 822.

[163] H. Zhao, E. S. Sterner, E. B. Coughlin, P. Theato, *Macromolecules* **2012**, *45*, 1723.

[164] J. F. Cameron, J. M. Frechet, *J. Am. Chem. Soc.* **1991**, *113*, 4303.

[165] A. Specht, M. Goeldner, *Angew. Chem.* **2004**, *116*, 2042.

[166] C. Marinzi, J. Offer, R. Longhi, P. E. Dawson, *Biorg. Med. Chem.* **2004**, *12*, 2749.

[167] Y. V. Il'ichev, M. A. Schwörer, J. Wirz, *J. Am. Chem. Soc.* **2004**, *126*, 4581.

[168] X. Chi, W. Cen, J. A. Queenan, L. Long, V. M. Lynch, N. M. Khashab, J. L. Sessler, *J. Am. Chem. Soc.* **2019**, *141*, 6468.

[169] I. Aujard, C. Benbrahim, M. Gouget, O. Ruel, J. B. Baudin, P. Neveu, L. Jullien, *Chem. Eur. J.* **2006**, *12*, 6865.

[170] C. C. Petropoulos, *J. Polym. Sci., Polym. Chem. Ed.* **1977**, *15*, 1637.

[171] E. Reichmanis, B. Smith, R. Gooden, *J. Polym. Sci., Polym. Chem. Ed.* **1985**, *23*, 1.

[172] E. Reichmanis, R. Gooden, C. W. Wilkins Jr., H. Schonhorn, *J. Polym. Sci., Polym. Chem. Ed.* **1983**, *21*, 1075.

[173] M. Kim, H. Chung, *Polym. Chem.* **2017**, *8*, 6300.

[174] A. Turanli, N. Demirbilek, T. N. Gevrek, *ACS Appl. Polym. Mater.* **2023**, *6*, 448.

[175] Y. Luo, M. S. Shoichet, *Biomacromolecules* **2004**, *5*, 2315.

[176] C. A. DeForest, K. S. Anseth, *Nat. Chem.* **2011**, *3*, 925.

[177] J. Hu, G. Zhang, Z. Ge, S. Liu, *Prog. Polym. Sci.* **2014**, *39*, 1096.

[178] A. S. Hoffman, *Adv. Drug Delivery Rev.* **2012**, *64*, 18.

[179] S. Lankalapalli, V. R. Kolapalli, *Indian J. Pharm. Sci.* **2009**, *71*, 481.

[180] S. J. Kim, S. R. Shin, K. B. Lee, Y. D. Park, S. I. Kim, *J. Appl. Polym. Sci.* **2004**, *91*, 2908.

[181] C. Vasile, D. Pieptu, R. P. Dumitriu, A. Pânzariu, L. Profire, *Rev. Med. Chir. Soc. Med. Nat. Iasi.* **2013**, *117*, 565.

[182] V. Bourganis, T. Karamanidou, O. Kammona, C. Kiparissides, *Eur. J. Pharm. Biopharm.* **2017**, *111*, 44.

[183] P. Visakh, *Polyelectrolytes: Thermodynamics and Rheology,* **2014**, 1.

[184] G. Morello, G. De Iaco, G. Gigli, A. Polini, F. Gervaso, *Gels* **2023**, *9*, 132.

[185] I. A. van Hees, A. H. Hofman, M. Dompé, J. van der Gucht, M. Kamperman, *Eur. Polym. J.* **2020**, *141*, 110034.

[186] C. L. Silva, J. C. Pereira, A. Ramalho, A. A. C. C. Pais, J. J. S. Sousa, *J. Membr. Sci.* **2008**, *320*, 268.

[187] C. Yang, Z. Suo, *Nat. Rev. Mater.* **2018**, *3*, 125.

[188] F. A. Simsek-Ege, G. M. Bond, J. Stringer, *J. Appl. Polym. Sci.* **2003**, *88*, 346.

[189] S. Srivastava, A. E. Levi, D. J. Goldfeld, M. V. Tirrell, *Macromolecules* **2020**, *53*, 5763.

[190] S. Gao, A. Holkar, S. Srivastava, *Polymers* **2019**, *11*, 1097.

[191] D. Li, T. Göckler, U. Schepers, S. Srivastava, *Macromolecules* **2022**, *55*, 4481.

[192] J. W. Lee, S. Y. Kim, S. S. Kim, Y. M. Lee, K. H. Lee, S. J. Kim, *J. Appl. Polym. Sci.* **1999**, *73*, 113.

[193] P. Matricardi, C. Di Meo, T. Coviello, W. E. Hennink, F. Alhaique, *Adv. Drug Delivery Rev.* **2013**, *65*, 1172.

[194] S. Srivastava, M. Andreev, A. E. Levi, D. J. Goldfeld, J. Mao, W. T. Heller, V. M. Prabhu, J. J. de Pablo, M. V. Tirrell, *Nat. Commun.* **2017**, *8*, 14131.

[195] S. Bian, Z. Zheng, Y. Liu, C. Ruan, H. Pan, X. Zhao, *J. Mater. Chem. B* **2019**, *7*, 6488.

[196] J. M. Townsend, E. C. Beck, S. H. Gehrke, C. J. Berkland, M. S. Detamore, *Prog. Polym. Sci.* **2019**, *91*, 126.

[197] D. Braun, *Int. J. Polym. Sci.* **2009**, 1, 893234.

[198] P. Nesvadba, "Radical Polymerization in Industry", in *Encyclopedia of Radicals in Chemistry, Biology and Materials*, **2012**.

[199] B. Yamada, P. B. Zetterlund, "General Chemistry of Radical Polymerization", in *Handbook of Radical Polymerization*, **2002**, 117.

[200] E. Andrzejewska, *Prog. Polym. Sci.* **2001**, *26*, 605.

[201] K. Anseth, S. Newman, C. Bowman, "Polymeric dental composites: properties and reaction behavior of multimethacrylate dental restorations", in *Biopolymers II*, Springer, **1995**, 177.

[202] J. G. Kloosterboer, "*Network formation by chain crosslinking photopolymerization and its applications in electronics"*, Springer, **1988**.

[203] A. Bagheri, J. Jin, *ACS Appl. Polym. Mater.* **2019**, *1*, 593.

[204] M. Kaur, A. K. Srivastava, *J. Macromol. Sci., Polym. Rev.* **2002**, *42*, 481.

[205] R. Chaudhary, P. Fabbri, E. Leoni, F. Mazzanti, R. Akbari, C. Antonini, *Prog. Addit. Manuf.* **2022**, *8*, 331.

[206] X. Pan, M. A. Tasdelen, J. Laun, T. Junkers, Y. Yagci, K. Matyjaszewski, *Prog. Polym. Sci.* **2016**, *62*, 73.

[207] M. Szwarc, M. Van Beylen, "*Ionic polymerization and living polymers"*, Springer Science & Business Media, **2012**.

[208] B. Wendel, D. Rietzel, F. Kühnlein, R. Feulner, G. Hülder, E. Schmachtenberg, *Macromol. Mater. Eng.* **2008**, *293*, 799.

[209] T. Jungst, W. Smolan, K. Schacht, T. Scheibel, J. Groll, *Chem. Rev.* **2016**, *116*, 1496.

[210] G. Ge, Q. Wang, Y. Z. Zhang, H. N. Alshareef, X. Dong, *Adv. Funct. Mater.* **2021**, *31,* 2107437.

[211] S. E. Bakarich, M. I. H. Panhuis, S. Beirne, G. G. Wallace, G. M. Spinks, *J. Mater. Chem. B* **2013**, *1*, 4939.

[212] R. Zhang, N. B. Larsen, *Lab Chip* **2017**, *17*, 4273.

[213] G. Burke, D. M. Devine, I. Major, *Polymers* **2020**, *12,* 2015.

[214] Y. Wang, N. Alizadeh, M. Barde, M. L. Auad, B. S. Beckingham, *ACS Appl. Polym. Mater.* **2022**, *4*, 971.

[215] J. H. Galarraga, A. P. Dhand, B. P. Enzmann, 3rd, J. A. Burdick, *Biomacromolecules* **2023**, *24*, 413.

[216] M. Taghizadeh, A. Taghizadeh, M. K. Yazdi, P. Zarrintaj, F. J. Stadler, J. D. Ramsey, S. Habibzadeh, S. Hosseini Rad, G. Naderi, M. R. Saeb, M. Mozafari, U. S. Schubert, *Green Chem.* **2022**, *24*, 62.

[217] R. Zhang, A. Liberski, F. Khan, J. J. Diaz-Mochon, M. Bradley, *Chem. Commun.* **2008**, 1317.

[218] Q. Liu, Q. Li, S. Xu, Q. Zheng, X. Cao, *Polymers* **2018**, *10,* 664.

[219] P. R. Martinez, A. Goyanes, A. W. Basit, S. Gaisford, *Int. J. Pharm.* **2017**, *532*, 313.

[220] S. Sultan, A. P. Mathew, *Nanoscale* **2018**, *10*, 4421.

[221] S. Waheed, J. M. Cabot, N. P. Macdonald, T. Lewis, R. M. Guijt, B. Paull, M. C. Breadmore, *Lab Chip* **2016**, *16*, 1993.

[222] W. Zhu, X. Qu, J. Zhu, X. Ma, S. Patel, J. Liu, P. Wang, C. S. E. Lai, M. Gou, Y. Xu, *Biomaterials* **2017**, *124*, 106.

[223] Z. Zhao, X. Tian, X. Song, *J. Mater. Chem. C* **2020**, *8*, 13896.

[224] W. Zhu, K. R. Tringale, S. A. Woller, S. You, S. Johnson, H. Shen, J. Schimelman, M. Whitney, J. Steinauer, W. Xu, *Mater. Today* **2018**, *21*, 951.

[225] Q. Mu, L. Wang, C. K. Dunn, X. Kuang, F. Duan, Z. Zhang, H. J. Qi, T. Wang, *Addit. Manuf.* **2017**, *18*, 74.

[226] A. Chiappone, E. Fantino, I. Roppolo, M. Lorusso, D. Manfredi, P. Fino, C. F. Pirri, F. Calignano, *ACS Appl. Mater. Interfaces* **2016**, *8*, 5627.

[227] J. Wang, S. Stanic, A. A. Altun, M. Schwentenwein, K. Dietliker, L. Jin, J. Stampfl, S. Baudis, R. Liska, H. Grützmacher, *Chem. Commun.* **2018**, *54*, 920.

[228] N. Murase, T. Ando, H. Ajiro, *J. Mater. Chem. B* **2020**, *8*, 1489.

[229] A. Radu, S. Scarmagnani, R. Byrne, C. Slater, K. Tong Lau, D. Diamond, *J. Phys. D: Appl. Phys.* **2007**, *40*, 7238.

[230] L. Chen, C. Zhao, J. Huang, J. Zhou, M. Liu, *Nat. Commun.* **2022**, *13*, 6821.

[231] W. Hu, C. Sun, Y. Ren, S. Qin, Y. Shao, L. Zhang, Y. Wu, Q. Wang, H. Yang, D. Yang, *Angew. Chem. Int. Ed. Engl.* **2021**, *60*, 19406.

[232] T. J. Gately, W. Li, S. H. Mostafavi, C. J. Bardeen, *Macromolecules* **2021**, *54*, 9319.

[233] B. Yang, M. Yu, H. Yu, *Chempluschem* **2020**, *85*, 2166.

[234] H. Cui, H. Liu, S. Chen, R. Wang, *Dyes Pigm.* **2015**, *115*, 50.

[235] A. Abdollahi, Z. Alinejad, A. R. Mahdavian, *J. Mater. Chem. C* **2017**, *5*, 6588.

[236] A. Gonzalez, E. S. Kengmana, M. V. Fonseca, G. G. D. Han, *Mater. Today Adv.* **2020**, *6*, 100058.

[237] X. Fang, H. Zhang, Y. Chen, Y. Lin, Y. Xu, W. Weng, *Macromolecules* **2013**, *46*, 6566.

[238] C.-C. Huang, M.-X. Du, B.-Q. Zhang, C.-Y. Liu, *Macromolecules* **2022**, *55*, 3189.

[239] K. E. Smith, S. Sawicki, M. A. Hyjek, S. Downey, K. Gall, *Polymer (Guildf)* **2009**, *50*, 5112.

[240] E. Samoylova, L. Ceseracciu, M. Allione, A. Diaspro, A. C. Barone, A. Athanassiou, *Appl. Phys. Lett.* **2011**, *99*, 201905.

[241] W. Tian, J. Tian, *Langmuir* **2014**, *30*, 3223.

[242] Y. Xue, J. Tian, W. Tian, P. Gong, J. Dai, X. Wang, *J. Phys. Chem. C* **2015**, *119*, 20762.

[243] H. Zhou, C. Xue, P. Weis, Y. Suzuki, S. Huang, K. Koynov, G. K. Auernhammer, R. Berger, H. J. Butt, S. Wu, *Nat. Chem.* **2017**, *9*, 145.

[244] L. Wang, Y. Liu, X. Zhan, D. Luo, X. Sun, *J. Mater. Chem. C* **2019**, *7*, 8649.

[245] Y. Li, Y. Liu, D. Luo, *J. Mater. Chem. C* **2019**, *7*, 15166.

[246] F. Horkay, *Gels* **2021**, *7,* 102.

[247] S. J. Kim, K. J. Lee, S. I. Kim, *J. Appl. Polym. Sci.* **2004**, *93*, 1097.

[248] J. Berger, M. Reist, J. M. Mayer, O. Felt, R. Gurny, *Eur. J. Pharm. Biopharm.* **2004**, *57*, 35.

[249] V. M. Gun'ko, I. N. Savina, S. V. Mikhalovsky, *Gels* **2017**, *3,* 37.

[250] C. Lin, I. Gitsov, *Macromolecules* **2010**, *43*, 3256.

[251] R. Foudazi, R. Zowada, I. Manas-Zloczower, D. L. Feke, *Langmuir* **2023**, *39*, 2092.

[252] G. S. Sailaja, P. Ramesh, T. V. Kumary, H. K. Varma, *Acta Biomater.* **2006**, *2*, 651.

[253] S. Suri, C. E. Schmidt, *Acta Biomater.* **2009**, *5*, 2385.

[254] R. Kocen, M. Gasik, A. Gantar, S. Novak, *Biomed. Mater.* **2017**, *12*, 025004.

[255] Q. Chen, X. Li, Y. Xie, W. Hu, Z. Cheng, H. Zhong, H. Zhu, *Carbohydr. Polym.* **2021**, *267,* 118152.

[256] C. E. Schanté, G. Zuber, C. Herlin, T. F. Vandamme, *Carbohydr. Polym.* **2011**, *85*, 469.

[257] G. Tripodo, C. Wischke, A. T. Neffe, A. Lendlein, *Carbohydr. Res.* **2013**, *381*, 59.

[258] Z. Yuan, Y. Ye, F. Gao, H. Yuan, M. Lan, K. Lou, W. Wang, *Int. J. Pharm.* **2013**, *446*, 191.

[259] Y. F. Chen, C. L. Hsieh, P. Y. Lin, Y. C. Liu, M. J. Lee, L. R. Lee, S. Zheng, Y. L. Lin, Y. L. Huang, J. T. Chen, *Small* **2024**, 20, 2305317.

[260] A. W. Zaibudeen, J. Philip, *Colloids Surf., A* **2018**, *550*, 209.

[261] C. Li, A. Iscen, L. C. Palmer, G. C. Schatz, S. I. Stupp, *J. Am. Chem. Soc.* **2020**, *142*, 8447.

[262] C. Pozos Vázquez, T. Boudou, V. Dulong, C. Nicolas, C. Picart, K. Glinel, *Langmuir* **2009**, *25*, 3556.

Appendix

Additional Figures of Chapter 4.1

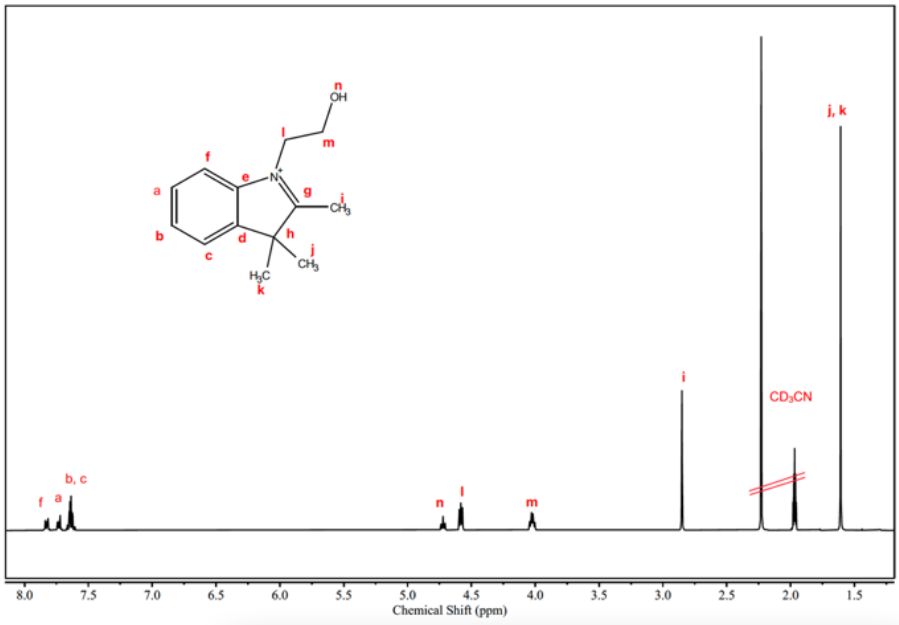

Figure A1 ^{1}H NMR spectrum of 1-(2-hydroxyethyl)-2,3,3-trimethyl-3H-indolium bromide in CD_3CN (400 MHz, 298 K).

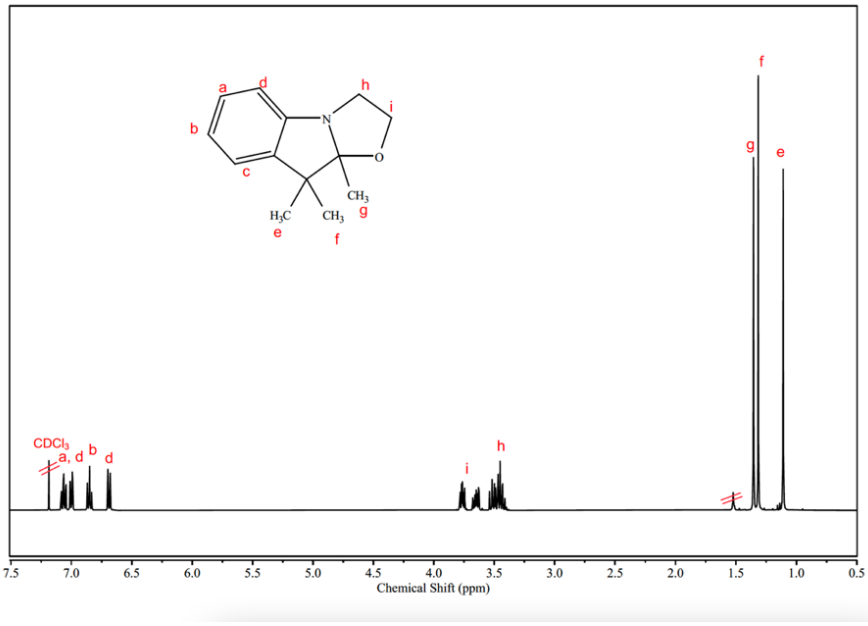

Figure A2 ^{1}H NMR spectrum of 9,9,9a -Trimethyl -2,3,9,9a- tetrahydro- oxazolo [3,2-a]indole in in $CDCl_3$ (400 MHz, 298 K).

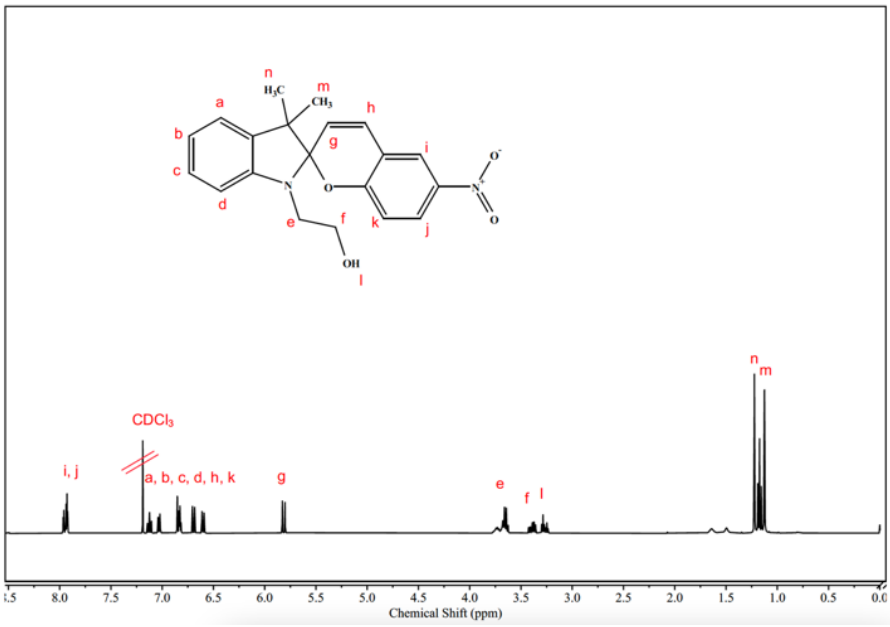

Figure A3 ^{1}H NMR spectrum of 2-(3',3'-Dimethyl-6-nitro-3'H-spiro[chromene-2,2'-indol]-1'-yl)-ethanol (SP-OH) in $CDCl_3$ (400 MHz, 298 K).

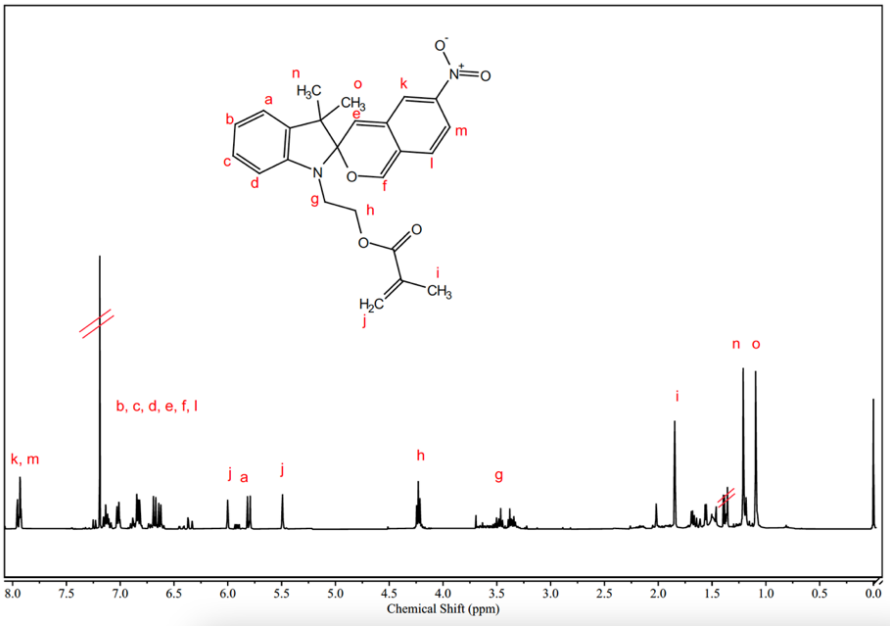

Figure A4 ^{1}H NMR spectrum of Spiropyran methacrylate (SpMa) in $CDCl_3$ (400 MHz, 298 K).

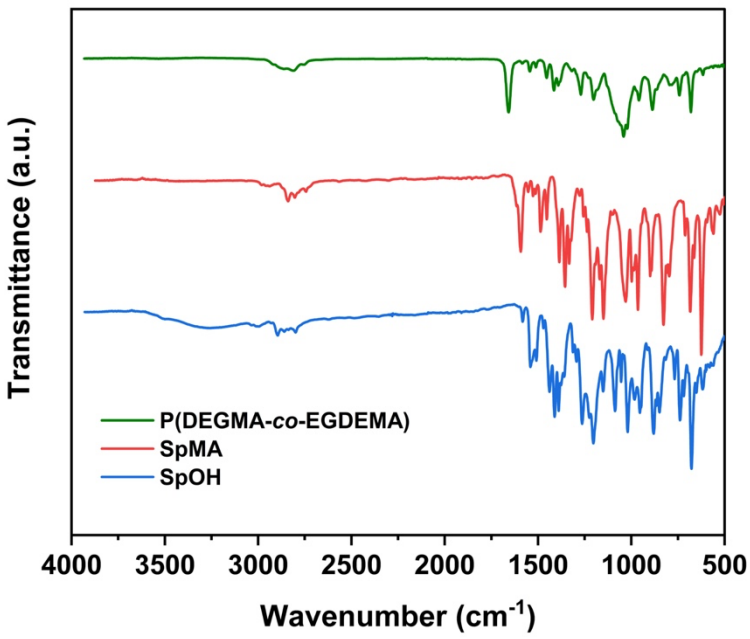

Figure A5 IR of P(DEGMA-*co*-SpMA) copolymer

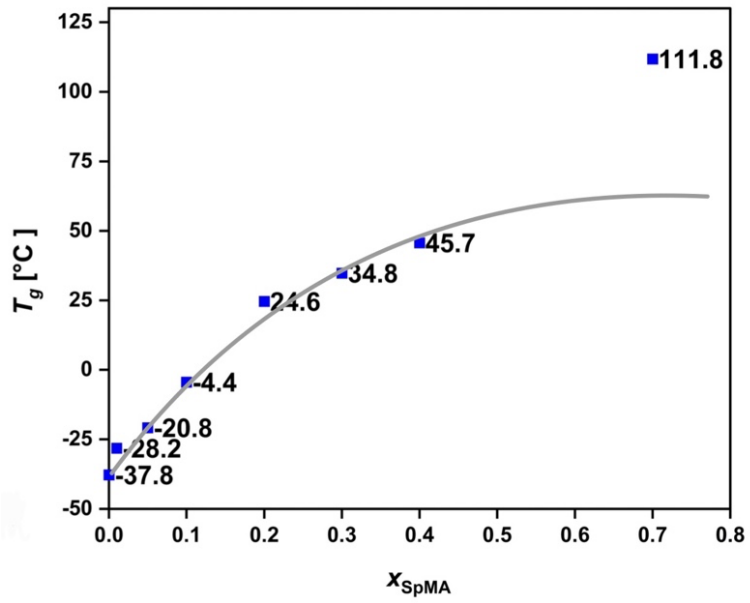

Figure A6 Graph representing the trend of T_g as a function of spiropyran content in the polymers

Additional Figures of Chapter 4.2

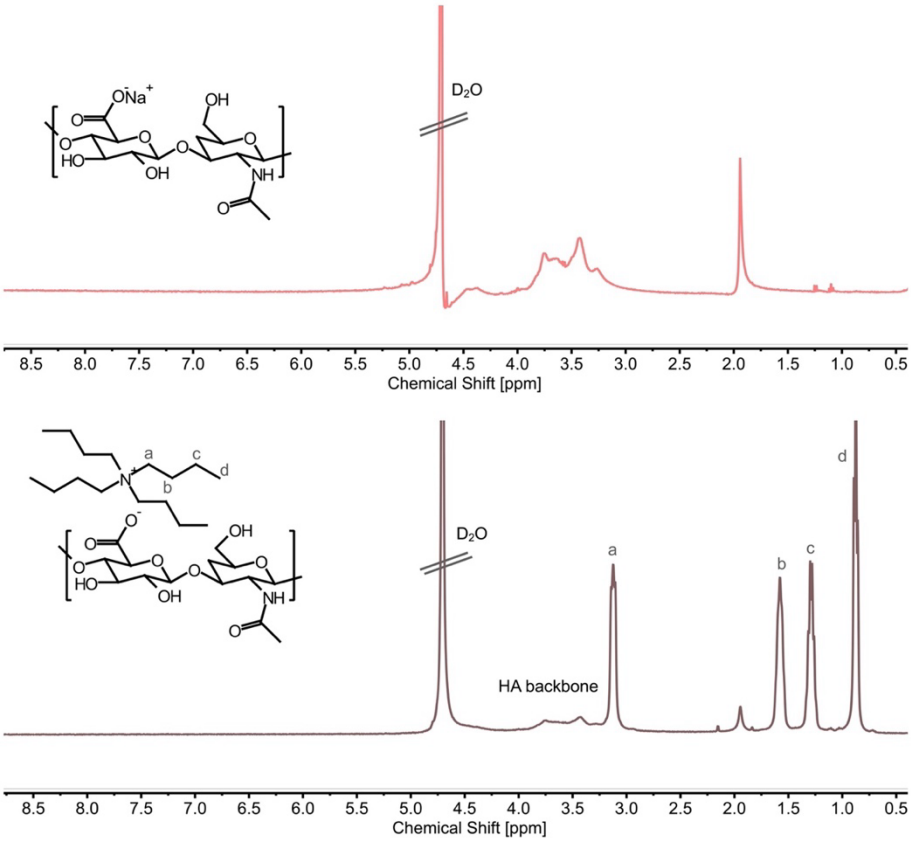

Figure A7 ^{1}H NMR spectra of HA-Na and HA-TBA in D_2O (400 MHz, 298 K).

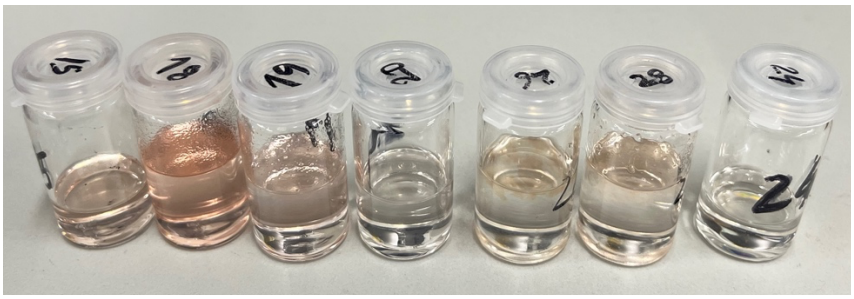

Figure A8 Different diverse HA-NBs exhibit varying color changes after UV exposure due to their different grafting ratios.

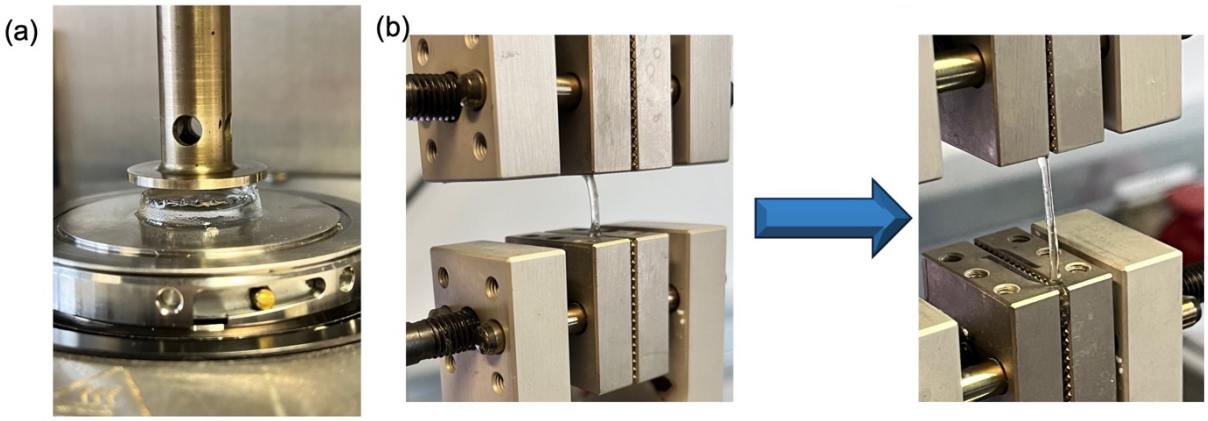

Figure A9 Figure displaying (a) shear rheology test of hydrogel, (b) tensile testing, showing high stretchability of hydrogel

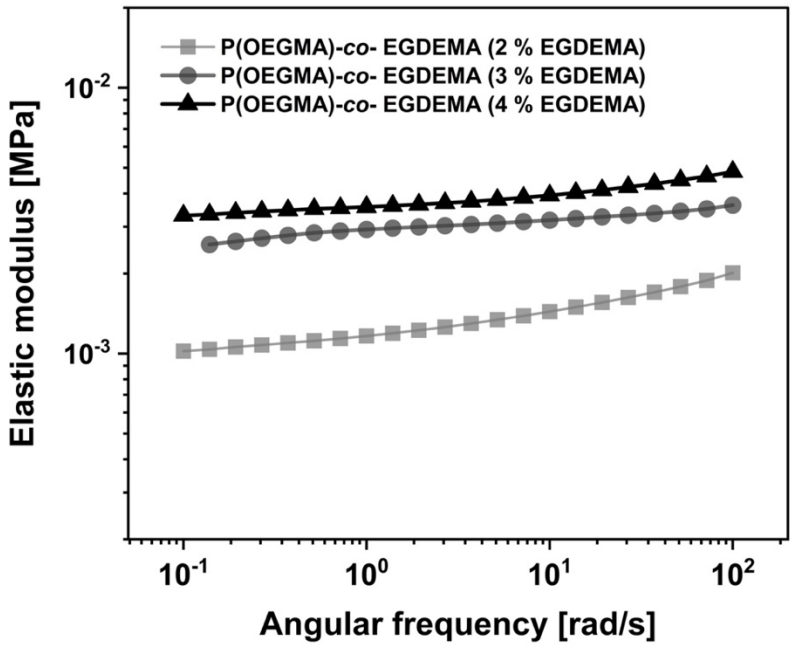

Figure A10 Frequency sweep analyses demonstrating the viscoelastic properties in P(OEGMA-*co*-EGDEMA) with different mol% of crosslinker.

Additional Figures of Chapter 4.3

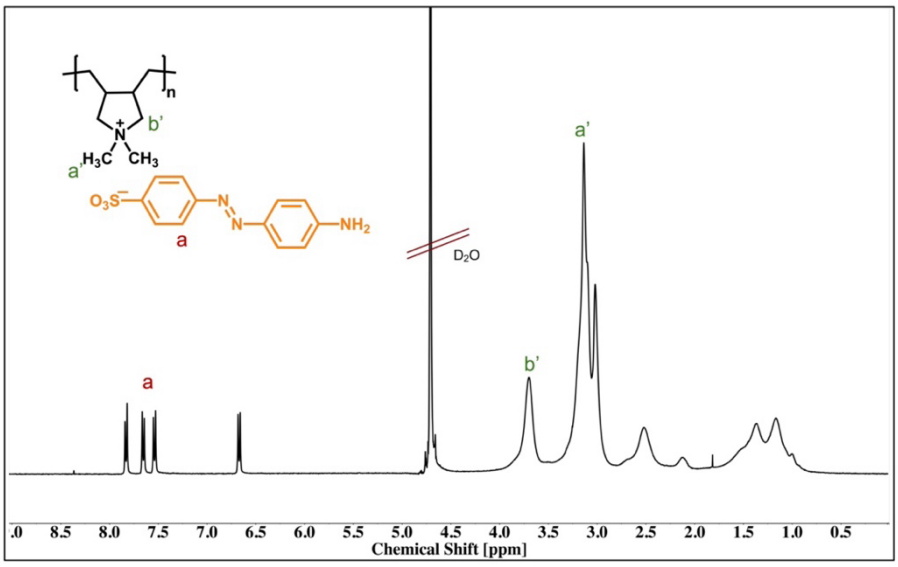

Figure A11 ^{1}H NMR spectrum of PDAC-Azo complex in D_2O (400 MHz, 298 K).

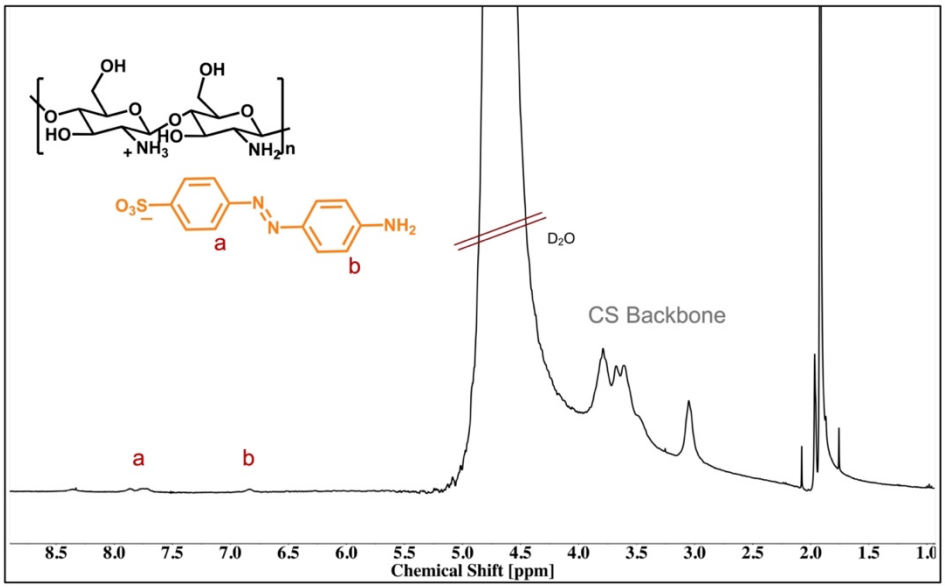

Figure A12 ^{1}H NMR spectrum of CS-Azo complex in D_2O (400 MHz, 298 K) (Note: 1% Acetic acid was added to the solution for better solubility).

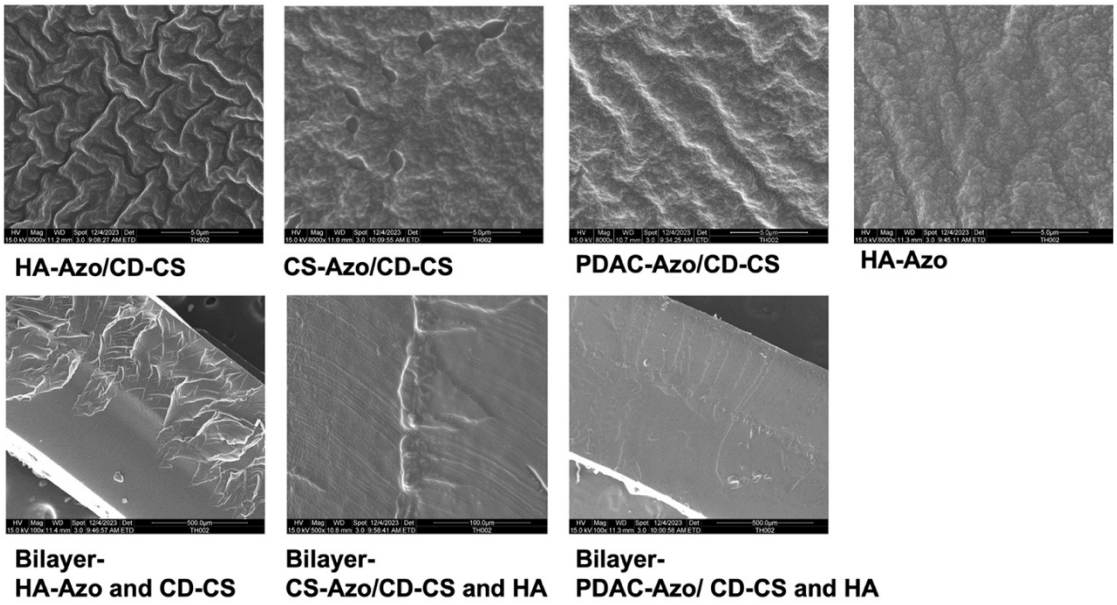

Figure A13 SEM images of IPNs, SPNs and Bilayers

List of Abbreviations

λ	Wavelength
β	Beta
γ	Gamma
ΔT	Difference in temperatures
°C	Degree Celsius
α	Alpha
ε	Molar extinction coefficient
δ	Chemical shift in NMR spectroscopy
a.u.	Atomic unit
AA	Acetic acid
AIBN	Azobisisobutyronitrile
ATRP	Atom transfer radical polymerization
Azo	Azobenzene
BL	Bilayer
CAD	Computer-Aided Design
CD	Cyclodextrin
CD-CS	β-Cyclodextrin-modified Chitosan
CD-oTs	monotosylated cyclodextrin
co	copolymer
CS	Chitosan
CS-Azo	Chitosan-Azobenzene Complex
D	Debye

Đ	Dispersity
DEGMA	di(ethylene glycol)methyl ether methacrylate
DLP	Digital Light Processing
DMSO	Dimethyl sulfoxide
DSC	Differential Scanning Calorimetry
E	Entgegen
EDC	1-Ethyl-3-(3-dimethylaminopropyl) carbodiimide
EGDEMA	ethylene glycol dimethylacrylate
et al.	Et alii
FRP	Free-radical polymerization
g	gram
G'	storage modulus
GPC	Gel Permeation Chromatography
HA	Hyaluronic Acid
HA-Azo	Azo-modified Hyaluronic Acid
HA-NB	*ortho*-nitrobenzyl ester of hyaluronic acid
HA-TBA	Tetrabutylammonium salt of HA
i.e.	Id est
IPN	Interpenetrating Polymer Network
IR	Infrared
IUPAC	International Union of Pure and Applied Chemistry
K_a	Association constant
kPa	kilopascal
LAP	lithium phenyl-2,4,6-trimethylbenzoylphosphinate
LCST	Lower critical solution temperature

mmol	Millimole
M_n	Number average molecular mass
mol%	Mole percentage
MR	Merocyanine
M_w	Weight average molecular mass
NHS	N-Hydroxysuccinimide
nm	Nanometer
NMR	Nuclear Magnetic Resonance
o-NB	*ortho*-nitrobenzyl
OEGMA	oligo(ethylene glycol) methyl ether methacrylate
PDAC	poly(diallyldimethylammonium chloride)
PDAC-Azo	poly(diallyldimethylammonium chloride)- Azobenzene complex
PDEGMA	Poly(di(ethylene glycol)methyl ether methacrylate)
PE	Polyelectrolyte
PEC	Polyelectrolyte Complex
PEC-IPN	Interpenetrating Polymer Networks integrated with Polyelectrolyte Complex
PEG	poly(ethylene glycol)
pH	Potential of hydrogen
PI	Photoinitiator
pK_a	Acid dissociation constant
PNIPAM	Poly(N-isopropylacrylamide)
PPG	Photo-protecting group
PRP	Photo-responsive Polymer

PSS	Photo-stationary state
RAFT	Reversible Addition fragmentation Transfer
ROMP	Ring-opening metathesis polymerisation
RP	Radical Polymerization
SEM	Scanning Electron Microscopy
SLA	Stereolithography
SP	Spiropyran
SpMA	Spiropyran methacrylate
SPN	Supramolecular Polymer Networks
T	Temperature
T_d	Thermal decomposition temperature
TEMPO	4-N-amino-2,2,6,6-tetramethylpiperidin-1-oxyl-4-yl
T_g	Glass transition temperature
TGA	Thermogravimetric Analysis
THF	Tetrahydrofuran
UV	Ultraviolet
Z	Zusammen

List of Schemes, Figures and Tables

List of Schemes

List of Figures

List of Tables

Acknowledgement

This journey of becoming a “Dr.”, which once felt like a distant dream, is now turning into a vivid reality. This path was paved not only by my own perseverance, but also through the support of numerous incredible individuals. I am profoundly grateful to each person who has played a role in this endeavor.

Foremost, I extend my deepest appreciation to my supervisor, Prof. Dr. Patrick Théato, for welcoming me into his group, for his faith in my potential, and his instrumental academic mentorship. I am particularly thankful for the scientific freedom he has offered, allowing me to forge my own path in research and pursue my interests with zeal. His generous support, motivational encouragement, financial backing, and patient guidance have been cornerstones of my experience here. The depth of knowledge and scientific insight I have acquired under his guidance are priceless assets I will take with me in my career ahead. I am keenly optimistic about our forthcoming collaborations.

Additionally, I would like to gratefully acknowledge the Ministry of Science, Research and Arts of Baden-Württemberg (MWK) for their generous support in the form of a doctoral scholarship through the esteemed 'Landesgraduiertenförderung', a Graduate Funding from the German States program. This scholarship has been a pillar of my academic journey, providing me with the financial stability to pursue my research with focus and dedication. Moreover, my heartfelt thanks go to the Karlsruhe House of Young Scientists (KHYS) for their pivotal role and support in facilitating this scholarship and aiding in my academic endeavors.

I would like to thank Dr. Dominik Voll for his pivotal role in the smooth operation of our lab's daily activities and instruments. I appreciate your assistance in times of need. My gratitude also goes to JProf. Dr. Hatice Mutlu for her valuable guidance during the initial phase of my doctoral research. I must express my special acknowledgement to our lab technician, Katharina Kuppinger, for her expert handling of lab supplies, and her skill in navigating the day-to-day hurdles of lab work. I am grateful to Dr. Yosuke Akae for his unwavering support and aid throughout my journey. Additionally, I would like to thank Dr. Christian Schmitt and Birgit Huber for their assistance. I am especially thankful to Bärbel Seufert-Dausmann and Martina Ritter for their generous assistance with bureaucratic processes and their consistent support throughout. I cherish the support of my dear friend and colleague, Dr. Azra Kocaarslan, whose academic and emotional support, especially in the demanding final year of my PhD, has been

a beacon of hope and encouragement in challenging times. A special expression of gratitude is reserved for Dr. Meryem S. Akdemir, who has been a constant support, a wonderful friend, an invaluable colleague and my well-wisher from my very first day at KIT till the end of my PhD. Thank you so much for being there for me and for all your kindness. To Dr. Wenyuan Dong, my labmate and Dr. Yunji Xie, my officemate, thank you for always helping, supporting and motivating me throughout my time here. Your presence and kindness made tough days a little easier to handle. A special note of thanks to Yi-Fan Chen, my short-term lab partner and exchange student, for her invaluable help and assistance in lab work during the last year. Your enthusiasm, support, and inspiring friendship have made our collaborative efforts a joy. And to Yibo, my endearing young colleague, your encouragement on challenging days was greatly appreciated and will always be remembered.

My heartfelt thanks go out to my valued colleagues, whose support and guidance, whether fleeting or enduring, have made a lasting impact on my journey. My sincere appreciation to Daniel and Alex for their readiness to help and offer thoughtful advice whenever needed. I must also acknowledge the generosity of Sven, Nico, Cornelius, Klara, and the alumni including Dr. Victoria Lee, Dr. David Sundermann, Dr. Miriam Khodier, Dr. Marvin Subarew, Dr. Isabella Weiß, Dr. Johannes Scheiger, Dr. Andreas Butzelaar, Dr. Stefan Frech, Dr. Sergej Baraban, Dr. Xiaohui Li, and Dr. Xia Huang, for their assistance and wise counsel.

Above all, I am deeply indebted to my family for their extraordinary and endless encouragement. To my dear Mumma and Papa, your constant motivation and inspiration, coupled with the unwavering emotional support and guidance you've provided, have been the bedrock of my success. You are truly the unsung heroes behind all my accomplishments.

Most importantly, I reserve my deepest gratitude for my beloved husband Dinesh, who has been my pillar of strength through thick and thin of my PhD journey. No words can adequately express my appreciation for the immeasurable love and support you have provided in every facet of my life, surpassing all that I could have ever hoped for. I am truly blessed to have you in my life.

I am immensely grateful to my lovely sister Mahima for her continuous uplifting words of encouragement. I am also thankful to my in-laws, my cherished friend Komal and my constant well-wishers Sourav and Bandhan for their unwavering support and motivation.

Lastly, to all the people I've had the pleasure of meeting on my PhD journey, THANK YOU!

"The cave you fear to enter holds the treasure you seek."
- Joseph Campbell